NASA TN D-444

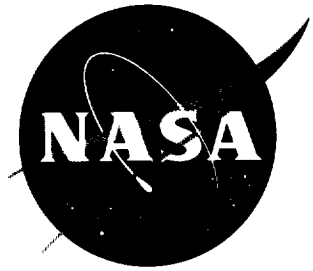

TECHNICAL NOTE
D-444

LATERAL STABILITY AND CONTROL CHARACTERISTICS OF A FOUR-PROPELLER DEFLECTED-SLIPSTREAM VTOL MODEL INCLUDING THE EFFECTS OF GROUND PROXIMITY

By Richard E. Kuhn and Kalman J. Grunwald

Langley Research Center
Langley Field, Va.

NATIONAL AERONAUTICS AND SPACE ADMINISTRATION

WASHINGTON

January 1961

NATIONAL AERONAUTICS AND SPACE ADMINISTRATION

TECHNICAL NOTE D-444

LATERAL STABILITY AND CONTROL CHARACTERISTICS OF A FOUR-PROPELLER DEFLECTED-SLIPSTREAM VTOL MODEL INCLUDING THE EFFECTS OF GROUND PROXIMITY

By Richard E. Kuhn and Kalman J. Grunwald

SUMMARY

The investigation of the lateral-directional stability and control characteristics of a four-propeller deflected-slipstream VTOL model in the transition speed range was conducted in the 17-foot test section of the Langley 300-MPH 7- by 10-foot tunnel. A large fairing on top of the rear fuselage was needed to eliminate directional instability in the power-off flaps-retracted condition. Even with this fairing some instability at small sideslip angles remained for power-on conditions with low flap deflections. The configuration exhibited a high level of dihedral effect which, coupled with the directional instability, will probably produce an undesirable Dutch roll oscillation.

INTRODUCTION

A wind-tunnel investigation has been made of a 1/5-scale model of a four-propeller deflected-slipstream VTOL (vertical take-off and landing) airplane to determine the performance and stability and control characteristics in hovering and in transition to forward flight. The transition investigation was made in the 17-foot test section of the Langley 300-MPH 7- by 10-foot tunnel; the hovering investigation was made in an adjacent static room.

The investigation covered the complete range of flap deflections and power conditions through the transition speed range from hovering to forward (flaps retracted) flight. This paper presents the results of the investigation of the lateral-directional stability and control characteristics, including tests in the region of ground effect. An analysis of some of the significant lateral-directional stability and control characteristics is included. The performance and longitudinal stability and control characteristics are presented in reference 1.

SYMBOLS

The force and moment coefficients presented are based on the dynamic pressure in the slipstream. This system is used because, when a wing is located in a propeller slipstream, large forces and moments can be produced even though the free-stream velocity decreases to zero. In this condition, coefficients based on the free-stream dynamic pressure approach infinity and therefore become meaningless. It appears appropriate, therefore, to base the coefficients on the dynamic pressure in the propeller slipstream. The coefficients based on this dynamic pressure are indicated in the present paper by the use of the subscript s. The relations between the thrust and dynamic pressure in the slipstream have been derived in reference 2. The more familiar coefficient forms based on the free-stream dynamic pressure can be found by dividing by $\left(1 - C_{T,s}\right)$; that is, $C_L = \frac{C_{L,s}}{1 - C_{T,s}}$. The positive sense of forces, moments, and angles is indicated in figure 1. The moments are presented with reference to the center of gravity located at the projection of the wing 40-percent-chord point on the thrust line as shown in figure 2(a).

L 8 9 5

b wing span, 6.55 ft

c wing chord, 1.166 ft

c_a aileron chord, 0.466 ft

$C_{h,a}$ aileron hinge-moment coefficient, $\frac{\text{Aileron hinge moment}}{q_s(2S_a)c_a}$

C_L lift coefficient based on free stream, $\frac{L}{\frac{\rho}{2}V_\infty{}^2 S}$

$C_{L,s}$ lift coefficient based on slipstream, $\frac{L}{q_s S}$

C_l rolling-moment coefficient, $\frac{M_X}{\frac{\rho}{2}V_\infty{}^2 Sb}$

$C_{l,s}$ rolling-moment coefficient, $\frac{M_X}{q_s Sb}$

$C_{m,s}$ pitching-moment coefficient, $\frac{M_Y}{q_s Sc}$

C_n yawing-moment coefficient, $\frac{M_Z}{\frac{\rho}{2}V_\infty^2 Sb}$

ΔC_{n_β} incremental change in directional-stability parameter

$C_{n,s}$ yawing-moment coefficient, $\frac{M_Z}{q_s Sb}$

$C_{T,s}$ thrust coefficient, $\frac{T}{q_s N \frac{\pi}{4} D^2}$

$C_{X,s}$ longitudinal-force coefficient, $\frac{F_X}{q_s S}$

$C_{Y,s}$ side-force coefficient, $\frac{F_Y}{q_s S}$

D propeller diameter, 1.55 ft

F resultant force, lb

F_X longitudinal force, lb

F_Y side force, lb

h height of wheels above ground, ft

i_t horizontal-tail incidence, deg

L lift, lb

M_X rolling moment, ft-lb

M_Y pitching moment, ft-lb

M_Z yawing moment, ft-lb

N number of propellers

q_s dynamic pressure in slipstream, $\frac{\rho}{2}V_\infty^2 + \frac{T}{N\frac{\pi}{4}D^2}$, lb/sq ft

S wing area, 7.65 sq ft

S_a aileron area per semispan, 0.692 sq ft

T total thrust, lb

V_∞ free-stream velocity, ft/sec

V velocity in flight, knots

α angle of attack, deg

β angle of sideslip, deg

δ_a aileron deflection, deg

$\delta_{f,S}$ sliding-flap deflection, deg

$\delta_{f,R}$ rear-flap deflection, deg

δ_r rudder deflection, deg

θ slipstream turning angle (static tests), $\tan^{-1}\frac{L}{F_X}$, deg

ρ mass density of air, slugs/cu ft

Subscripts:

0 power-off flaps-retracted condition

s based on slipstream

S sliding flap

R rear flap

MODEL

Drawings of the model with pertinent dimensions are presented in figure 2; photographs of the model mounted for testing are presented in figure 3. The wing employed an NACA 4415 airfoil section and was set at 5° nose-up incidence to the fuselage reference line, which was parallel to the normal position of the propeller thrust axis. The flap system consisted of a 50-percent-chord sliding flap and a 30-percent-chord slotted flap as shown in figure 2(b). The radius of the sliding flap was approximately 20 percent of the wing chord, and the ordinates of the slotted flap are shown in figure 2(b). The combinations of flap deflections used in the investigation and the system used to designate the flap deflections in the figures and text are as follows:

Sliding-flap deflection, $\delta_{f,S}$, deg	Rear-flap deflection, $\delta_{f,R}$, deg	Designation: $\delta_{f,S}/\delta_{f,R}$
0	0	0/0
10	8.2	10/8.2
20	15	20/15
30	20.7	30/20.7
40	24	40/24
50	25	50/25

In addition, the rear or slotted flap was constructed in two pieces so that the outboard element could be deflected as an aileron.

The model was constructed of a steel frame to carry the loads and wood covering to give the desired contours. The three-blade propellers were made of aluminum alloy and driven by variable-frequency electric motors. The speed of each propeller was determined by observing a stroboscopic-type indicator into which was fed the output frequency of small alternators connected to each motor shaft. The outboard propellers rotated against the tip vortices (right-hand rotation on the right wing; left-hand rotation on the left wing) and for most of the tests the inboard propellers rotated in the opposite direction.

The lift, longitudinal force, pitching moment, rolling moment, yawing moment, and side force were measured on an internally mounted strain-gage balance; also, the hinge moment of the aileron was measured by a strain-gage beam. The reference point for this hinge moment is shown in figure 2(b).

The flap and aileron settings were fixed by interchangeable blocks; the stabilizer and rudder were set at fixed positions by inserting dowels in predrilled setting holes.

Several modifications to the fuselage and vertical tail were tested during the investigation. These are shown in figures 4, 5, and 6. The top fuselage fairing (figs. 4(b) and 5) was constructed of balsa wood and heavy manila paper. The dorsal fin, spoilers, lower fuselage fairing, and vertical-tail extension were made of heavy cardboard and the auxiliary vertical tails were made of sheet aluminum.

TESTS AND CORRECTIONS

The investigation was made in the 17-foot test section of the Langley 300-MPH 7- by 10-foot tunnel, which is described in the appendix to reference 3. In order to minimize the time required for the tests, the operating conditions were chosen so that only two propeller-blade angles were required. A blade angle of 5° was used for tests at thrust coefficients of 0.60 and above and a blade angle of 13° was used for the lower thrust coefficients and for propeller-windmilling tests. A propeller rotational speed of 6,000 rpm was used with the 5° blade angle and 4,000 rpm was used with the 13° blade angle. The thrust of the four propellers was determined at each tunnel speed by taking the difference between the measured longitudinal force with the propellers operating and the propeller-off longitudinal force (drag) at zero angle of attack with the flaps retracted.

The test procedure consisted of setting the propeller rotational speed with the model at zero angle of attack and then increasing the tunnel speed until zero longitudinal force was reached. This tunnel speed, which corresponded to the condition for steady level flight at zero angle of attack (when lift is scaled up to the airplane weight), was held constant as the data were taken through the sideslip-angle range. Usually, subsequent tests were made at angles of attack with speeds above and below the tunnel speed for steady level flight at zero angle of attack in order to provide data for the conditions of acceleration and deceleration.

The slipstream dynamic pressure varied from about 3.8 to 5.0 pounds per square foot. A free-stream dynamic pressure of 5.0 pounds per square foot was used for the propeller-off and propeller-windmilling tests. The Reynolds number of the flow in the slipstream based on the wing chord of 1.166 feet varied from 0.42×10^6 to 0.49×10^6.

Errors in the free-stream velocity due to blockage and slipstream contraction were estimated and were found to be small, and therefore corrections were not applied. The jet-boundary corrections applied to the angle of attack and longitudinal force were estimated for a square test section by a method similar to that of reference 4. Inasmuch as

these corrections depend on the circulation about the wing, it was necessary to subtract the direct thrust contribution to lift before applying them. The following relations were used:

$$\alpha = \alpha_{measured} + 0.239C_{L,l}$$

$$C_{X,s} = C_{X,s,measured} - 0.0042(C_{L,l})^2(1 - C_{T,s})$$

where $C_{L,l}$ is the increment of lift coefficient that is approximately proportional to circulation and is obtained by subtracting the direct thrust contribution as follows:

$$C_{L,l} = \frac{C_{L,s} - C_{T,s}\frac{\frac{4\pi D^2}{4}}{S}\frac{F}{T}\sin(\theta + \alpha)}{1 - C_{T,s}}$$

where θ and F/T are the turning angle and thrust-recovery factor determined from static tests (ref. 1).

PRESENTATION OF RESULTS

The results of the investigation are presented in the following figures:

	Figures
Basic data:	
Flaps-retracted condition:	
Characteristics of original configuration (power-off)	7
Effect of modifications (power-off)	8 to 10
Effect of power	11
Effect of flap deflection and power-on stability:	
Out of ground-effect region	12
In ground-effect region	13
Aileron effectiveness:	
Out of ground-effect region	14
In ground-effect region	15
Rudder effectiveness	16
Characteristics through 180° sideslip-angle range	17 to 18
Aileron hinge moment	19

Figures

Analysis:
Stability:
Out of ground-effect region 20
Effect of ground proximity 21
Aileron effectiveness 22
Rudder effectiveness 23

Extraneous symbols on the zero axes of figures 7 to 18 are reference points printed by the machine used for plotting the data.

DISCUSSION

Stability Characteristics, Power Off

Original configuration.- The basic tail-on and tail-off lateral-directional stability characteristics of the model, before modification, are shown in figure 7. The tail-on data show directional stability at large sideslip angles but indicate instability at sideslip angles near zero. This instability is about equivalent to the directional instability with the tail off and indicates the equivalent of zero vertical-tail effectiveness at small sideslip angles. Several factors contributed to this loss in directional stability. A large separated wake originated on the steep slope of the fuselage upper surface near the wing trailing edge. This wake reduced the effective dynamic pressure at the vertical tail. Also, the rear part of the fuselage has an inverted-triangular cross section and is inclined at a large angle to the direction of flight so that a component of the flow approaches from the base of the triangle. Through the use of tufts on the fuselage sides, it was observed that the flow, when the model was at a sideslip angle, was attached on the side from which the relative wind approached and was separated on the opposite side. The data of reference 5 indicate that the side force on this part of the fuselage under these flow conditions was probably toward the side with the attached flow and thus in a direction to reduce the stability. Also, changing the horizontal-tail incidence from 0° to -7.5° increased the instability, probably because of flow separation at the juncture. Reference 1 indicates, however, that positive incidence settings will be required through most of the flight regime and that negative incidence angles of about 7.5° will be needed only in demonstrating power-off stalls.

Effect of modifications.- Numerous attempts were made to reduce or eliminate the instability at small yaw angles. Some of these attempts were also made to gain an insight into the reasons for the loss in

stability described in the preceding section. Figure 8 shows the effect of adding vertical surface area. As can be seen, the stability was improved, but a small unstable or neutrally stable region remained, primarily because these fixes did not affect the basic causes of the problem.

Figure 9 presents the results of some attempts to prevent flow attachment on the sides of the inverted-triangular fuselage by placing spoilers vertically along the side of the fuselage a short distance behind the wing trailing edge and longitudinally along the top edge of the fuselage. In general, the spoilers were not able to maintain a separated flow condition except when both systems were used together (side and top spoilers). In fact, the top spoilers alone increased the instability somewhat.

The addition of a fairing to the top of the fuselage (as shown in figs. 4(b) and 5) produced a configuration with directional stability throughout the sideslip-angle range (fig. 10). This fairing eliminated the separated-flow region on the top of the fuselage and was faired into the sides of the fuselage so that separation from the fuselage sides was minimized. Refairing the lower rear part of the fuselage, as shown in figure 6, with the top fairing off also reduced the instability (fig. 10) but was not as effective as fairing the top of the fuselage.

The effect of enclosing the cockpit (fig. 10) was small and generally within the accuracy of the data.

Stability and Control Characteristics, Power On

Effect of power and flap deflection on stability.- The characteristics of the model with the windmilling propeller are not very different from the characteristics of the model with the propeller off. (See figs. 7 to 11.) In general, the propellers would be expected to produce a destabilizing contribution because of their fin effect, as discussed in reference 6; however, in the present tests the propellers are only a short distance ahead of the moment-reference point. As a result the expected decrease in directional stability as calculated from reference 6 is about $\Delta C_{n_\beta} = -0.00027$, which, as can be seen from the scatter of the data, is about the order of accuracy of the present results.

The effect on the directional stability of applying power with flaps retracted is also shown in figure 11 $\left(C_{T,s} = 0.33\right)$ and is destabilizing, as would be expected. The magnitude of the reduction in stability, however, is much greater than would be expected. Estimates of the destabilizing effect of applying power, made by the method

of reference 6, indicate a destabilizing moment from the propellers of only about $\Delta C_{n_\beta} = 0.00032$. Even adding the direct moments on the propellers from the data of reference 3 (which are also destabilizing and which were not considered in ref. 6) increases this increment to only $\Delta C_{n_\beta} = 0.0005$, whereas the experimental data (fig. 11) indicate an increment of $\Delta C_{n_\beta} = -0.0012$.

The lateral stability characteristics of the modified model (top fuselage fairing on) with the combinations of flap deflection and thrust coefficients required throughout the transition speed range are presented in figure 12 and are summarized in figure 20. At the lower speeds and flap deflections of 50/25 and 40/24, the model exhibits neutral stability or a low level of directional instability which is generally independent of angle of attack (figs. 12(e) and (f)). With flap deflections of 20/15 and 10/8.2 (figs. 12(b) and (c)) the model is directionally stable at angles of attack of 10° and 20° within the sideslip-angle range of the investigation; however, it is directionally unstable for small sideslip angles at $\alpha = 0°$ and $\alpha = -10°$. It is believed that the instability at zero and negative angles of attack (flaps retracted and deflected) is due to the previously discussed flow across the inverted-triangular cross section of the rear fuselage. Although the fuselage fairing is installed, some flow separation apparently occurs on the side of the fuselage (downstream side with respect to the component of velocity due to sideslip) with the result that the attached flow on the upstream side produces a force on the rear part of the fuselage in a destabilizing direction. The increased slipstream velocity due to power and the increased downward component of this velocity due to flap deflection aggravate the situation, whereas increasing the angle of attack more nearly alines the rear part of the fuselage with the free-stream velocity, thus reducing the component of flow across the fuselage and reducing or eliminating the destabilizing forces. If the reduction in directional stability were caused by flow separation with a corresponding reduction in dynamic pressure in the region of the vertical tail, the effects of increasing angle of attack would be expected to reduce the directional stability rather than increase it.

The variations of the directional-stability parameter $\frac{\partial M_Z}{\partial \beta}$ and the dihedral-effect parameter $\frac{\partial M_X}{\partial \beta}$ experienced in steady-level-flight transition are shown in figure 20 and compared with the variations that would exist if the power-off characteristics were maintained for all flap deflections and thrust coefficients required in the transition. As previously discussed, the configuration exhibits directional instability at small sideslip angles for the lower flap deflections (40 to 50 knot-speed range) but exhibits directional stability at large sideslip angles.

There appears to be little effect of power on dihedral effect $\frac{\partial M_X}{\partial \beta}$ (fig. 20); however, the general level of dihedral effect is very high, as might be expected from the high wing-fuselage juncture, the four high wing-nacelle junctures, and the high vertical tail topped by a horizontal tail. This high level of dihedral effect coupled with the directional instability at small sideslip angles will probably produce poor flying qualities, such as a poorly damped Dutch roll oscillation, in the transition speed range.

L
8
9
5

Effects of ground on stability.- The effects of proximity of the ground on the characteristics with flap deflections of 50/25 and 30/20.7 are presented in figure 13, and summarized in figure 21. Very large increases in both dihedral effect $\frac{\partial M_X}{\partial \beta}$ and directional stability $\frac{\partial M_Z}{\partial \beta}$ were experienced with the 50/25 flap setting. Similar effects of the ground have been experienced on another deflected-slipstream configuration in an unpublished investigation. The reasons for these large effects of the ground are not understood but may be associated with the tendency of the free-stream flow to decrease the spanwise flow of the slipstream from under the forward wing tip when the model is side slipped. Decreasing the amount of air escaping at the wing tip would increase both the turning angle and the thrust-recovery factor of the leading wing and thus would increase both the directional stability and the dihedral effect.

Aileron effectiveness.- The aileron effectiveness is shown in figures 14 and 15 and is summarized in figure 22. The power-off flaps-retracted data of figure 14(a) show roll-control effectiveness with only moderate yawing moment due to aileron deflection (except at high angles of attack and high deflections), as would be expected. As the flaps are deflected and the speed is decreased, the yawing moment due to aileron deflection increases (fig. 22) and the rolling moment decreases until, with a flap setting of 50/25, the ailerons give primarily yaw control and little roll control. The exact manner in which the aileron deflections are to be phased out and the change in propeller-blade angle phased in as roll control on the airplane when the flap deflection is increased is not known. The data of figures 14, 15, and 22 can be used in designing proper programing of aileron deflection and propeller-blade-angle change with flap deflection. Another point to consider in matching such a control system is the almost complete lack of roll control at angles of attack beyond the stall with flaps deflected (figs. 14(a), (b), and (c)), which would indicate the desirability of using the propeller-blade-angle change for control in at least part of the roll control down to very low flap deflections. The large yawing moments obtained from the ailerons are in the direction

to counter the yawing moments that would result from using the change in propeller-blade angle as roll control at low flap deflections.

The data also indicate the possibility of using the ailerons for yaw control at high flap deflections. This will eliminate the need for using the tail fan for yaw control and will increase the amount of tail-fan thrust available for pitch control.

Comparison between the data of figure 15, obtained with the model in the presence of the ground board, and the data from tests with the ground board removed (fig. 14) indicate very little effect of the ground board on the aileron effectiveness.

Rudder effectiveness.- The effects of rudder deflection are presented in figure 16 and summarized in figure 23. Also in figure 23, the rudder effectiveness with power on and flaps retracted is compared with variations that would be obtained if the power-off level of effectiveness were maintained through the transition speed range. The good agreement shown indicates that, as with the horizontal tail (ref. 1), the rudder is operating in essentially free-stream conditions.

Effect of 180° Sideslip Angles

A few tests were made with the flaps deflected for hovering (50/25) through a sideslip-angle range from -35° to 180° to obtain some information about flying sideways and backwards. The data are presented in figures 17 and 18. Note the large changes in longitudinal-force coefficient and the losses in lift associated with large sideslip angles for all thrust coefficients except the highest ($C_{T,s} = 0.995$). Apparently very high nose-up attitudes will be required for rearward flight, and large rolling and yawing moments will have to be countered in order to fly sideways.

CONCLUSIONS

The wind-tunnel investigation of the lateral stability and control characteristics of a 1/5-scale model of a deflected-slipstream VTOL airplane indicates the following conclusions:

1. The original model exhibited directional instability under power-off flaps-retracted conditions, primarily because of the peculiarities of the shape of the rear part of the fuselage. Adding a large fairing to the top of the fuselage eliminated the instability for the power-off flaps-retracted condition, but some instability

remained at small sideslip angles for the low to moderate flap deflections with power on.

2. The configuration exhibited a high level of dihedral effect which, coupled with the directional instability at small sideslip angles, will probably result in an undesirable Dutch roll oscillation.

3. Aileron effectiveness followed the expected trend of producing primarily roll control at low flap deflections and primarily yaw control at high flap deflections.

L
8
9
5

Langley Research Center,
National Aeronautics and Space Administration,
Langley Field, Va., June 3, 1960.

REFERENCES

1. Kuhn, Richard E., and Grunwald, Kalman J.: Longitudinal Aerodynamic Characteristics of a Four-Propeller Deflected Slipstream VTOL Model Including the Effects of Ground Proximity. NASA TN D-248, 1960.

2. Kuhn, Richard E., and Draper, John W.: Investigation of the Aerodynamic Characteristics of a Model Wing-Propeller Combination and of the Wing and Propeller Separately at Angles of Attack up to 90°. NACA Rep. 1263, 1956. (Supersedes NACA TN 3304 by Draper and Kuhn.)

3. Kuhn, Richard E., and Hayes, William C., Jr.: Wind-Tunnel Investigation of Longitudinal Aerodynamic Characteristics of Three Propeller-Driven VTOL Configurations in the Transition Speed Range, Including Effects of Ground Proximity. NASA TN D-55, 1960.

4. Gillis, Clarence L., Polhamus, Edward C., and Gray, Joseph L., Jr.: Charts for Determining Jet-Boundary Corrections for Complete Models in 7- by 10-Foot Closed Rectangular Wind Tunnels. NACA WR L-123, 1945. (Formerly NACA ARR L5G31.)

5. Polhamus, Edward C., Geller, Edward C., and Grunwald, Kalman J.: Pressure and Force Characteristics of Noncircular Cylinders as Affected by Reynolds Number With a Method Included for Determining the Potential Flow About Arbitrary Shapes. NASA Rep. R-46, 1959.

6. Ribner, Herbert S.: Notes on the Propeller and Slipstream in Relation to Stability. NACA WR L-25, 1944. (Formerly NACA ARR L4I12a.)

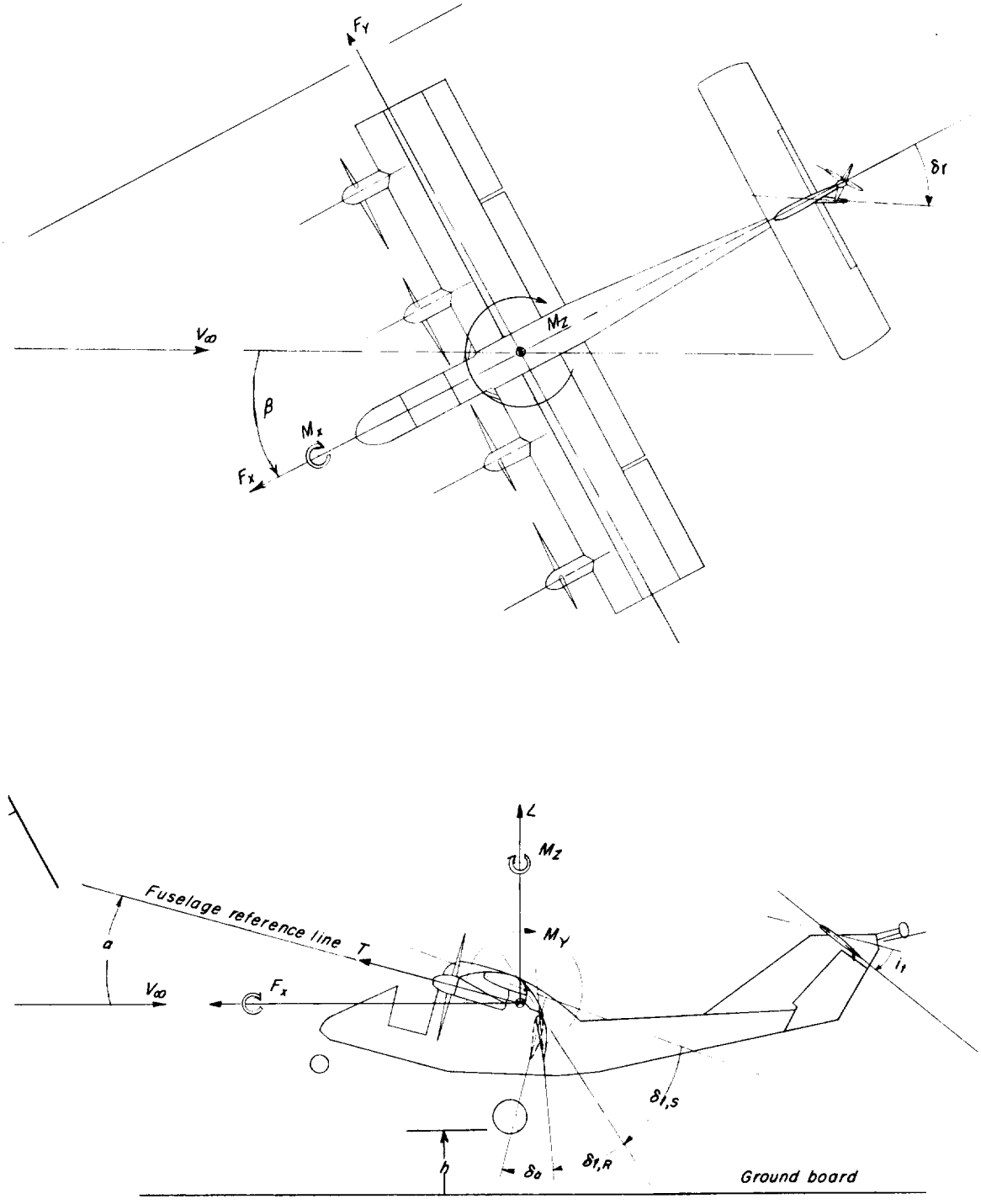

Figure 1.- System of axes showing positive sense of forces, moments, and angles.

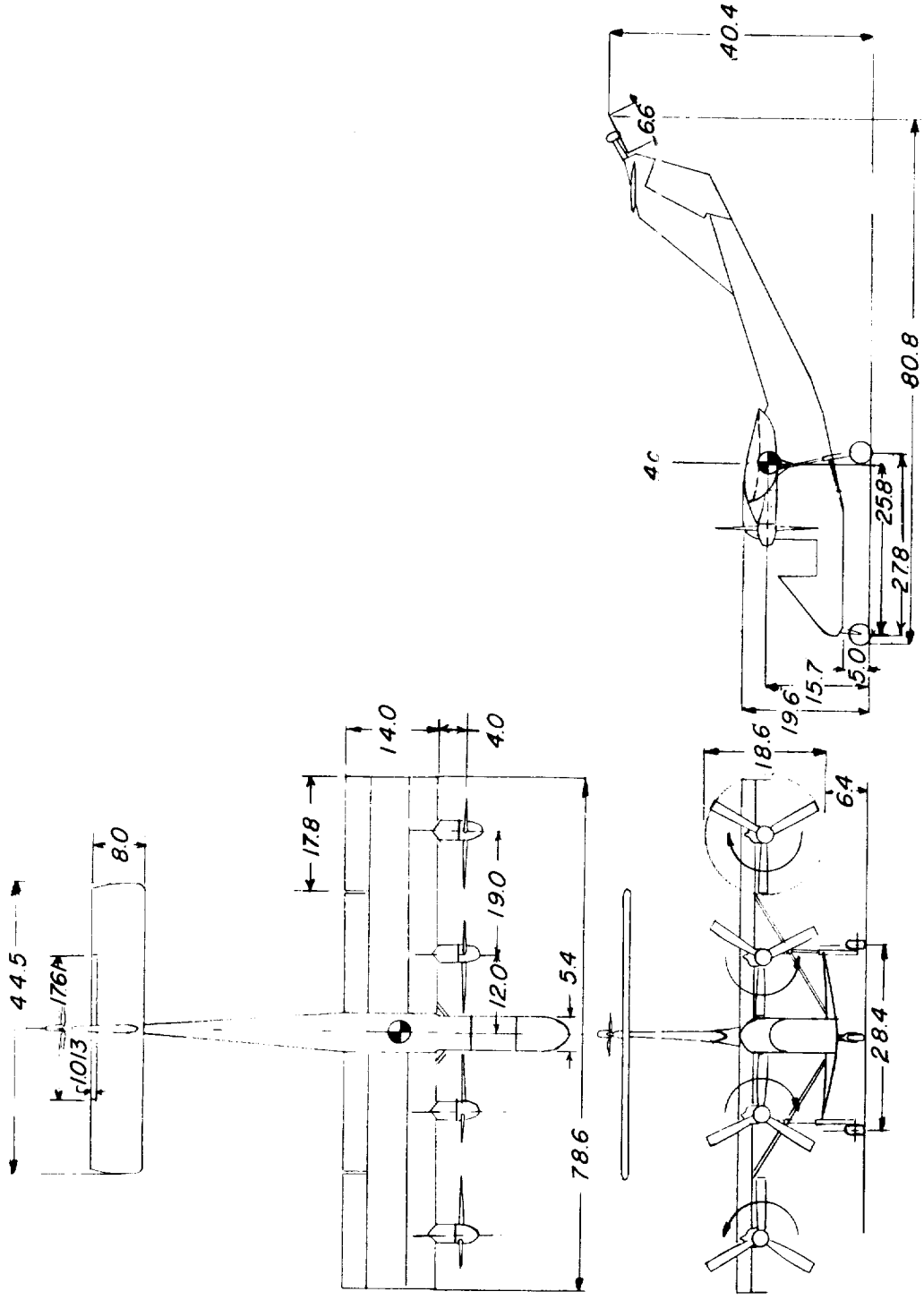

(a) Three-view drawing.

Figure 2.- Drawings of 1/5-scale model. All dimensions are in inches.

SLOT ORDINATES

Station	y_u	Station	y
7.310	-0.362	8.593	0.566
7.550	-.319	8.788	.697
7.755	-.235	9.369	.953
7.925	-.113	9.950	1.061
8.062	.031	10.150	1.070
8.120	.103	10.350	1.066
8.200	.194	10.550	1.052
8.400	.386	10.750	1.025
8.600	.542	10.950	.989
8.800	.668	11.150	.944
9.100	.816	11.350	.889
9.400	.920		
9.600	.971		
9.800	1.007		
10.000	1.025		

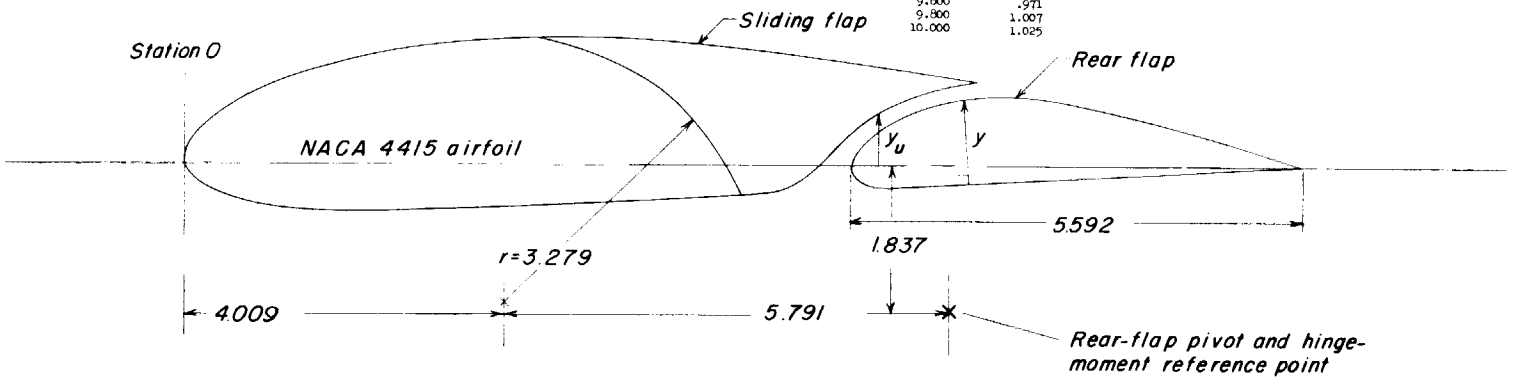

(b) Drawing of wing profile.

Figure 2.- Concluded.

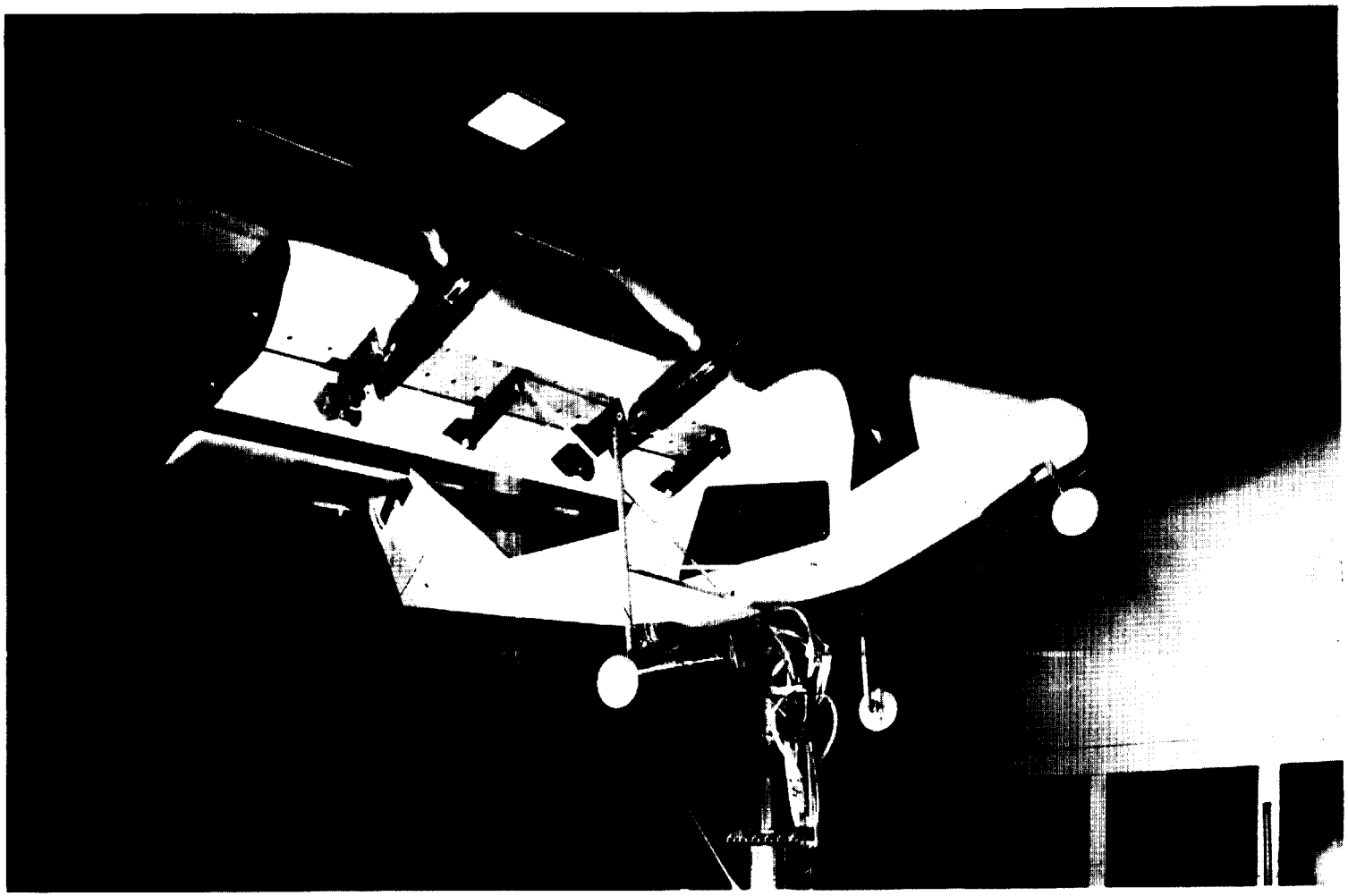

(a) Three-quarter front view of model (flaps retracted). L-58-2886

Figure 3.- Photographs of model.

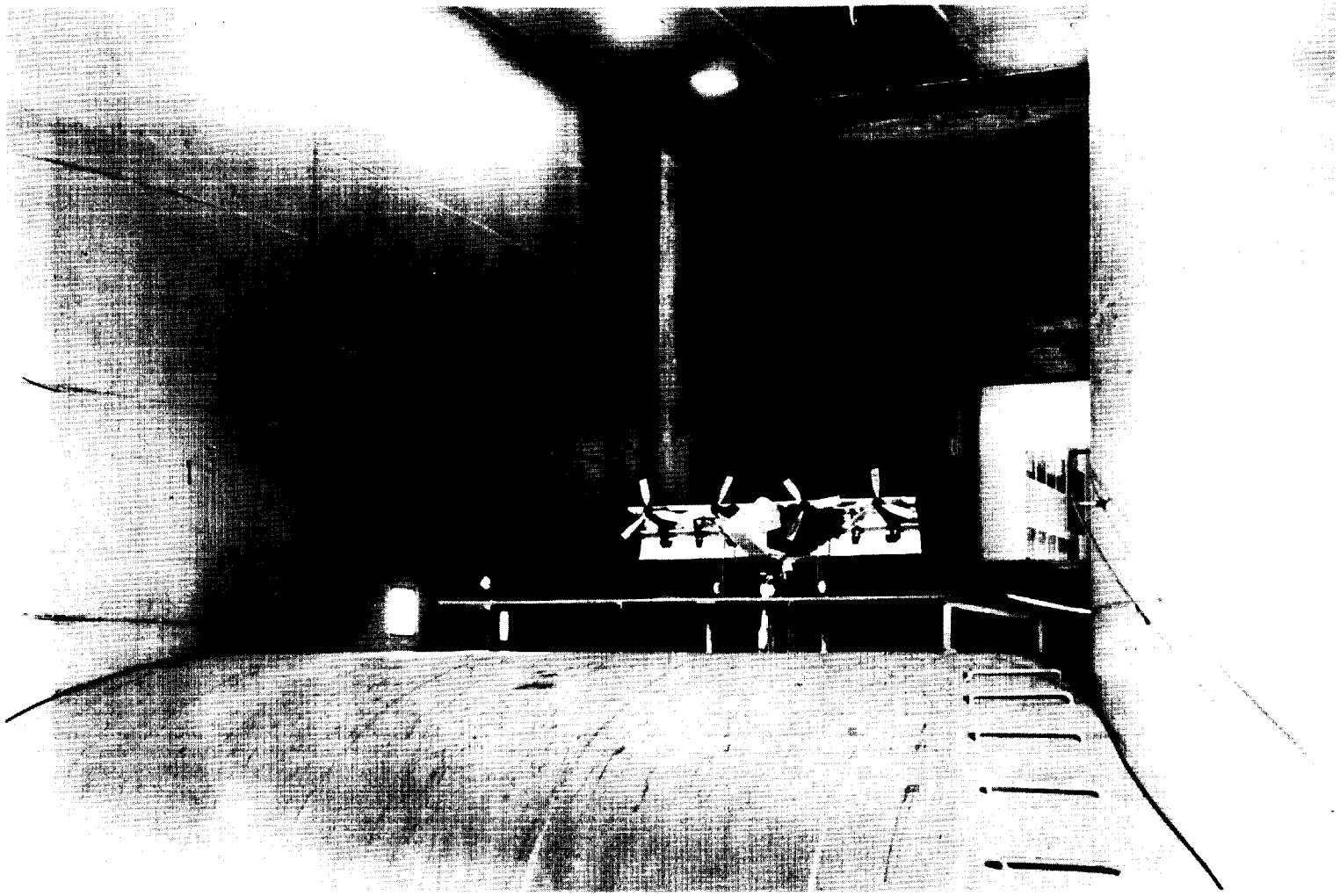

(b) Model in low position with ground board. L-58-3277

Figure 3.- Concluded.

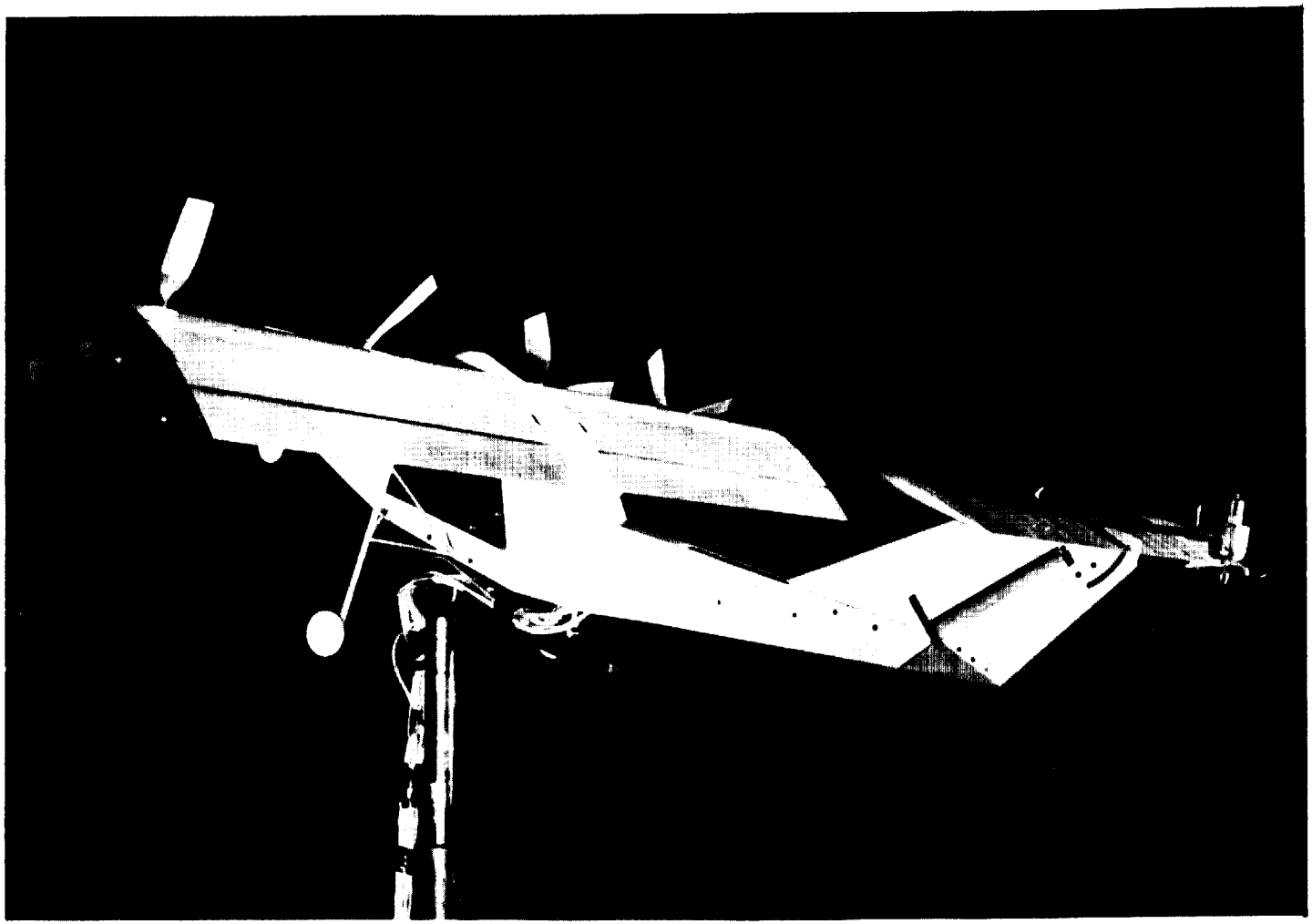

(a) Three-quarter rear view of original configuration. L-58-2887

Figure 4.- Photographs of fuselages.

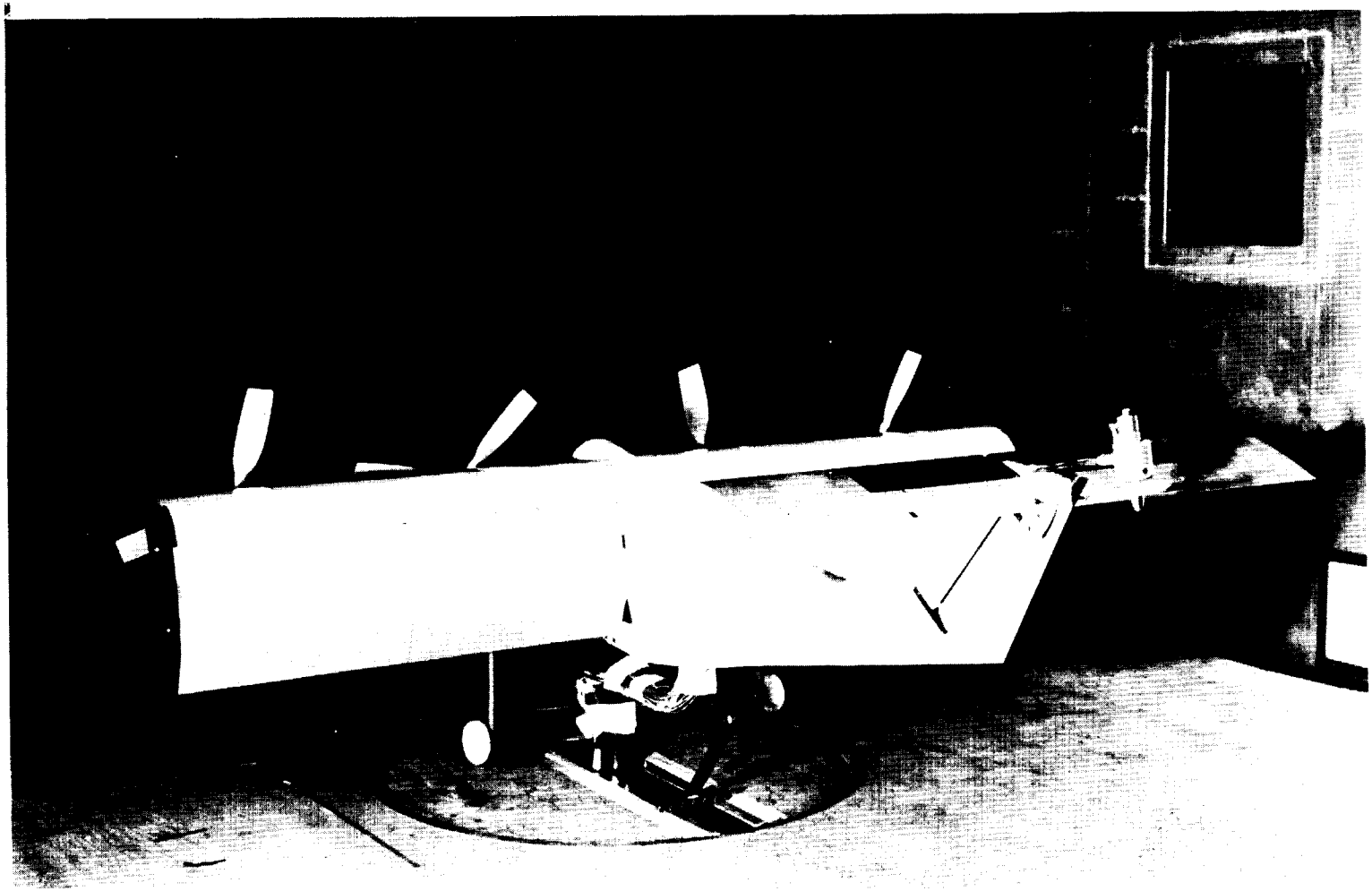

(b) Top fuselage fairing installed. L-58-3278

Figure 4.- Concluded.

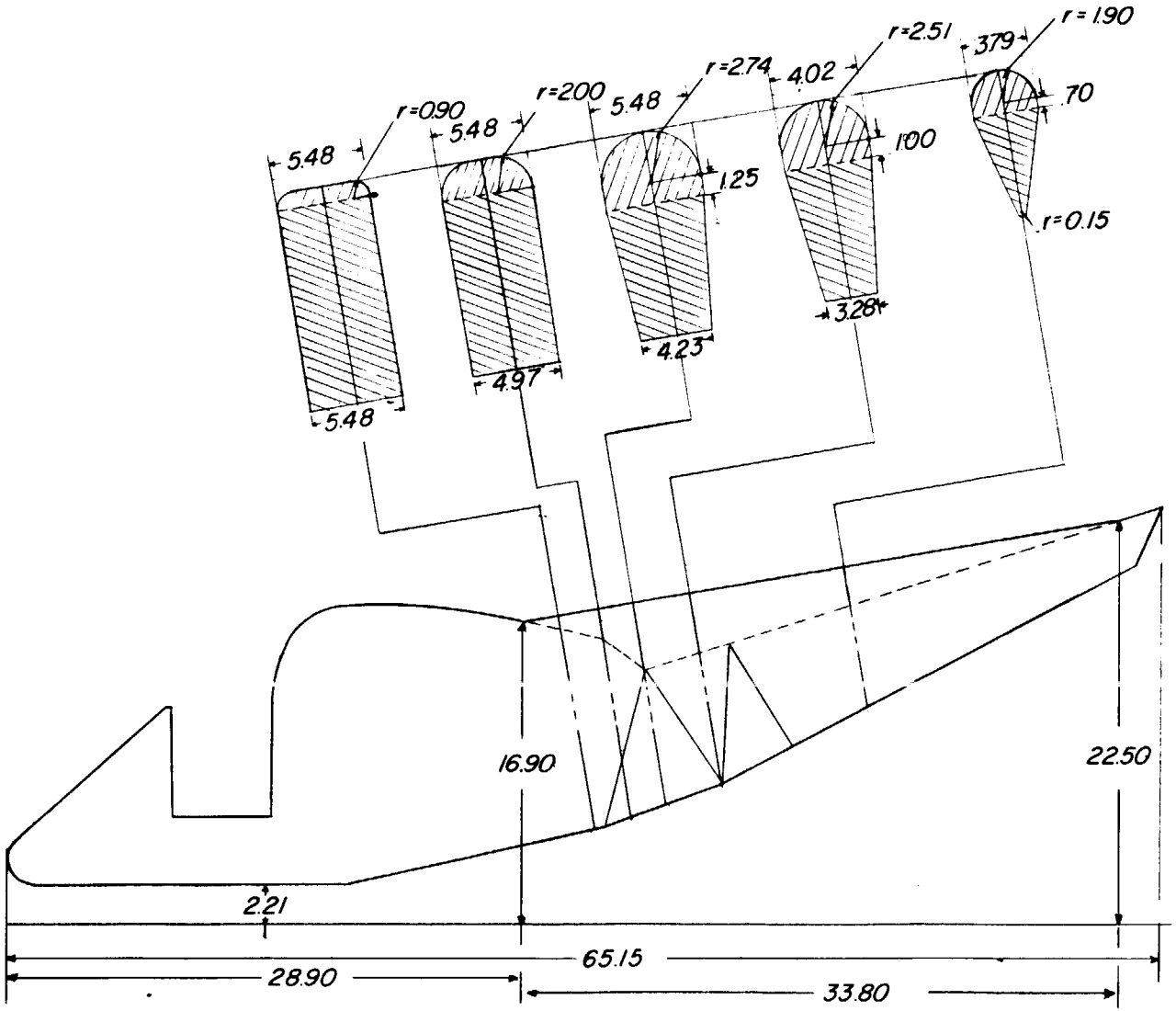

Figure 5.- Drawing of fuselage-fairing modification.

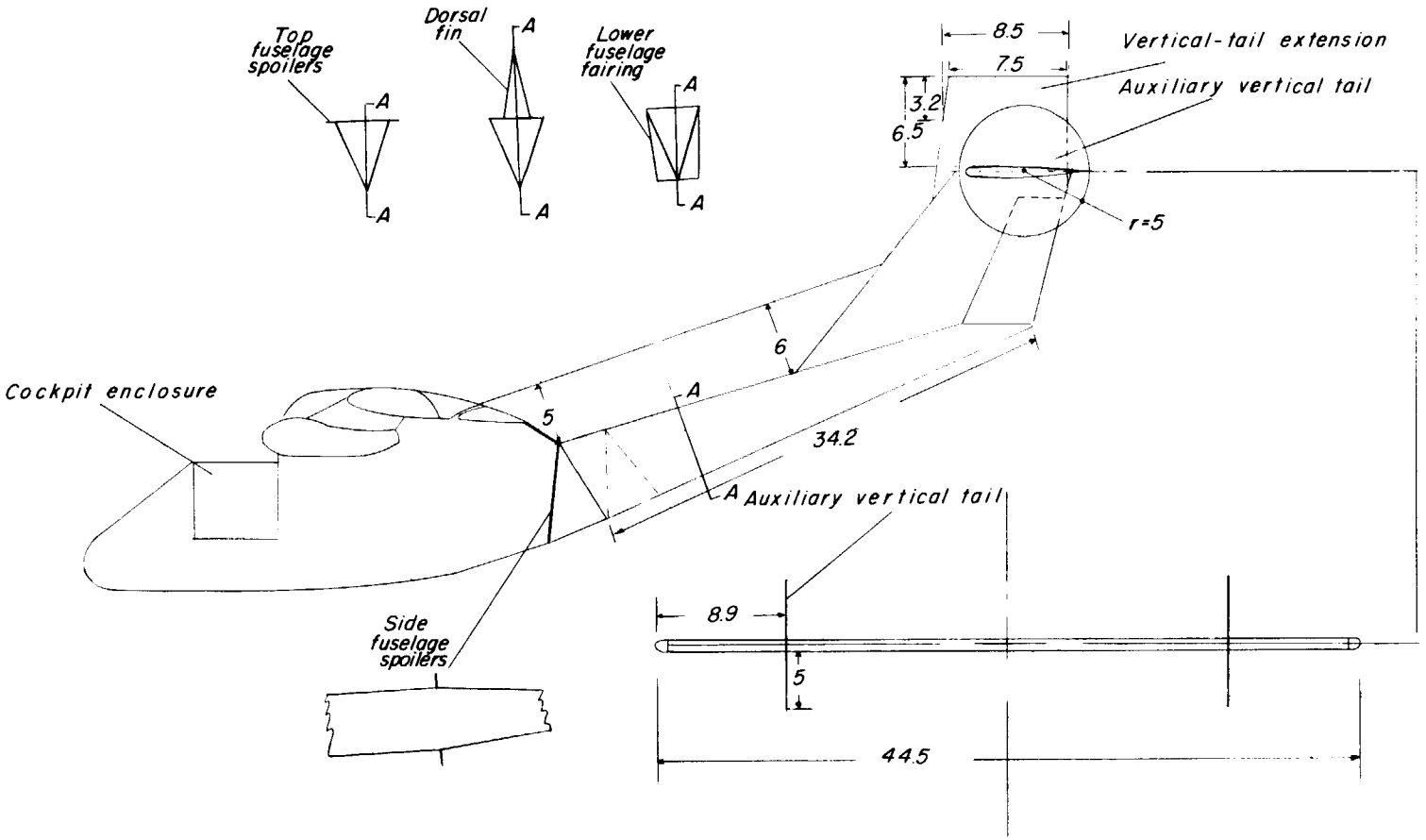

Figure 6.- Drawing of fuselage and vertical-tail modifications.

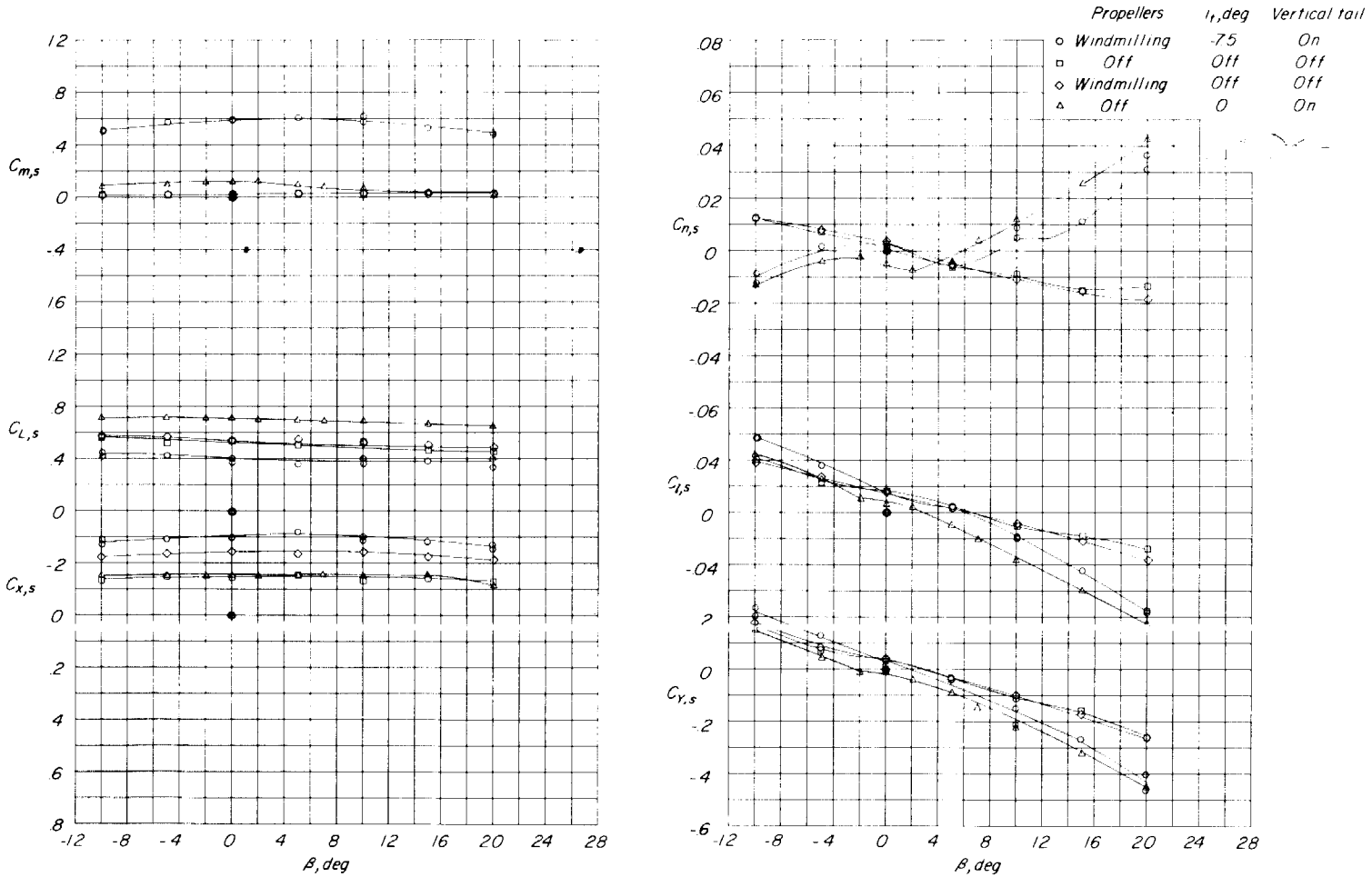

Figure 7.- Characteristics of original configuration. Flaps retracted; $\alpha = 0^{o}$; $C_{T,s} = 0$; $\delta_{f,S}/\delta_{f,R} = 0/0$; $h/D = \infty$.

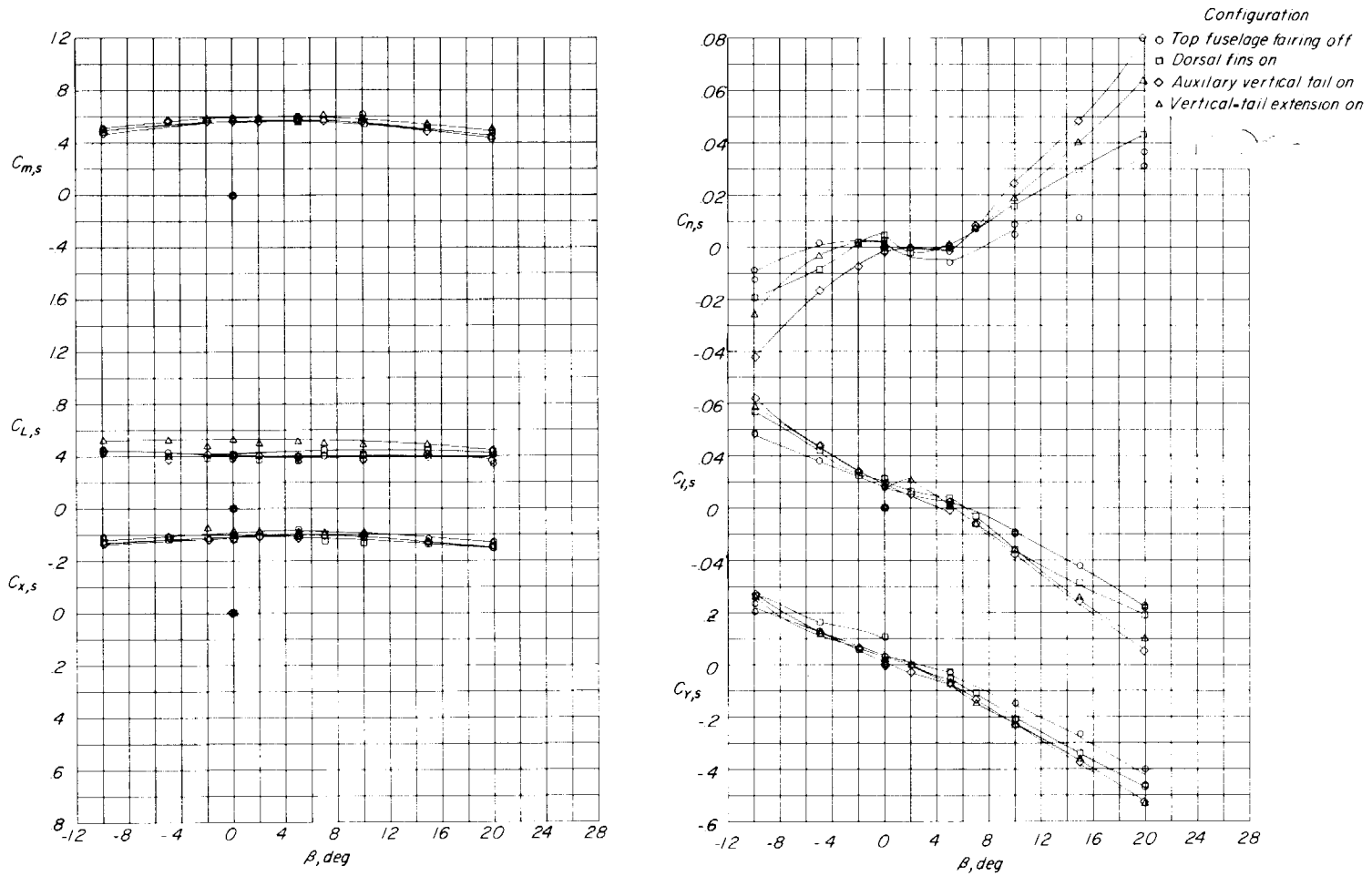

Figure 8.- Effect of vertical-tail modification. Flaps retracted; propellers windmilling; $\alpha = 0^{\circ}$; $i_t = -7.5^{\circ}$; $h/D = \infty$; $C_{T,s} = 0$; $\delta_{f,S}/\delta_{f,R} = 0/0$.

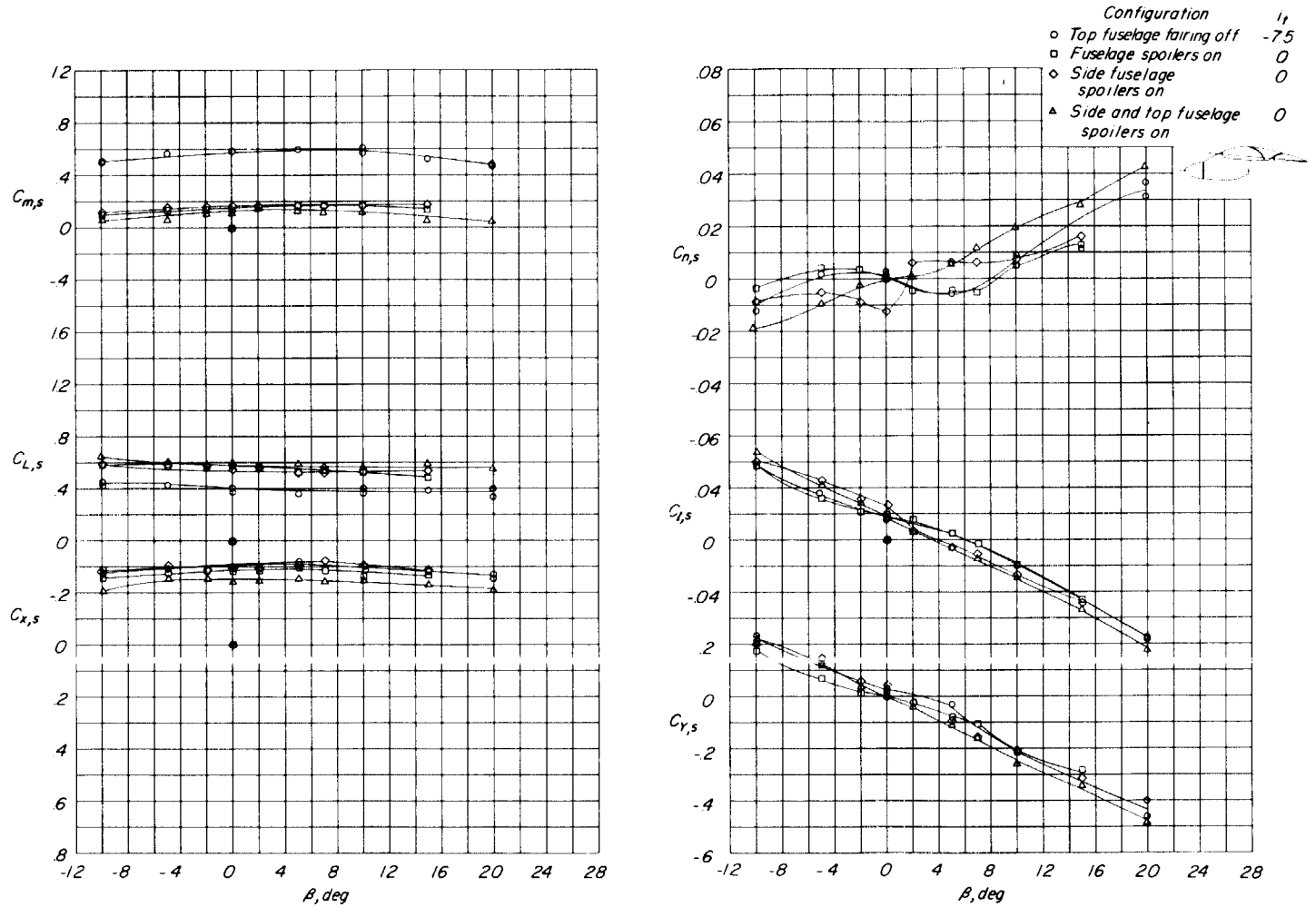

Figure 9.- Effect of fuselage spoilers. Flaps retracted; propellers windmilling; landing gear on; $\alpha = 0^{\circ}$; $\delta_{f,S}/\delta_{f,R} = 0/0$.

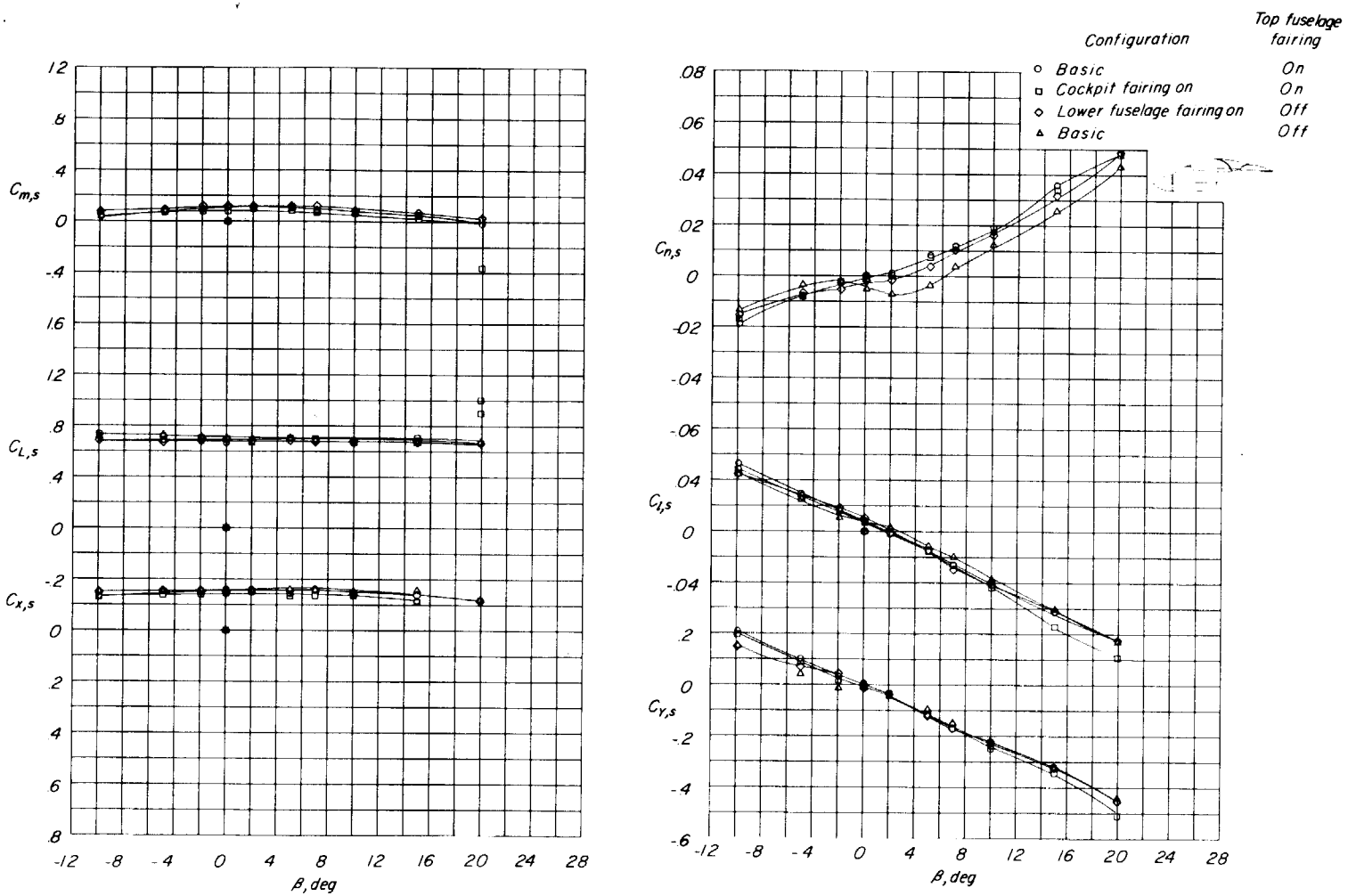

Figure 10.- Effect of fuselage modification. Flaps retracted; propellers off; landing gear off; $\alpha = 0^{\circ}$; $\delta_{f,S}/\delta_{f,R} = 0/0$; $C_{T,s} = 0$; $h/D = \infty$.

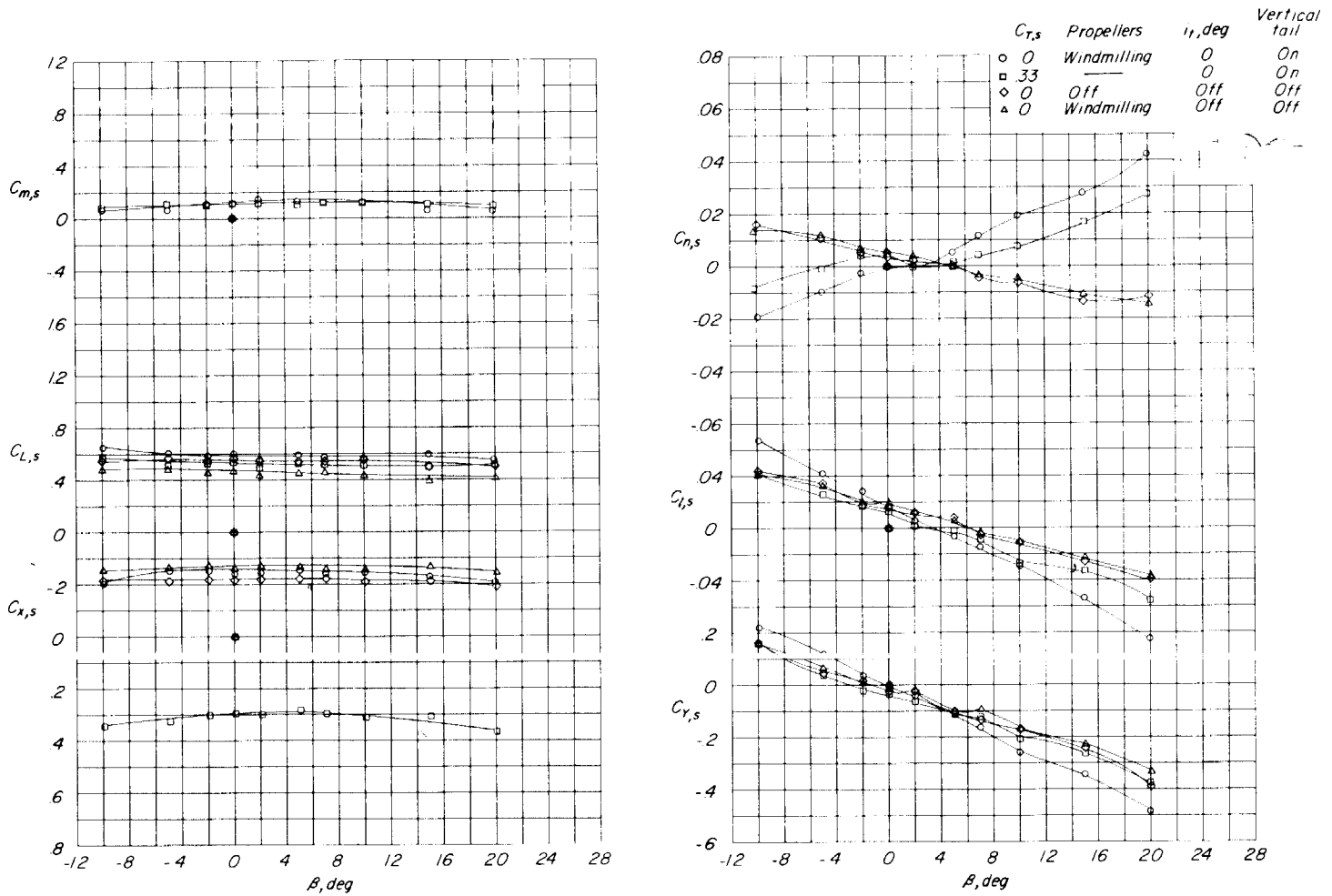

Figure 11.- Effect of thrust coefficient. Flaps retracted; top fuselage fairing on; $\alpha = 0^{\circ}$; $\delta_{f,S}/\delta_{f,R} = 0/0$.

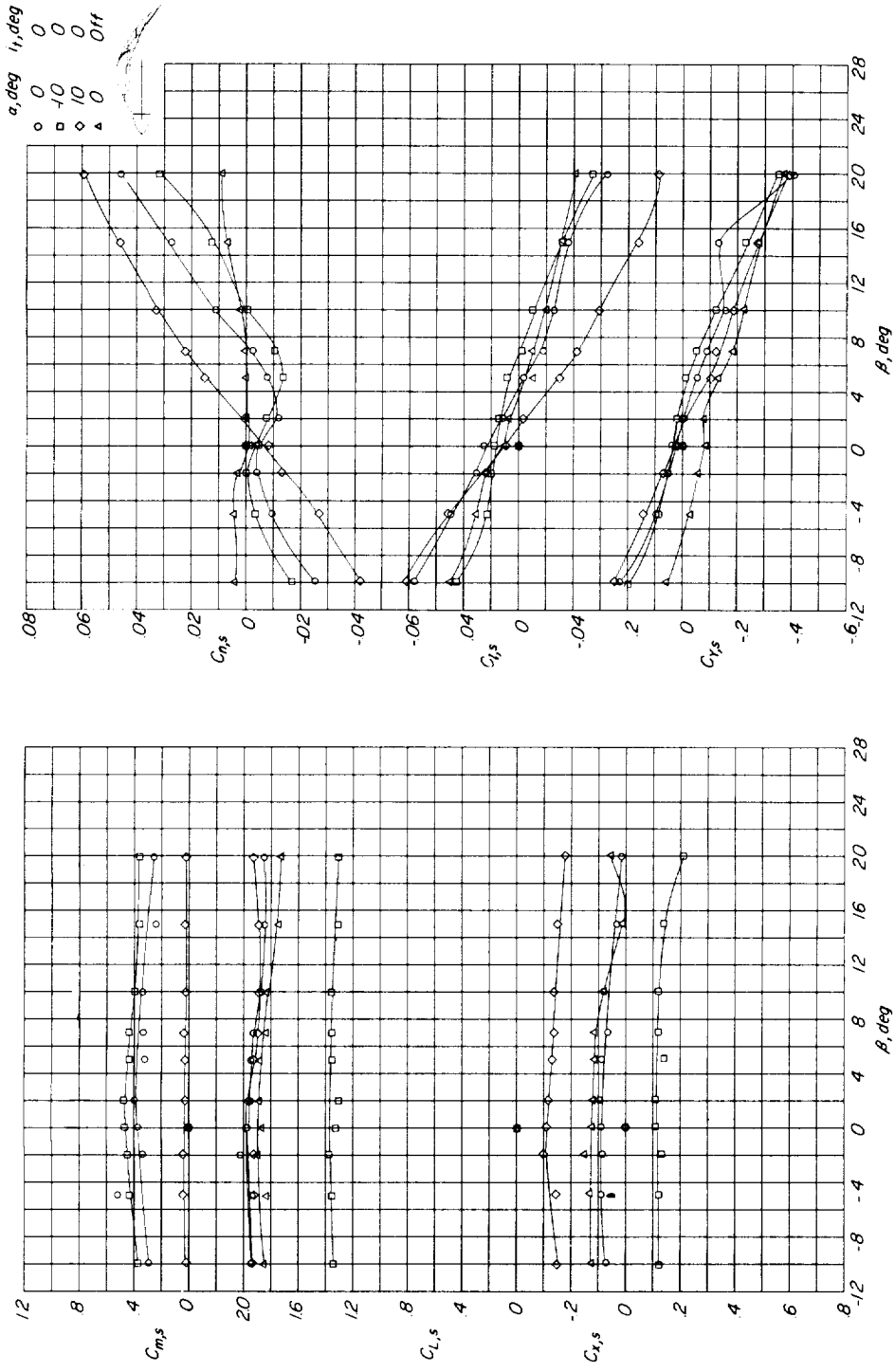

(c) $\delta_{f,s}/\delta_{f,R} = 20/15$; $C_{T,s} = 0.366$.

Figure 12.- Continued.

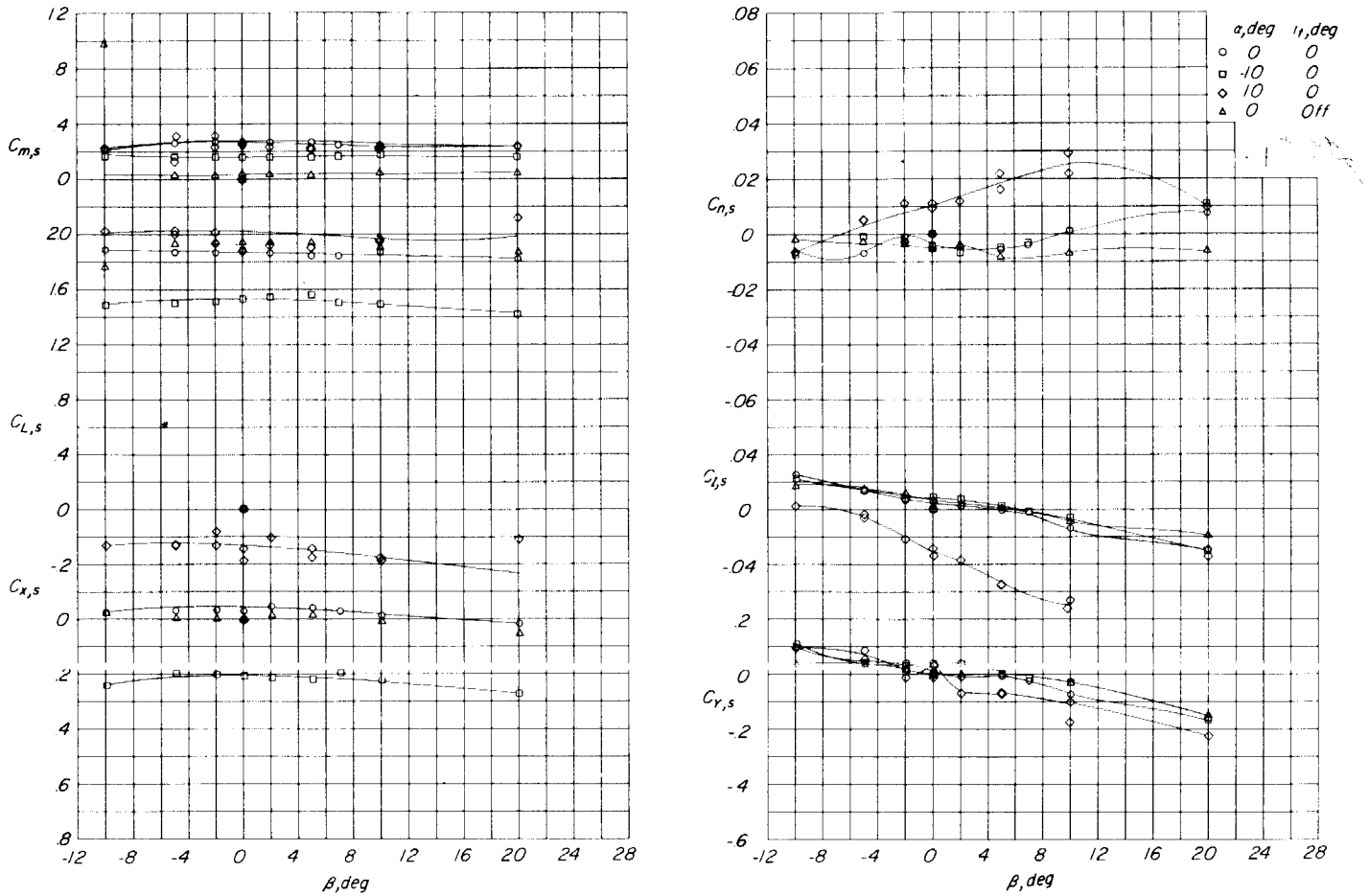

(d) $\delta_{f,S}/\delta_{f,R}$ = 30/20.7; $C_{T,s}$ = 0.744.

Figure 12.- Continued.

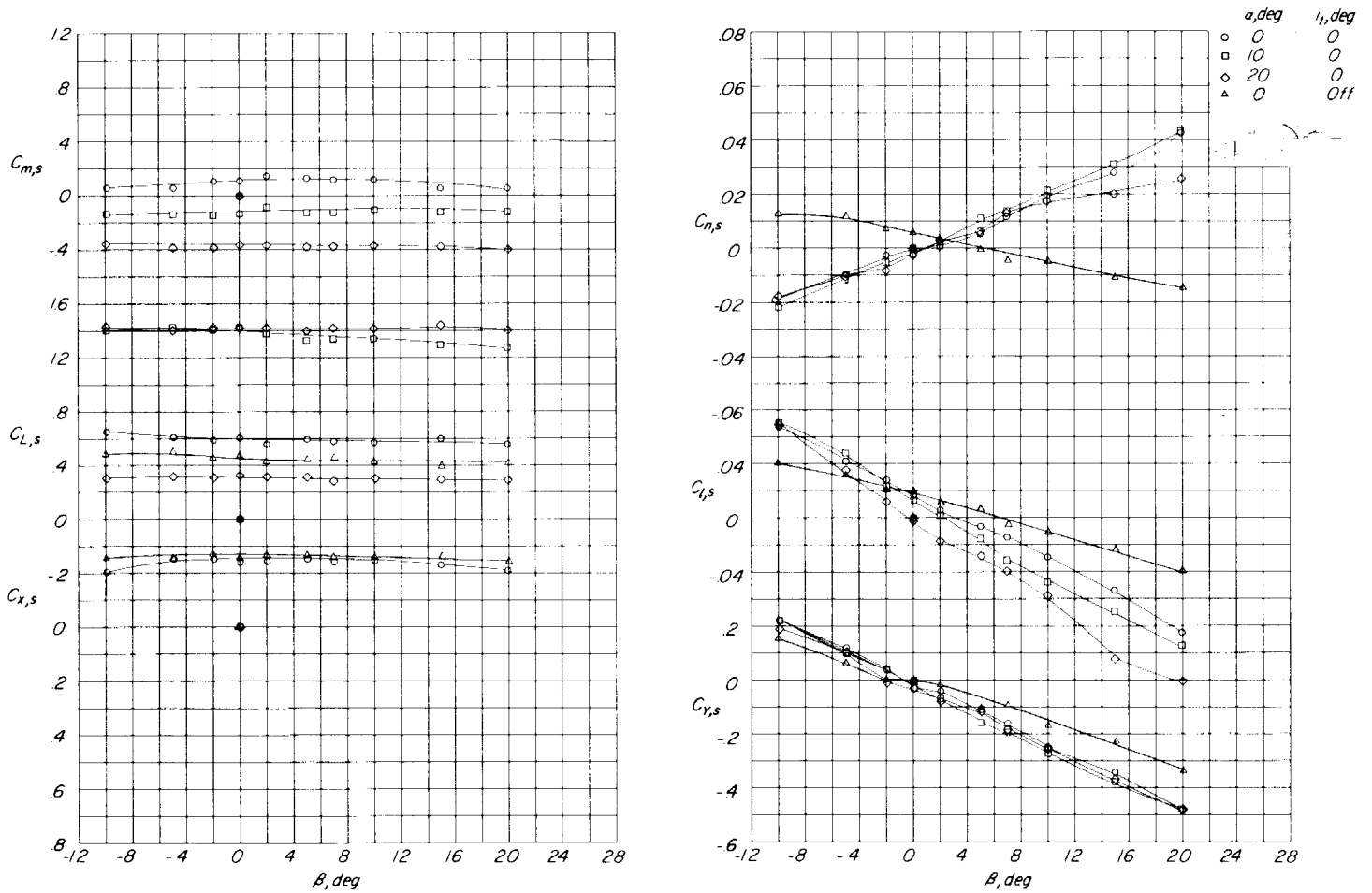

(a) $\delta_{f,S}/\delta_{f,R}$ = 0/0; propellers windmilling.

Figure 12.- Effect of flap deflection and thrust coefficient. Top fuselage fairing on; h/D = ∞.

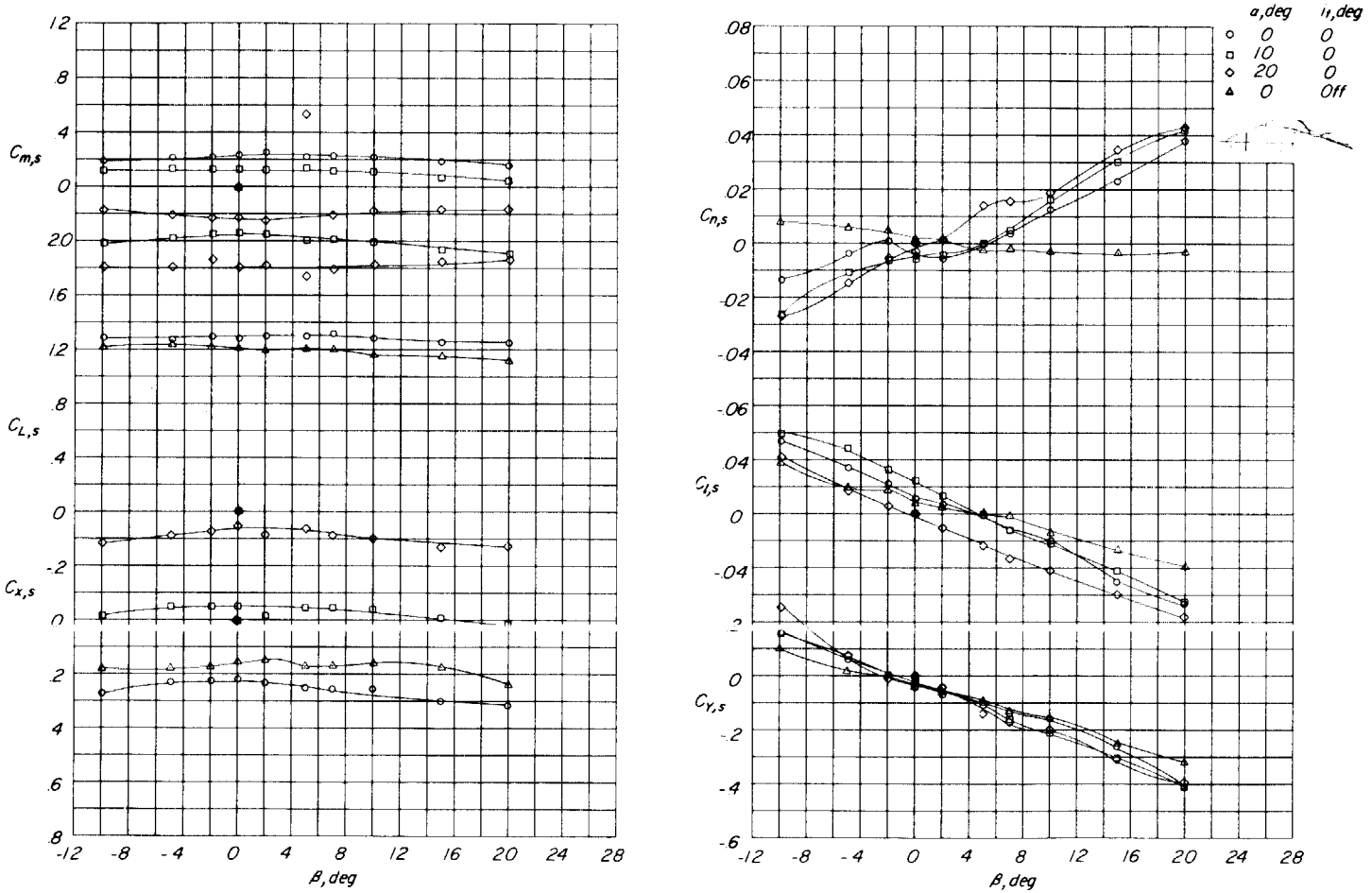

(b) $\delta_{f,S}/\delta_{f,R}$ = 10/8.2; $C_{T,s}$ = 0.366.

Figure 12.- Continued.

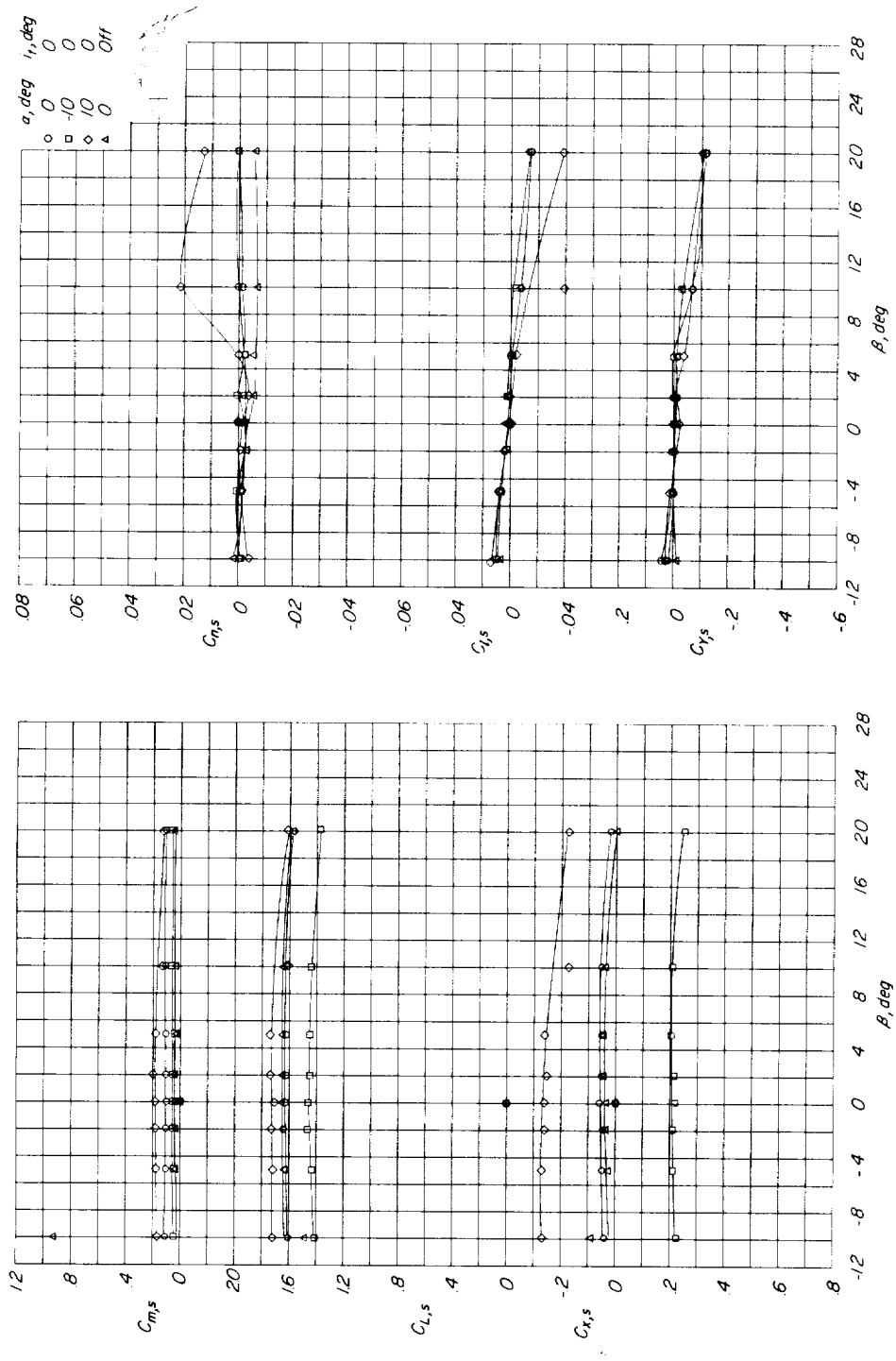

(e) $\delta_{f,S}/\delta_{f,R} = 40/24$; $C_{T,s} = 0.882$.

Figure 12.- Continued.

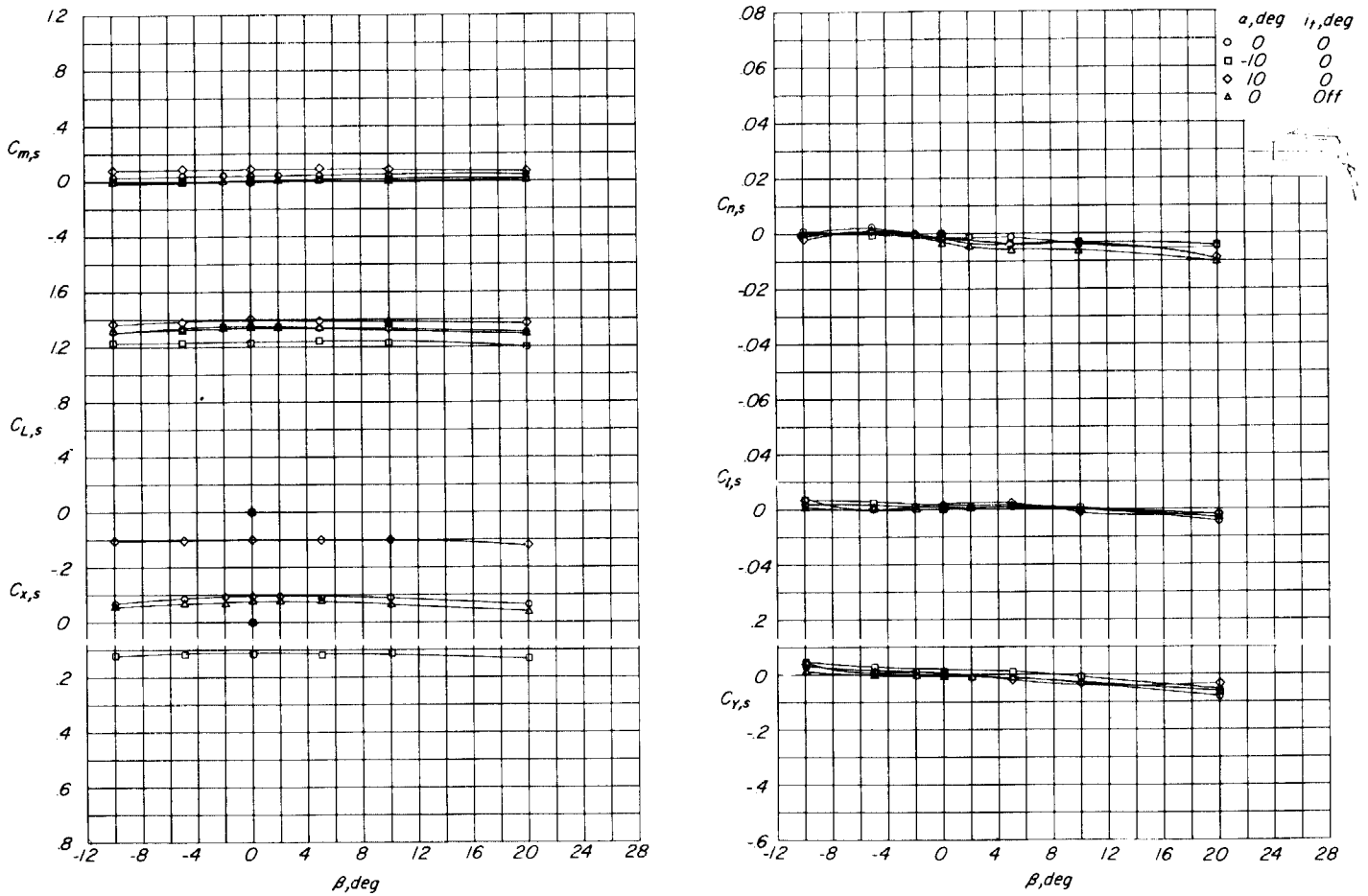

(f) $\delta_{f,S}/\delta_{f,R}$ = 50/25; $C_{T,s}$ = 0.944.

Figure 12.- Continued.

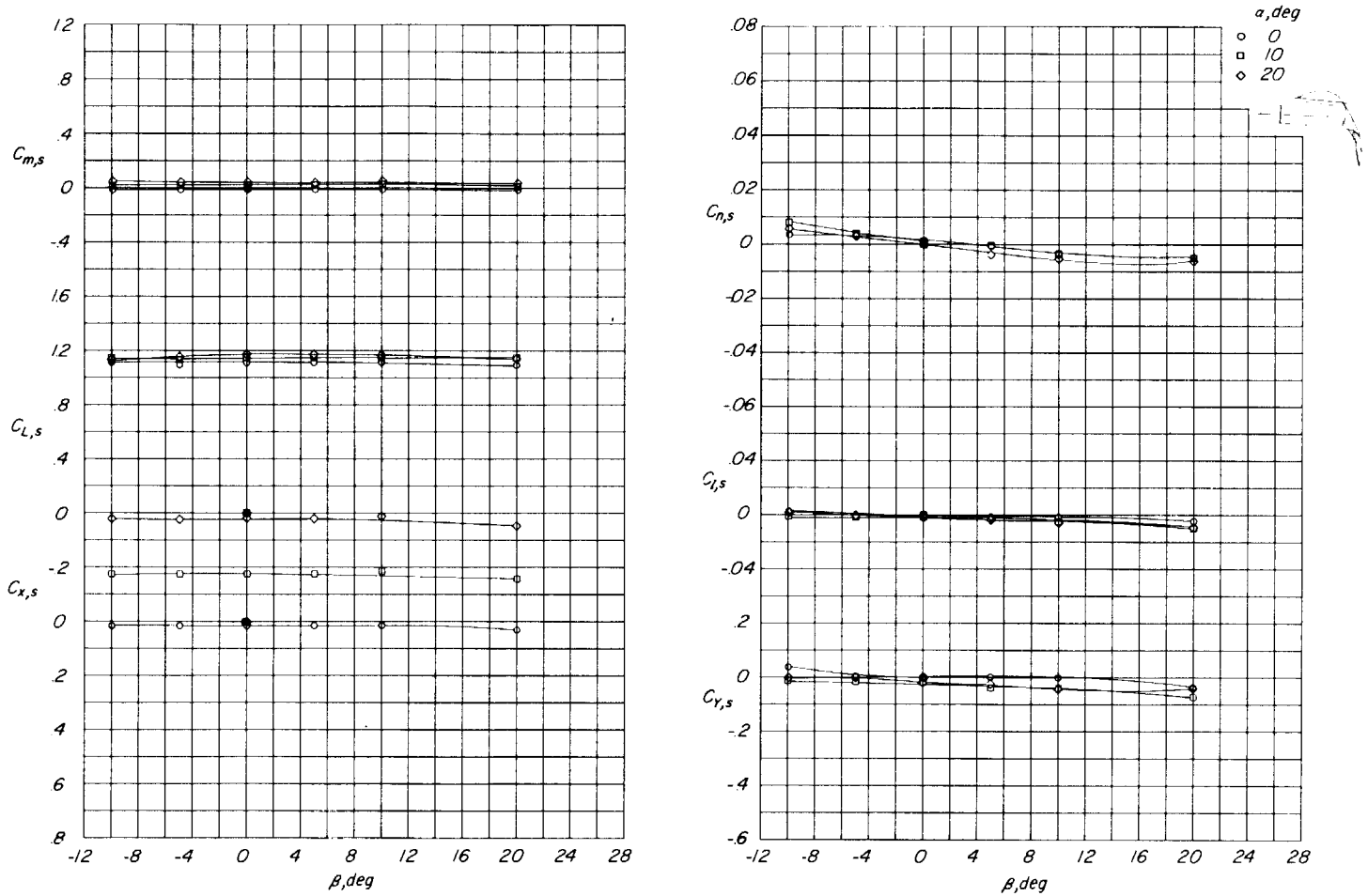

(g) $\delta_{f,S}/\delta_{f,R} = 50/25$; $C_{T,s} = 0.978$.

Figure 12.- Concluded.

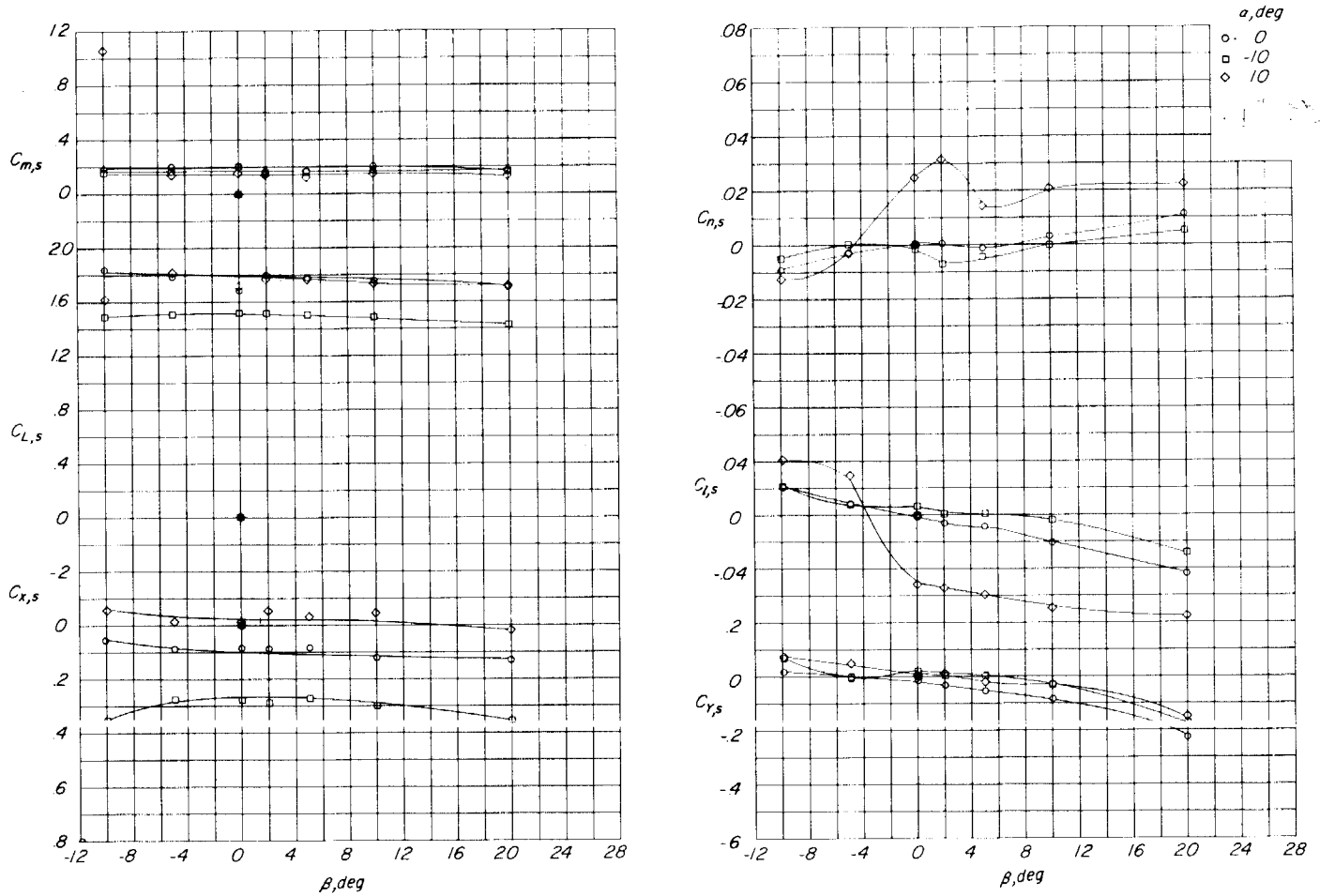

(a) h/D = 0.33; $\delta_{f,S}/\delta_{f,R}$ = 30/20.7; $C_{T,s}$ = 0.745.

Figure 13.- Effect of flap deflection and thrust coefficient in the region of ground effect. Top fuselage fairing on; $i_t = 0^o$.

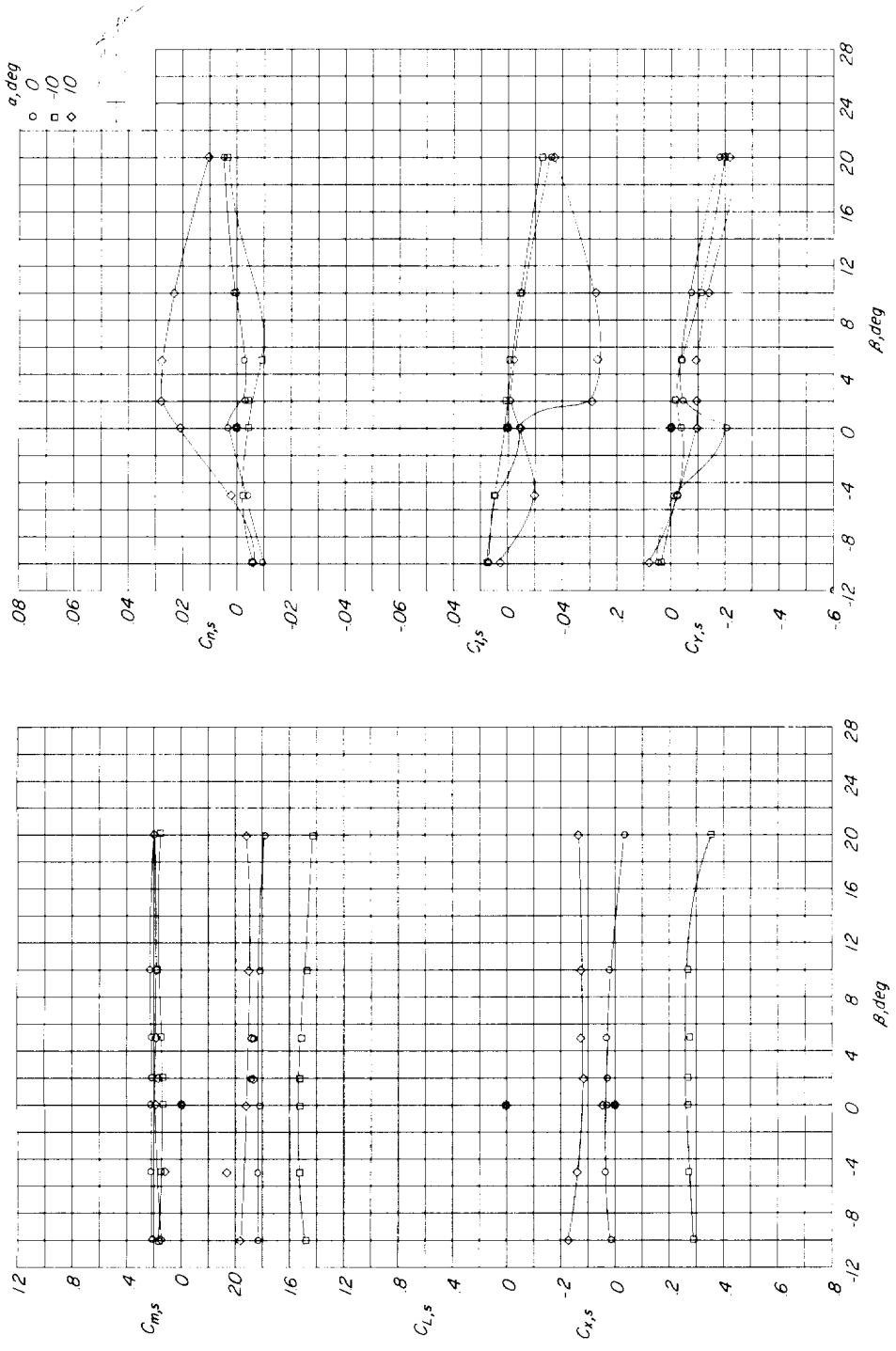

(b) h/D = 1.0; $\delta_{f,S}/\delta_{f,R}$ = 30/20.7; $C_{T,s}$ = 0.745.

Figure 13.- Continued.

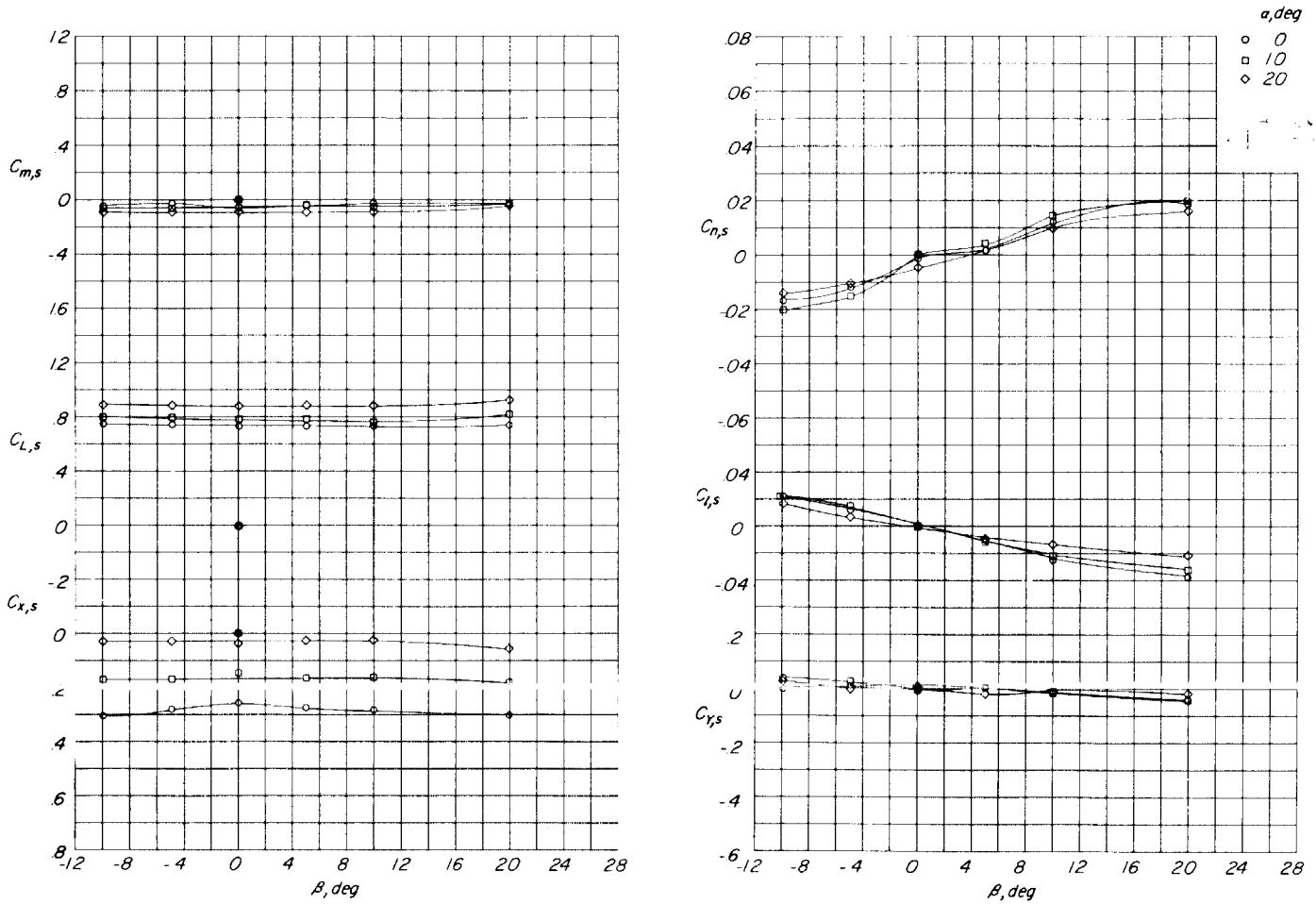

(c) h/D = 0.33; $\delta_{f,S}/\delta_{f,R}$ = 50/25; $C_{T,s}$ = 0.943.

Figure 13.- Continued.

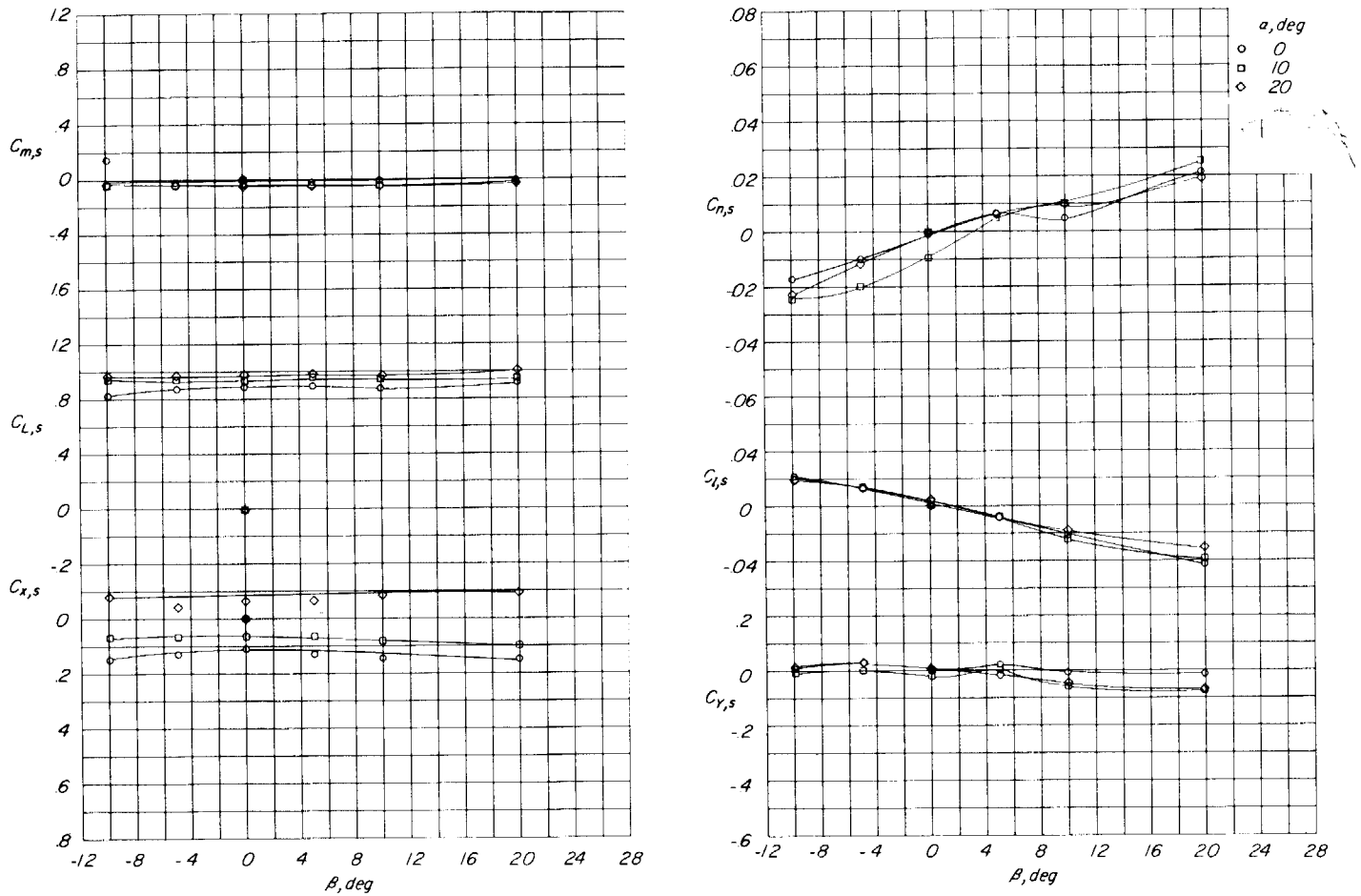

(d) $h/D = 1.0$; $\delta_{f,S}/\delta_{f,R} = 50/25$; $C_{T,s} = 0.943$.

Figure 13.- Continued.

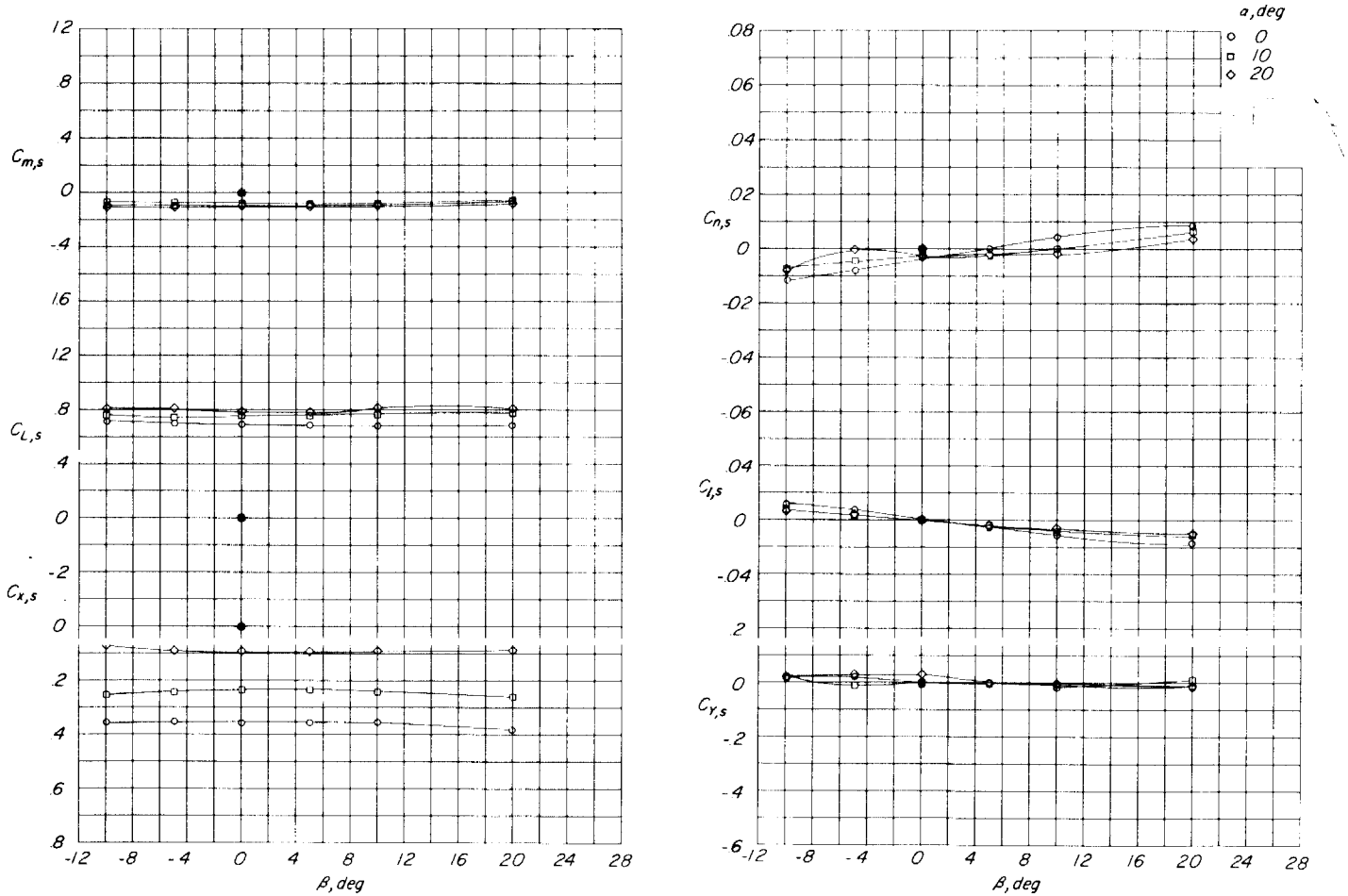

(e) $h/D = 0.33$; $\delta_{f,S}/\delta_{f,R} = 50/25$; $C_{T,s} = 0.978$.

Figure 13.- Continued.

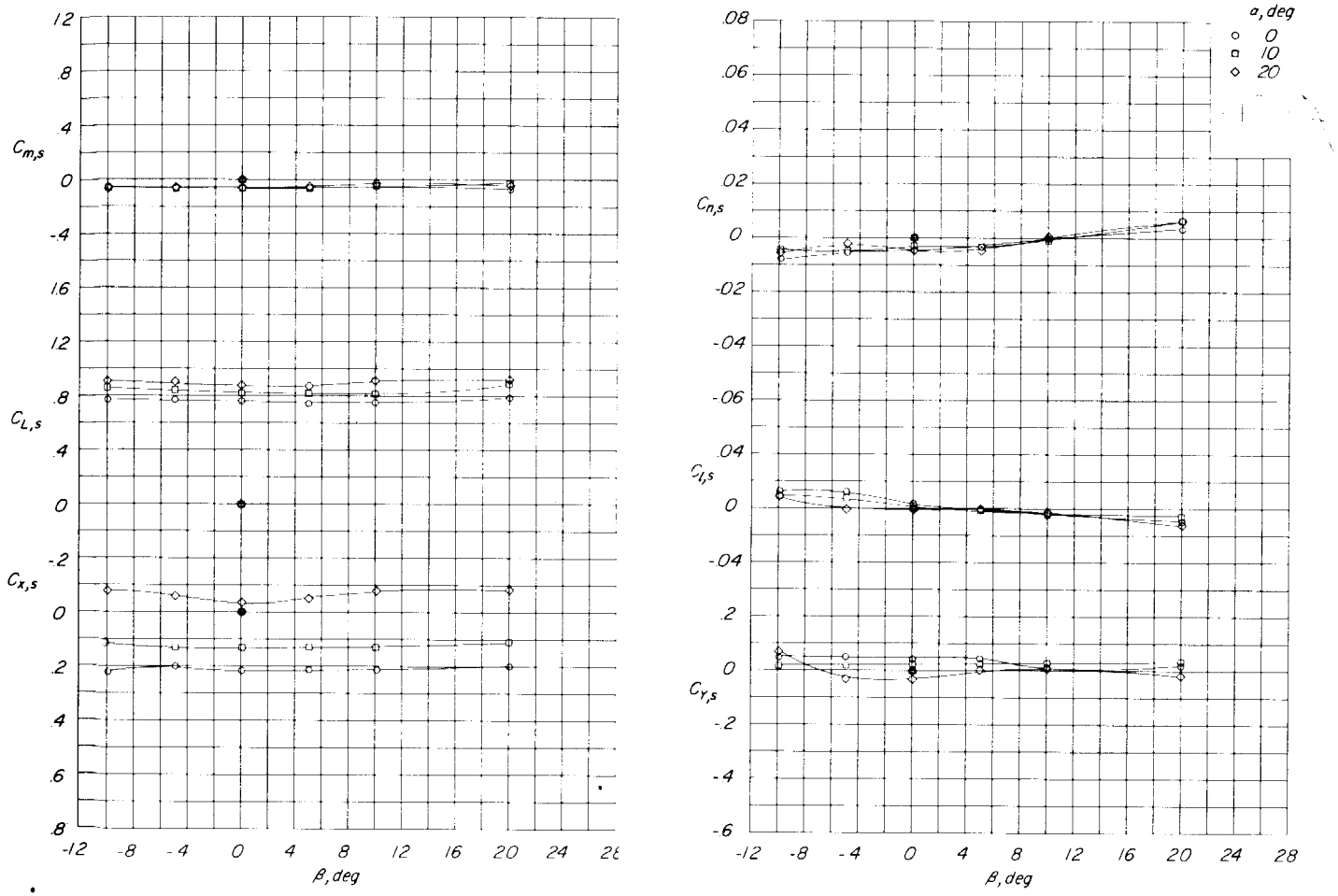

(f) h/D = 1.0; $\delta_{f,S}/\delta_{f,R}$ = 50/25; $C_{T,s}$ = 0.978.

Figure 13.- Concluded.

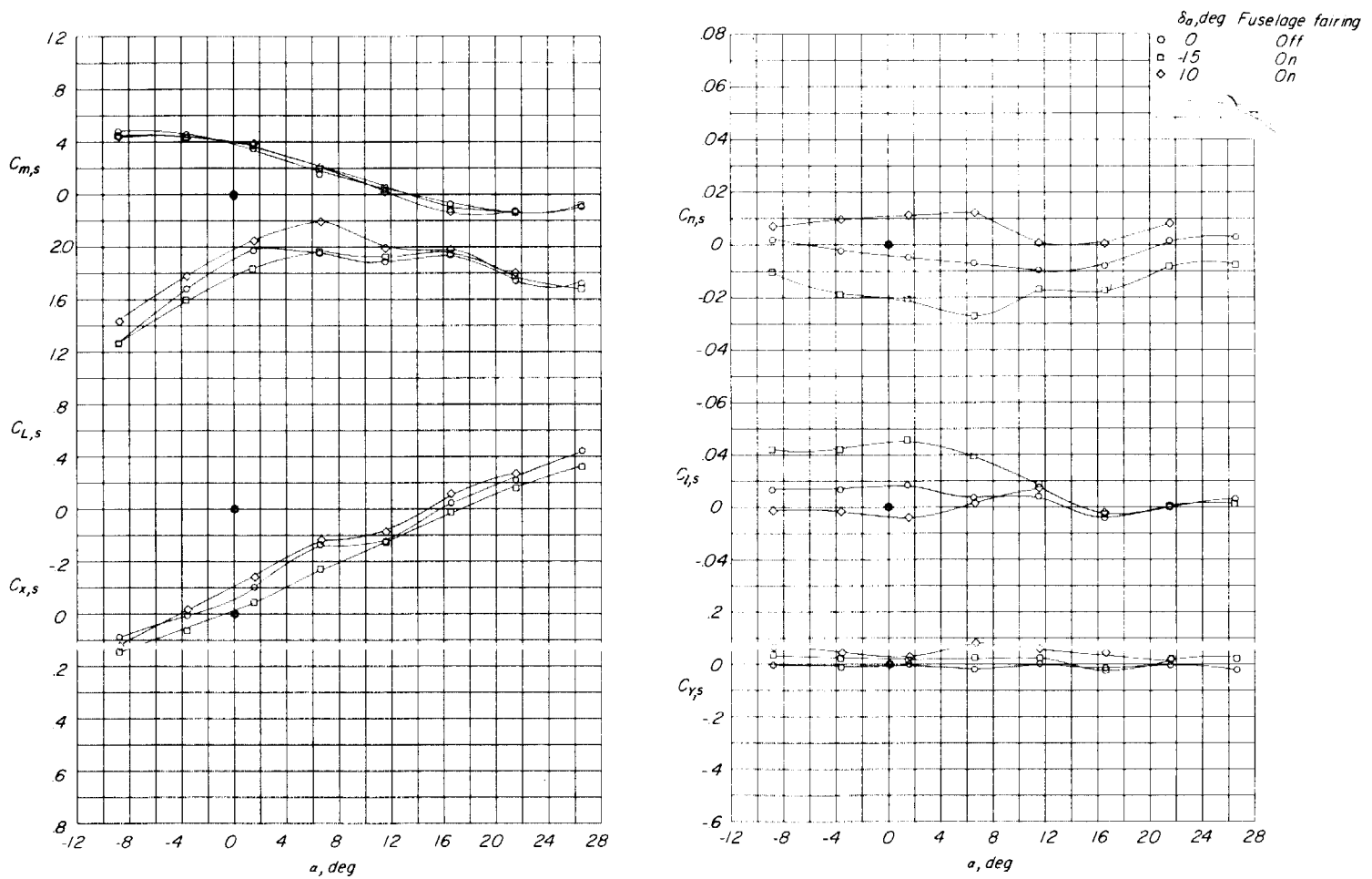

(c) $\delta_{f,S}/\delta_{f,R}$ = 20/15; $C_{T,s}$ = 0.366.

Figure 14.- Continued.

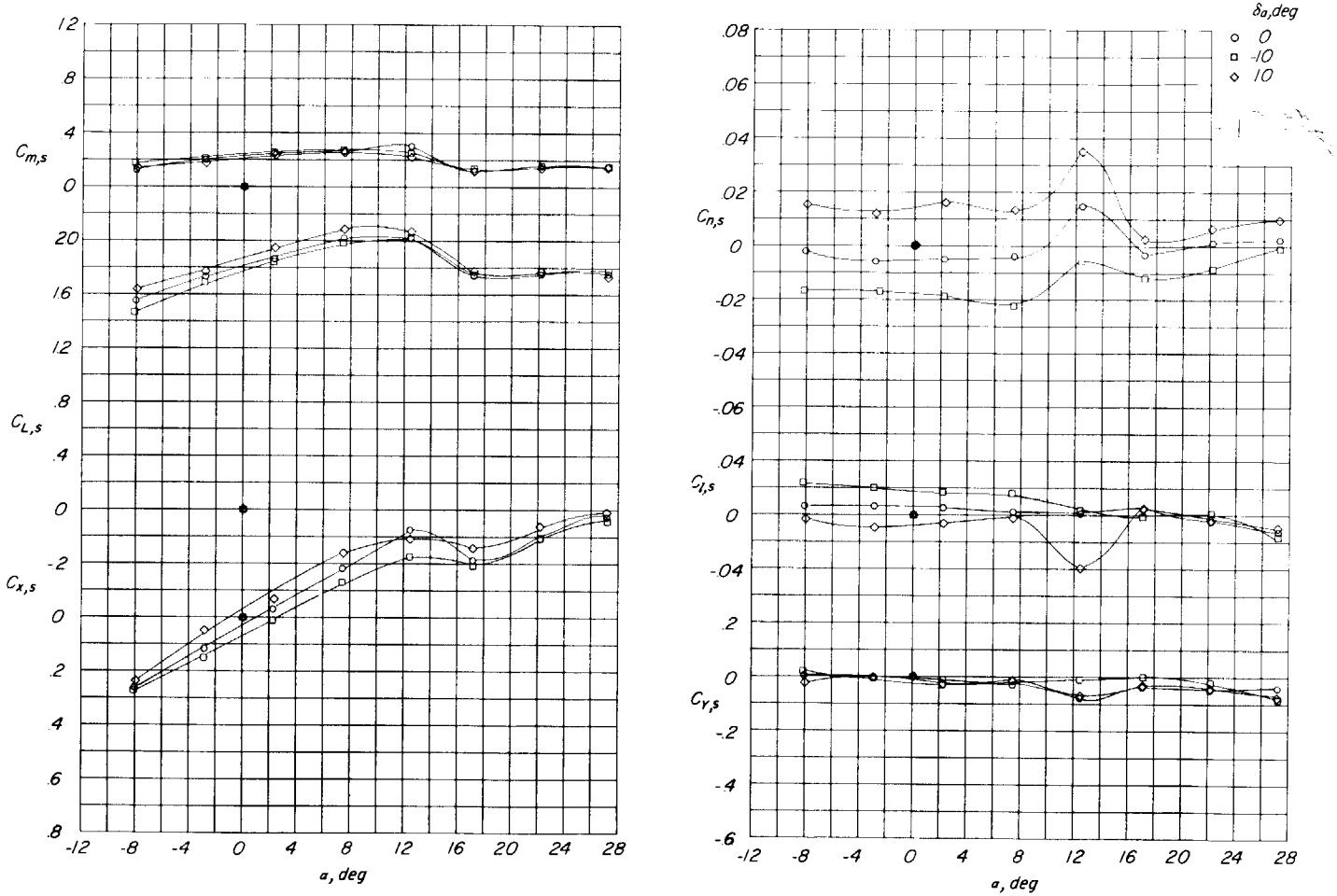

(d) $\delta_{f,S}/\delta_{f,R}$ = 30/20.7; $C_{T,s}$ = 0.744.

Figure 14.- Continued.

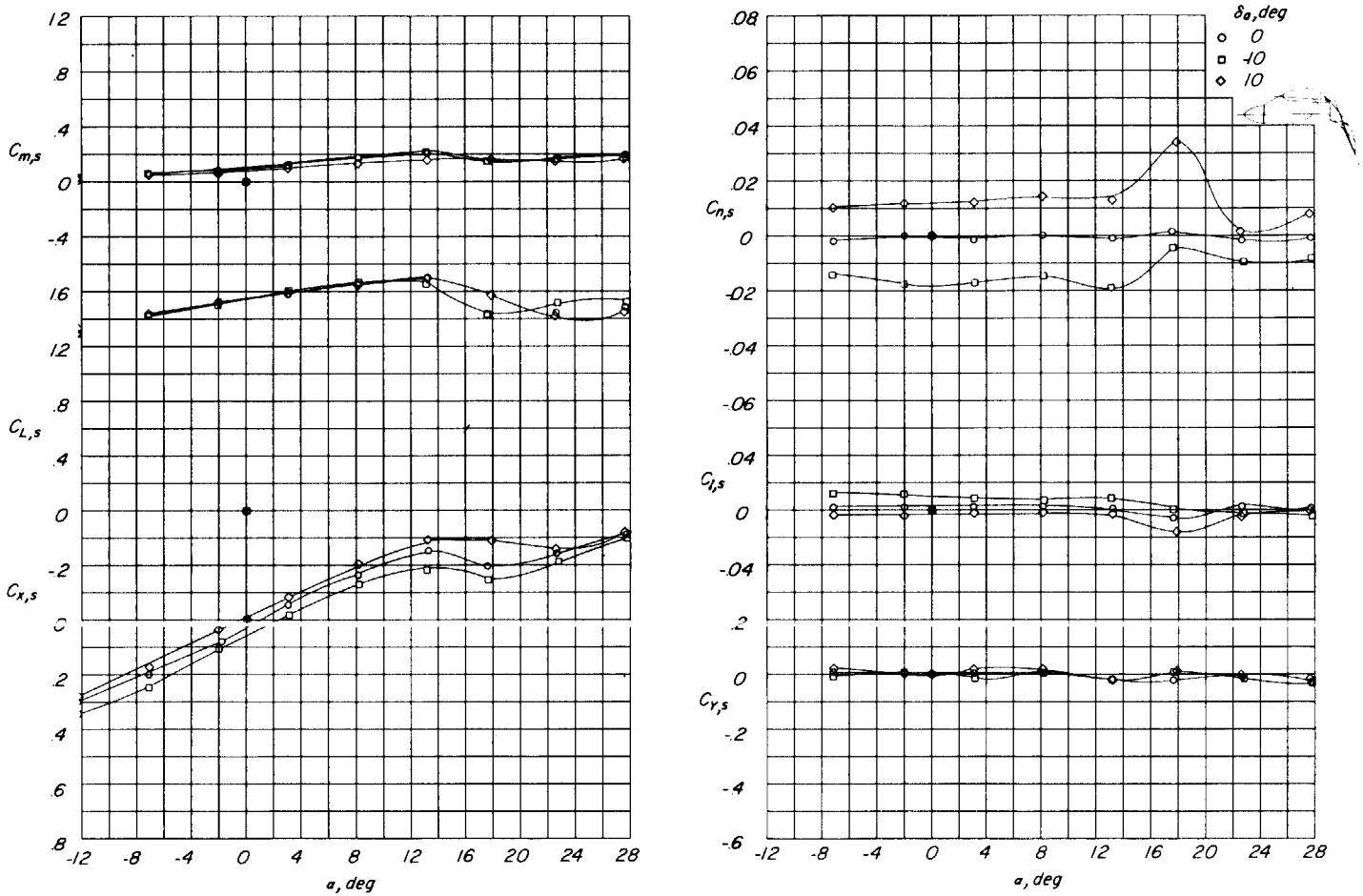

(e) $\delta_{f,S}/\delta_{f,R}$ = 40/24; $C_{T,s}$ = 0.882.

Figure 14.- Continued.

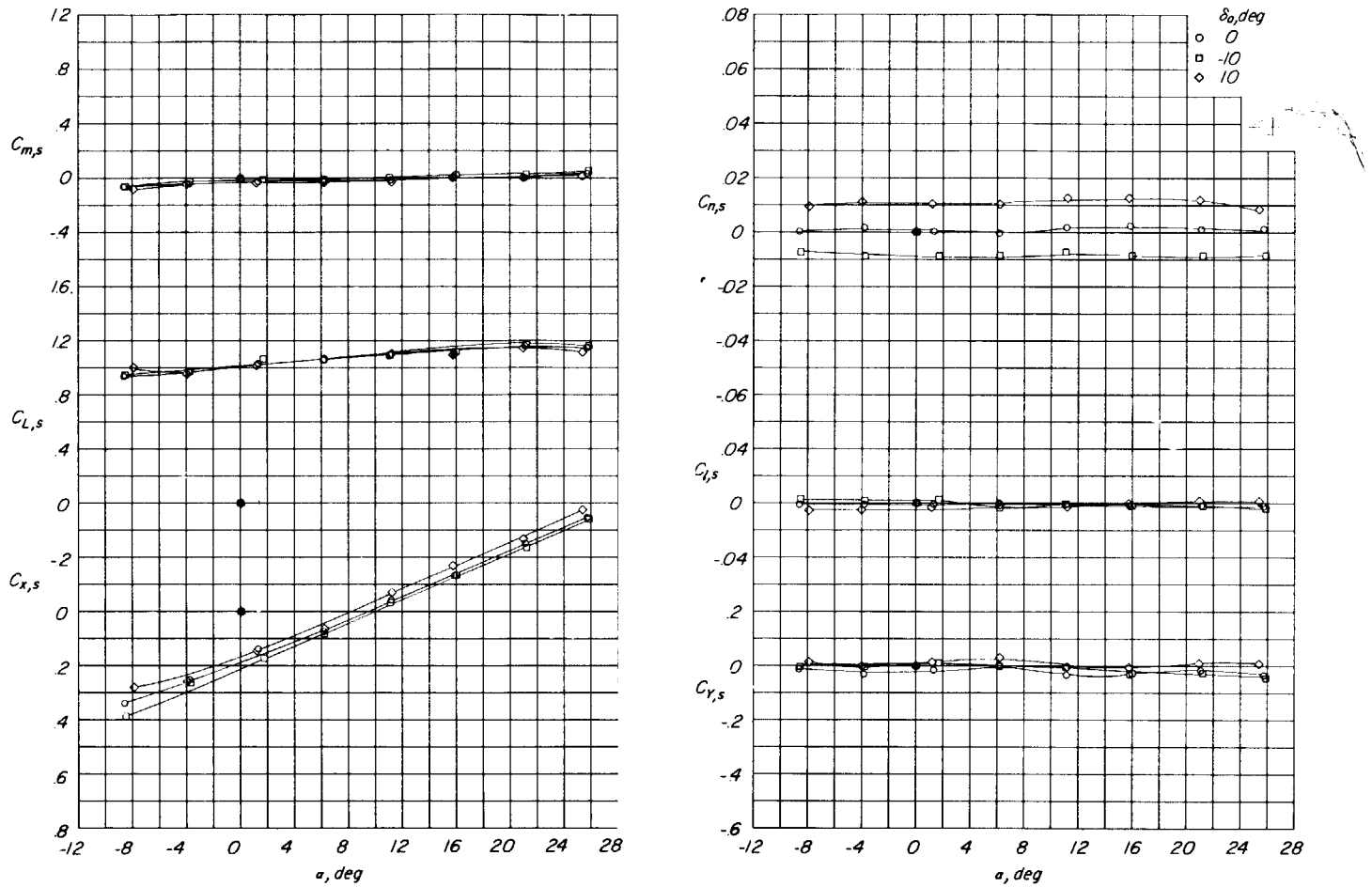

(f) $\delta_{f,S}/\delta_{f,R}$ = 50/25; $C_{T,s}$ = 0.978.

Figure 14.- Concluded.

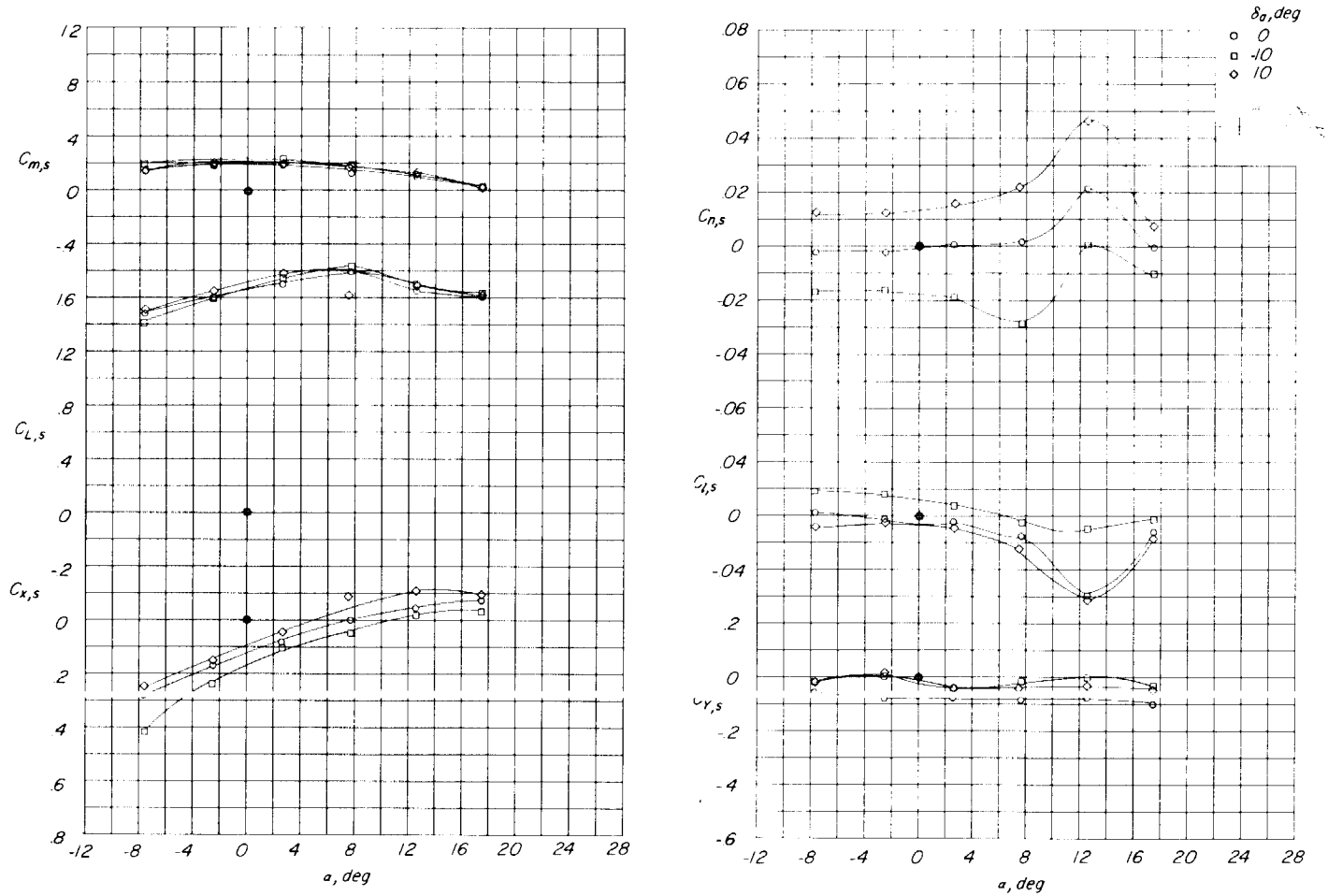

(a) $h/D = 0.33$; $\delta_{f,S}/\delta_{f,R} = 30/20.7$; $C_{T,s} = 0.745$.

Figure 15.- Effect of aileron deflection in the region of ground effect. Top fuselage fairing on; $i_t = 0^o$.

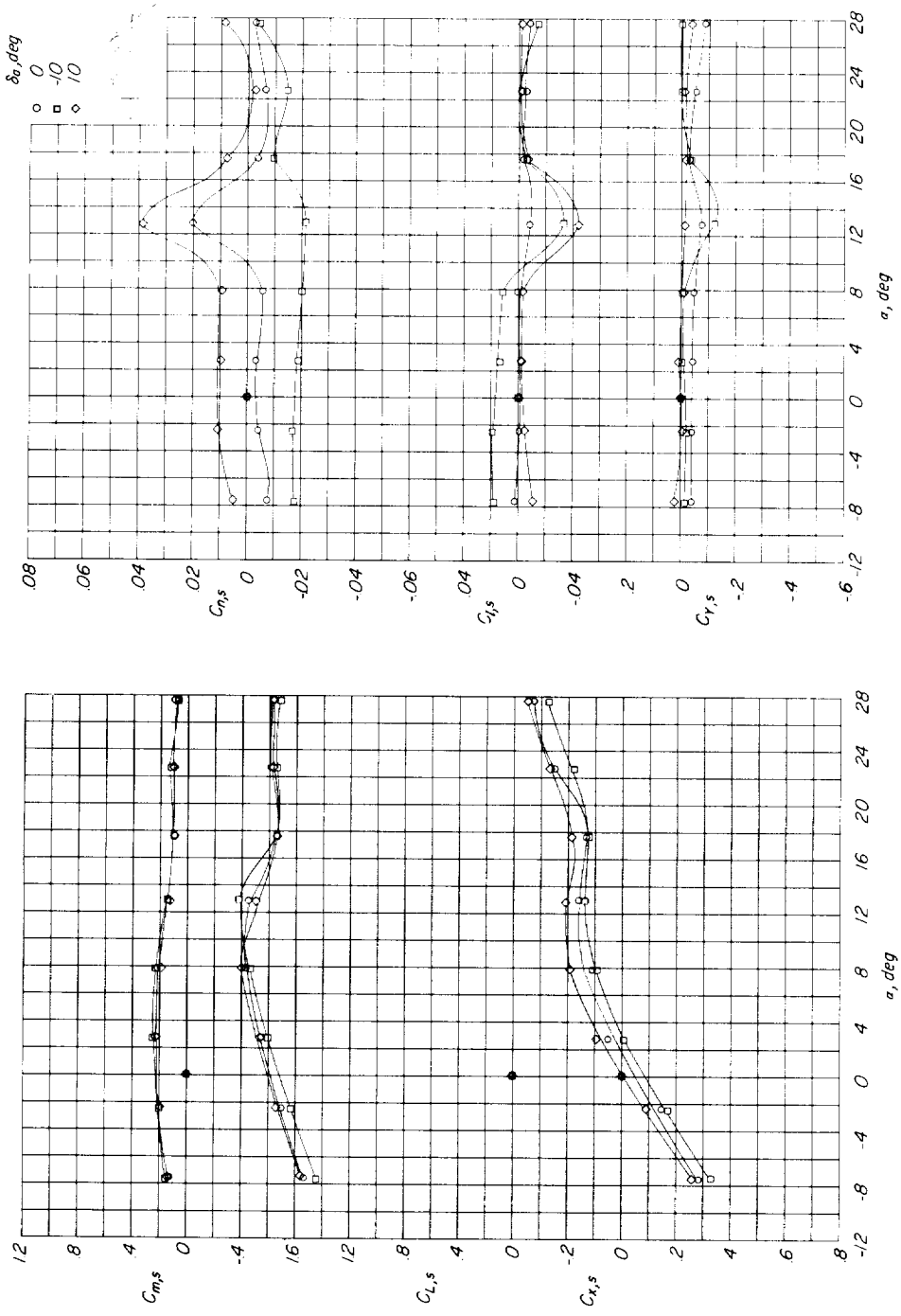

(b) $\delta_{f,s}/\delta_{f,R}$ = 30/20.7; $C_{T,s}$ = 0.744; h/D = 1.0.

Figure 15.- Continued.

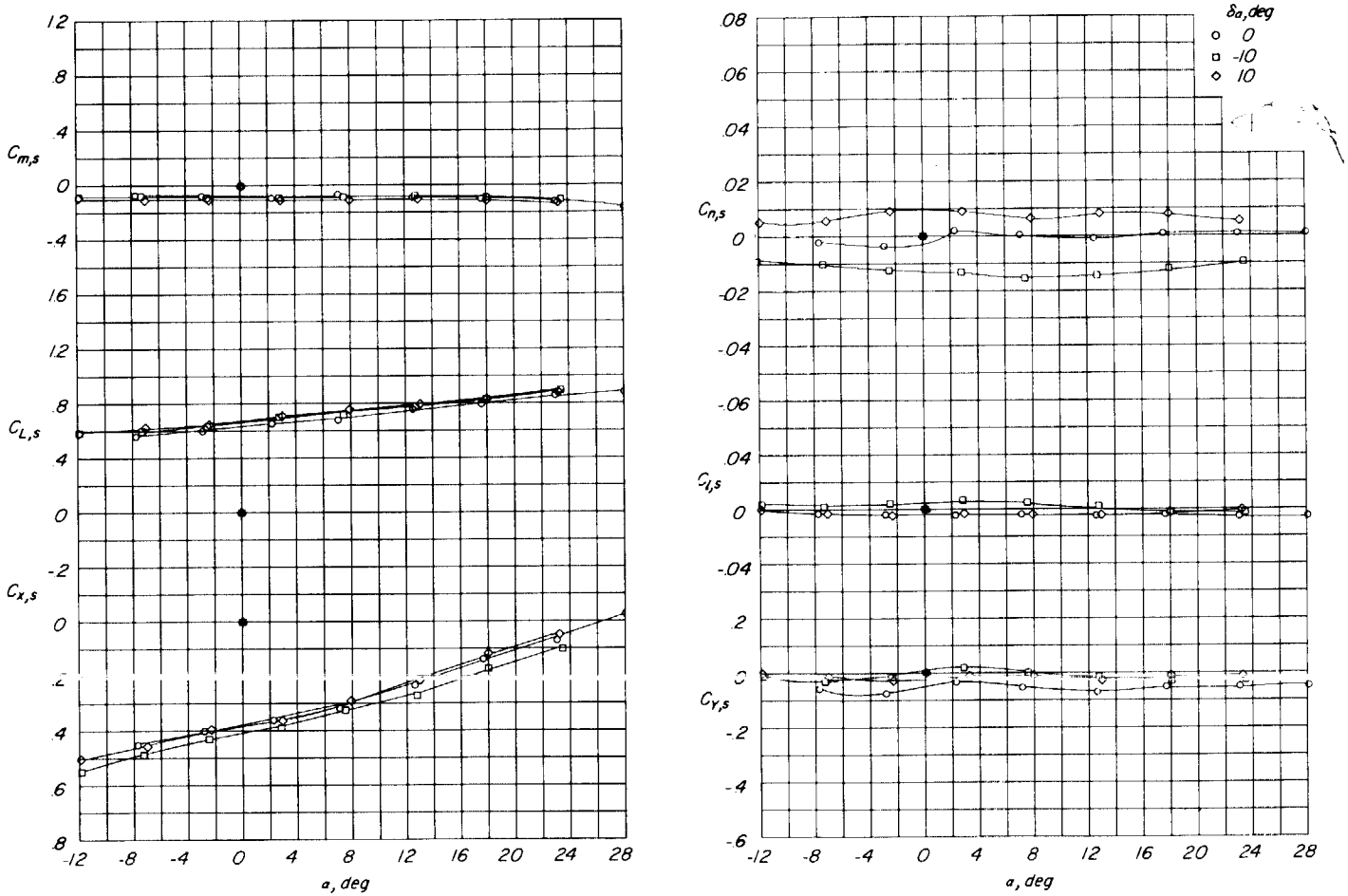

(c) $\delta_{f,S}/\delta_{f,R}$ = 50/25; $C_{T,s}$ = 0.978; h/D = 0.33.

Figure 15.- Continued.

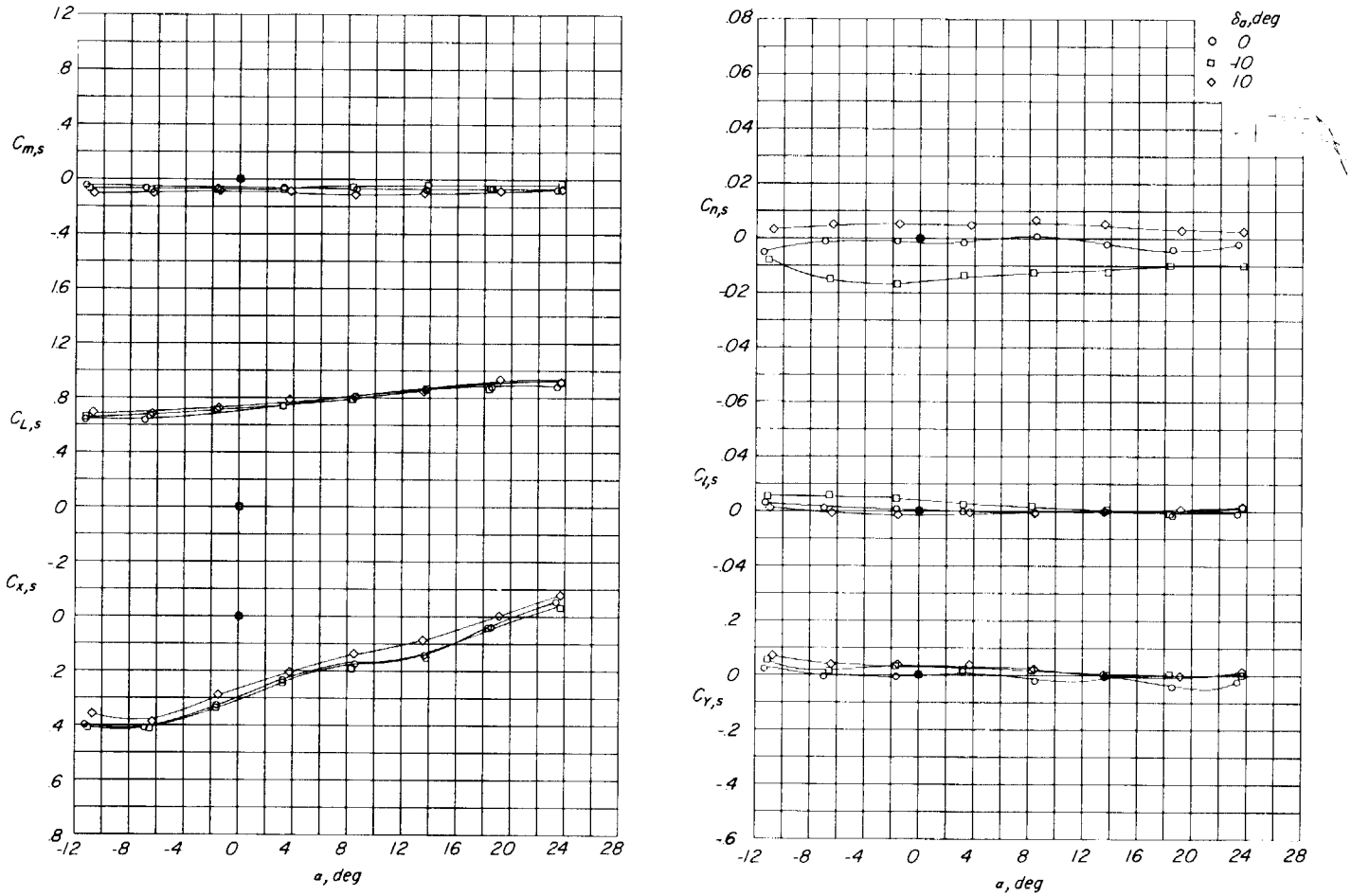

(d) $\delta_{f,S}/\delta_{f,R}$ = 50/25; $C_{T,s}$ = 0.978; h/D = 1.0.

Figure 15.- Concluded.

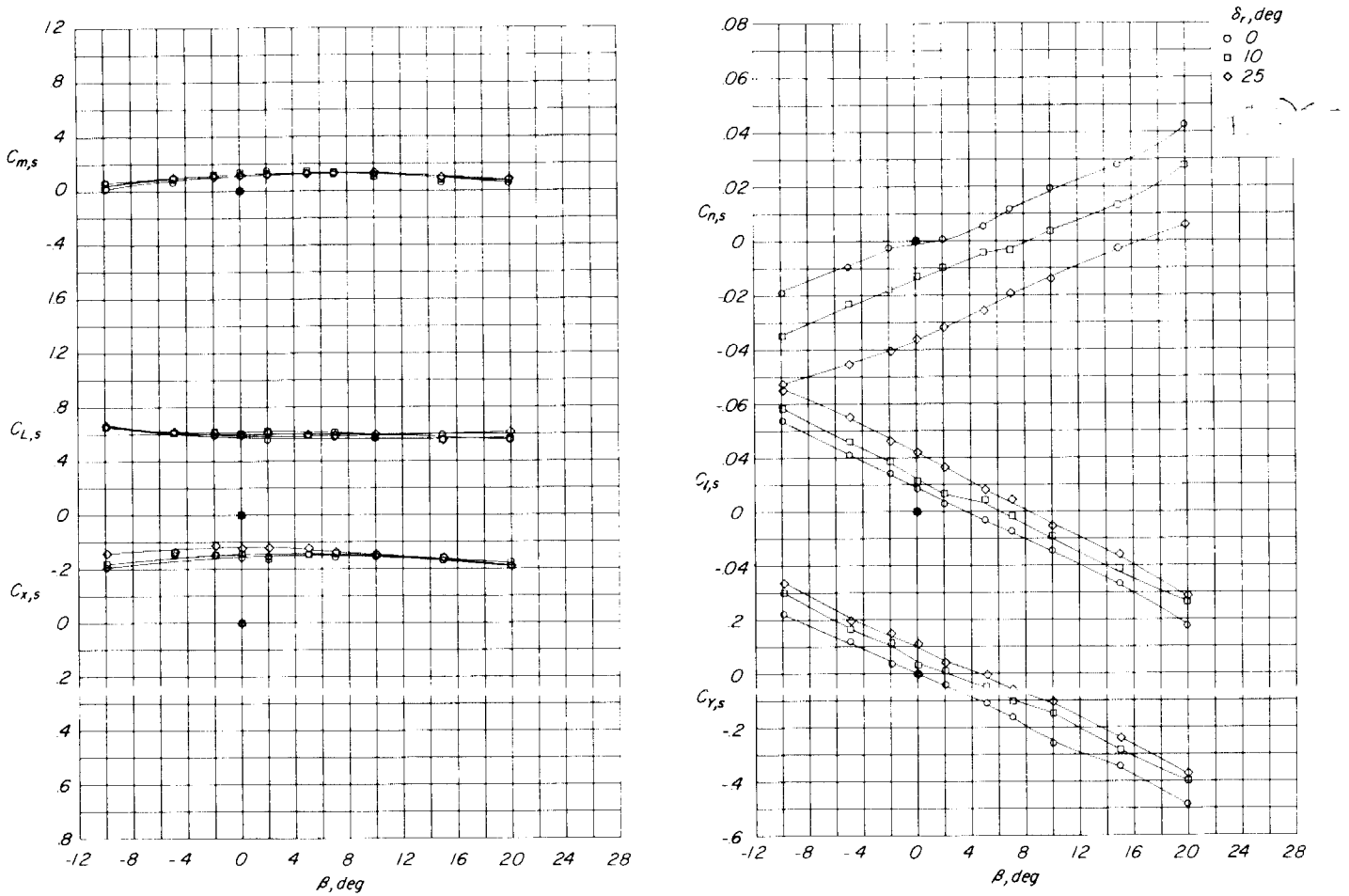

(a) $\delta_{f,S}/\delta_{f,R}$ = 0/0; propellers windmilling.

Figure 16.- Effect of rudder deflection. Top fuselage fairing on; $i_t = 0^\circ$; $\alpha = 0^\circ$; $h/D = \infty$.

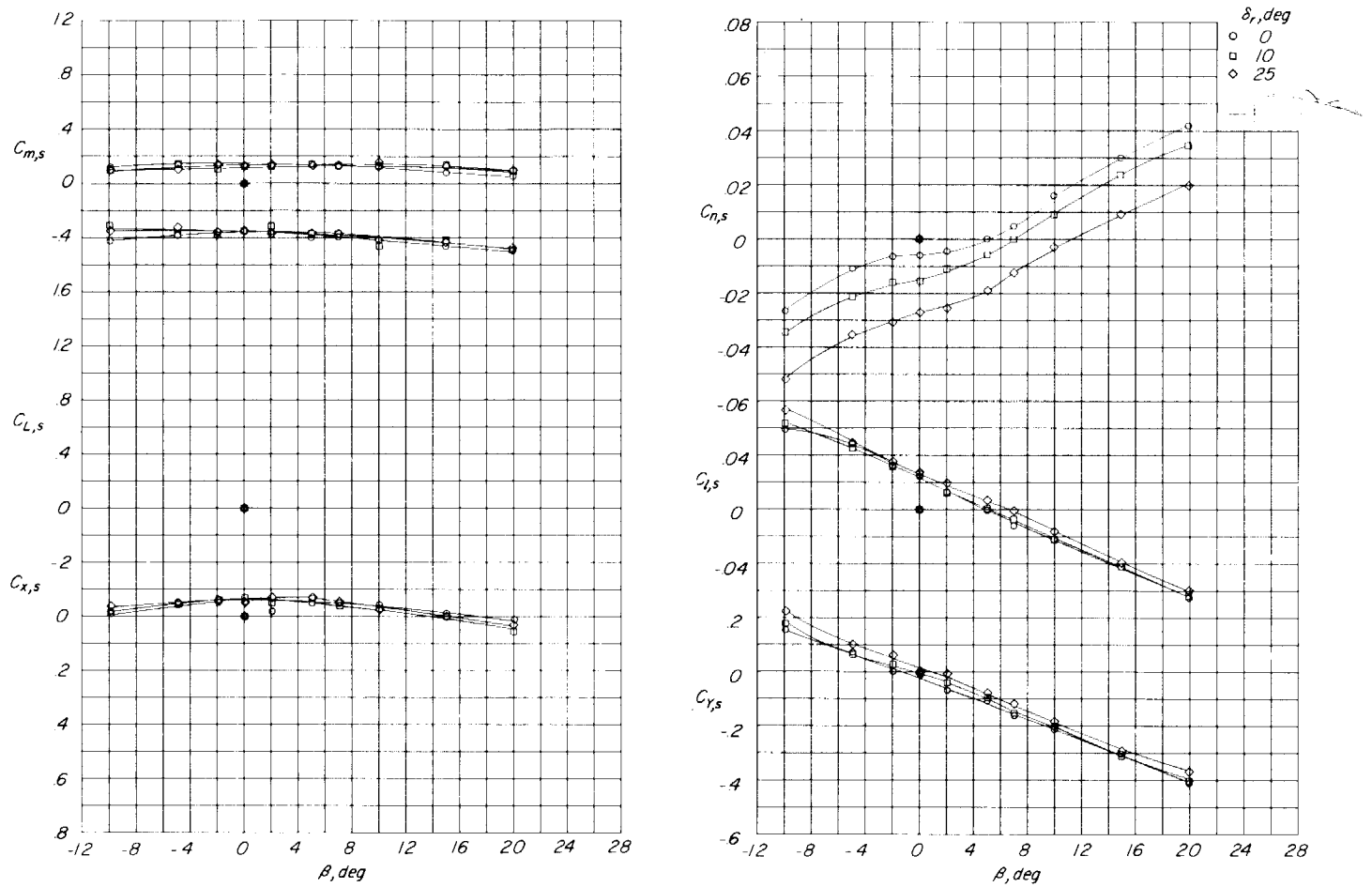

(b) $\delta_{f,S}/\delta_{f,R}$ = 10/8.2; $C_{T,s}$ = 0.366.

Figure 16.- Continued.

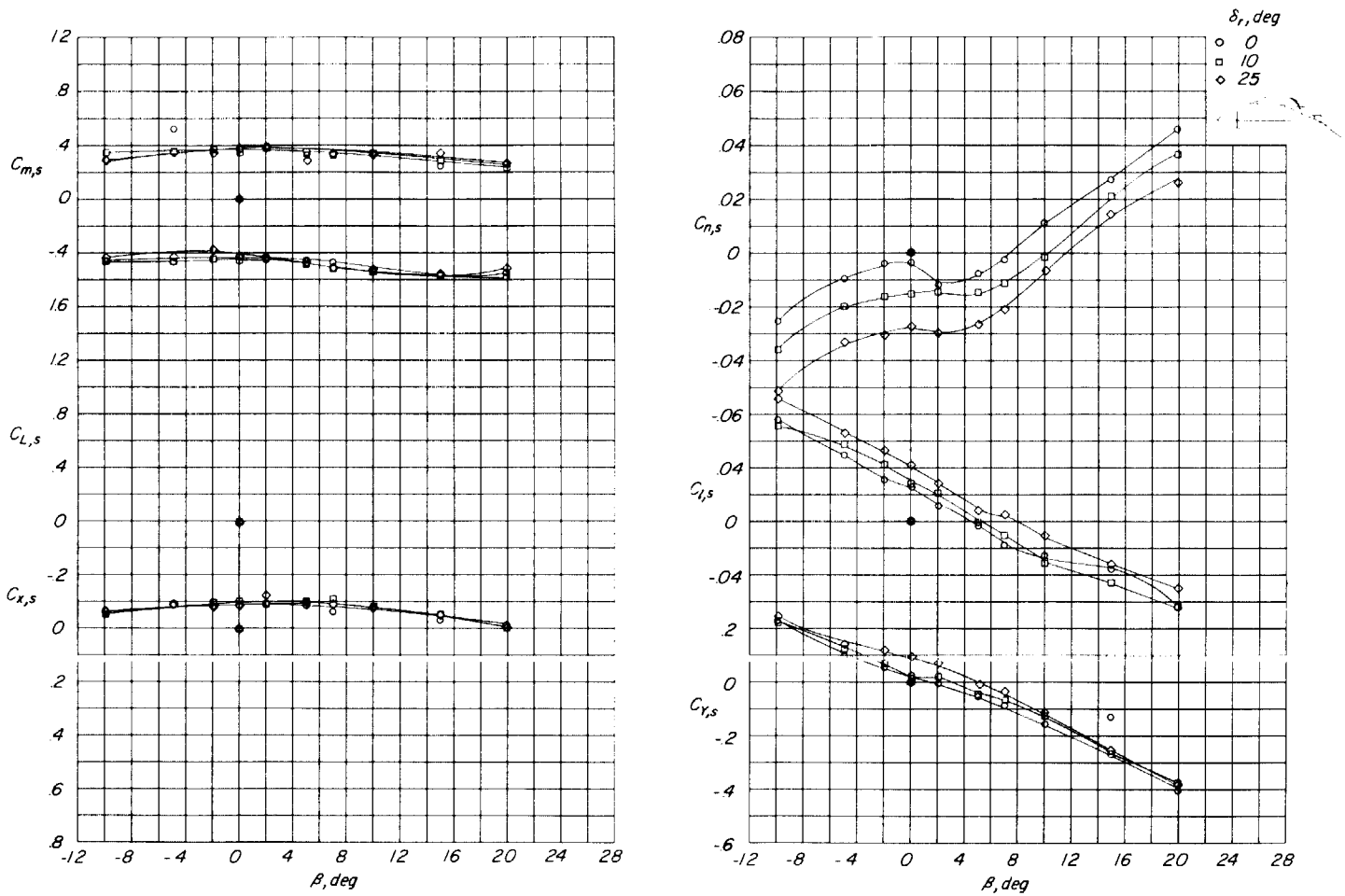

(c) $\delta_{f,S}/\delta_{f,R}$ = 20/15; $C_{T,s}$ = 0.366.

Figure 16.- Continued.

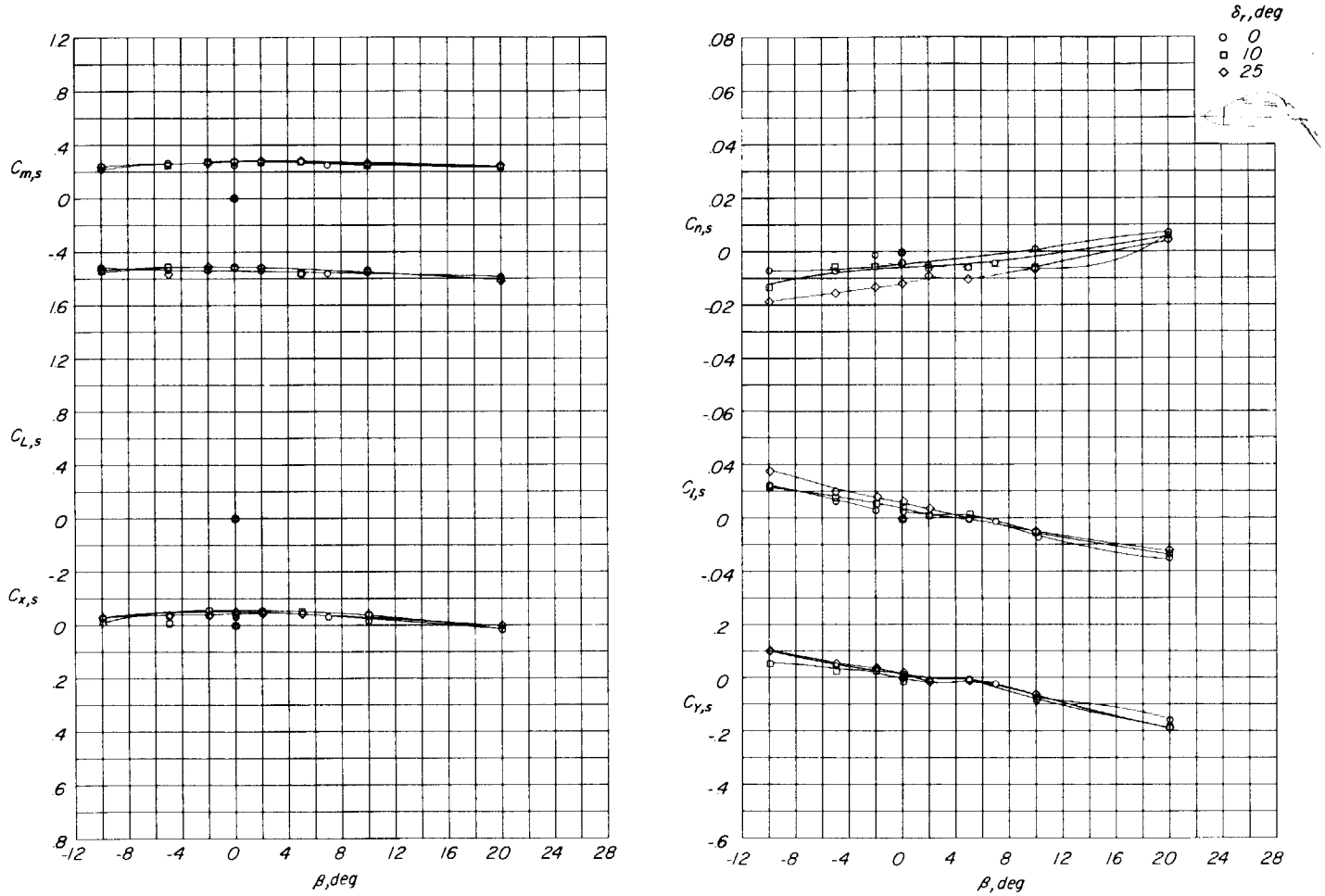

(d) $\delta_{f,S}/\delta_{f,R}$ = 30/20.7; $C_{T,s}$ = 0.744.

Figure 16.- Concluded.

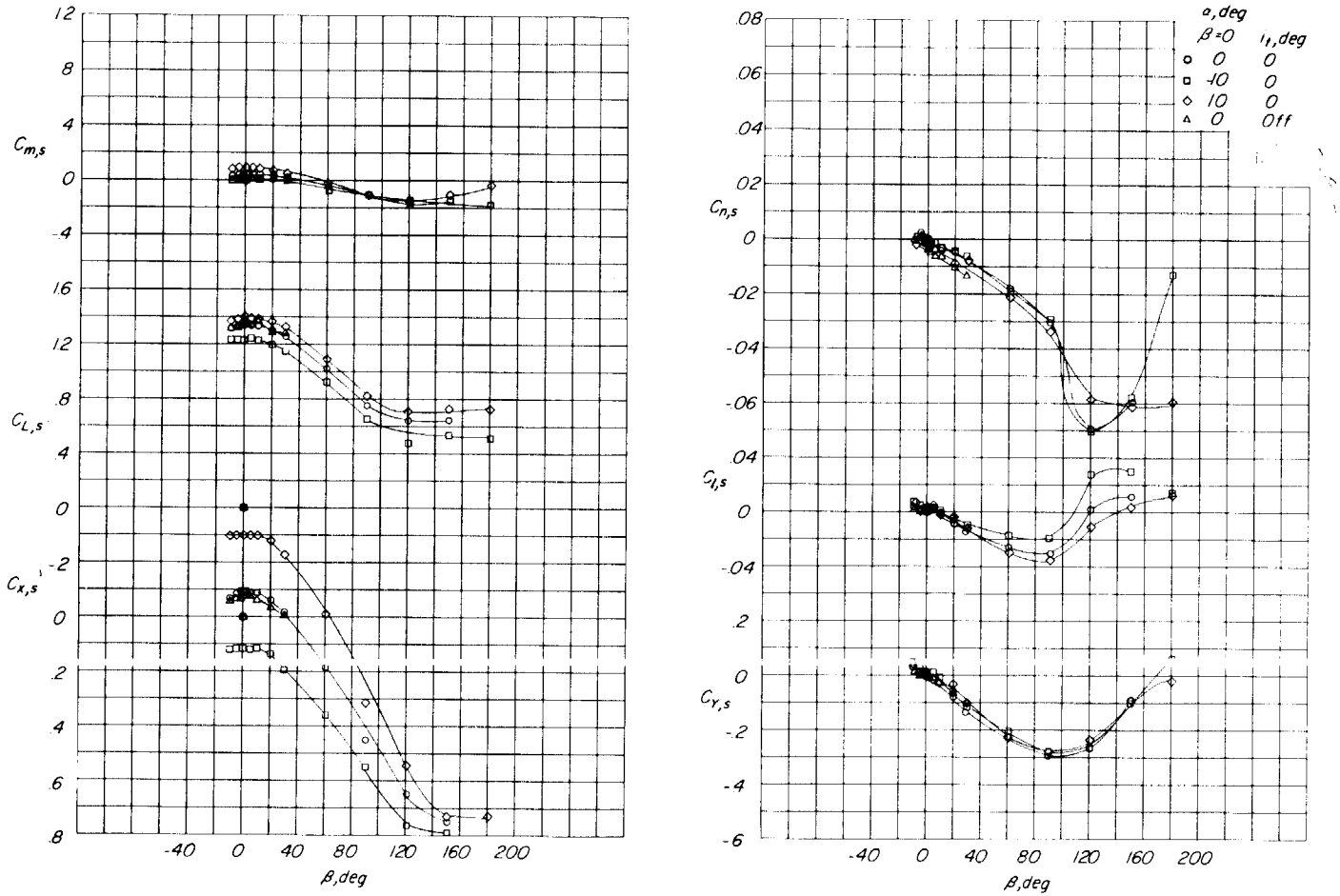

(a) $h/D = \infty$; $C_{T,s} = 0.944$; $\delta_{f,S}/\delta_{f,R} = 50/25$.

Figure 17.- Effect of angle of attack on the aerodynamic characteristics through a 180° sideslip-angle range. Fuselage fairing on.

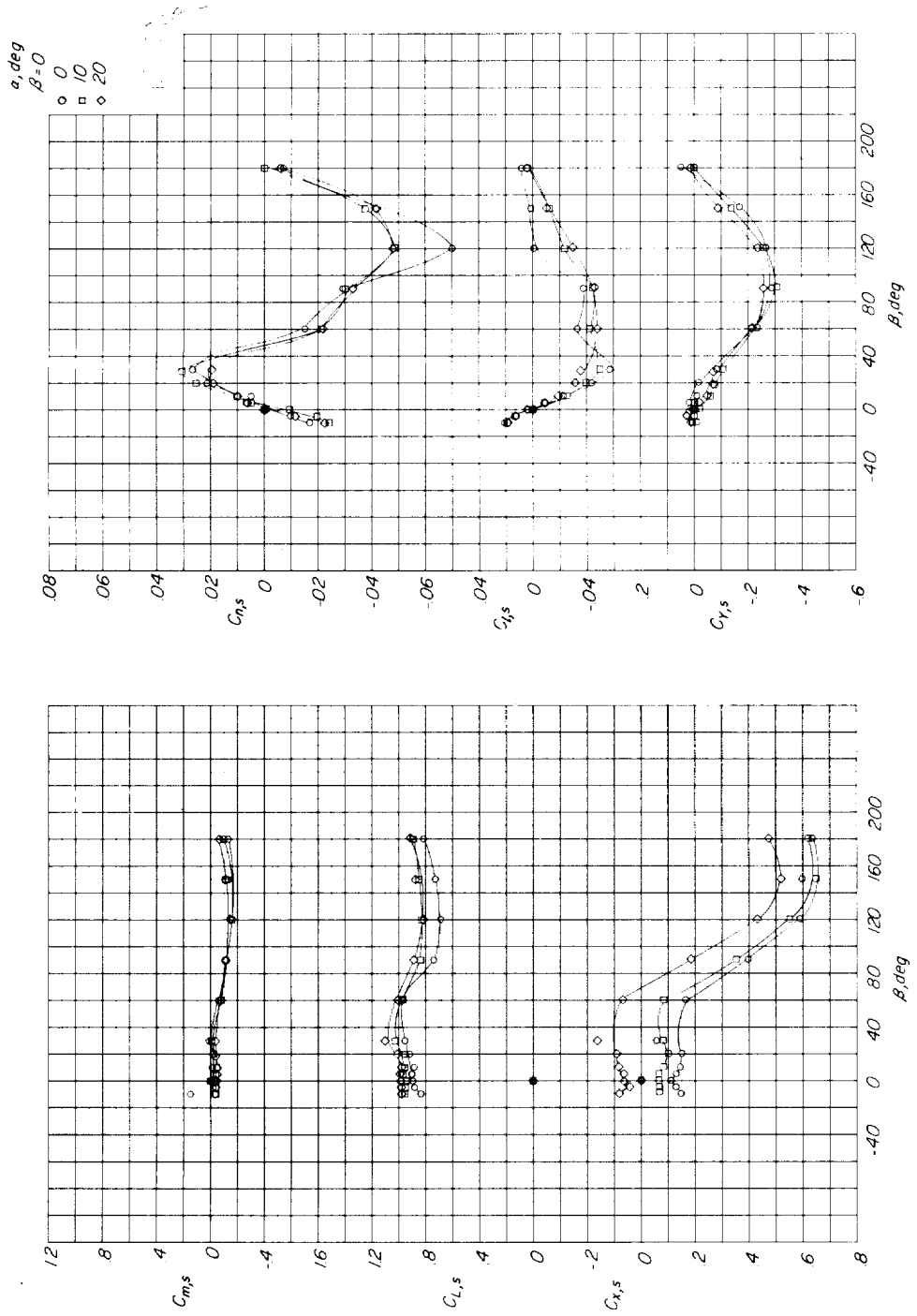

(b) h/D = 1.0; $C_{T,s}$ = 0.944; $\delta_{f,s}/\delta_{f,R}$ = 50/25.

Figure 17.- Continued.

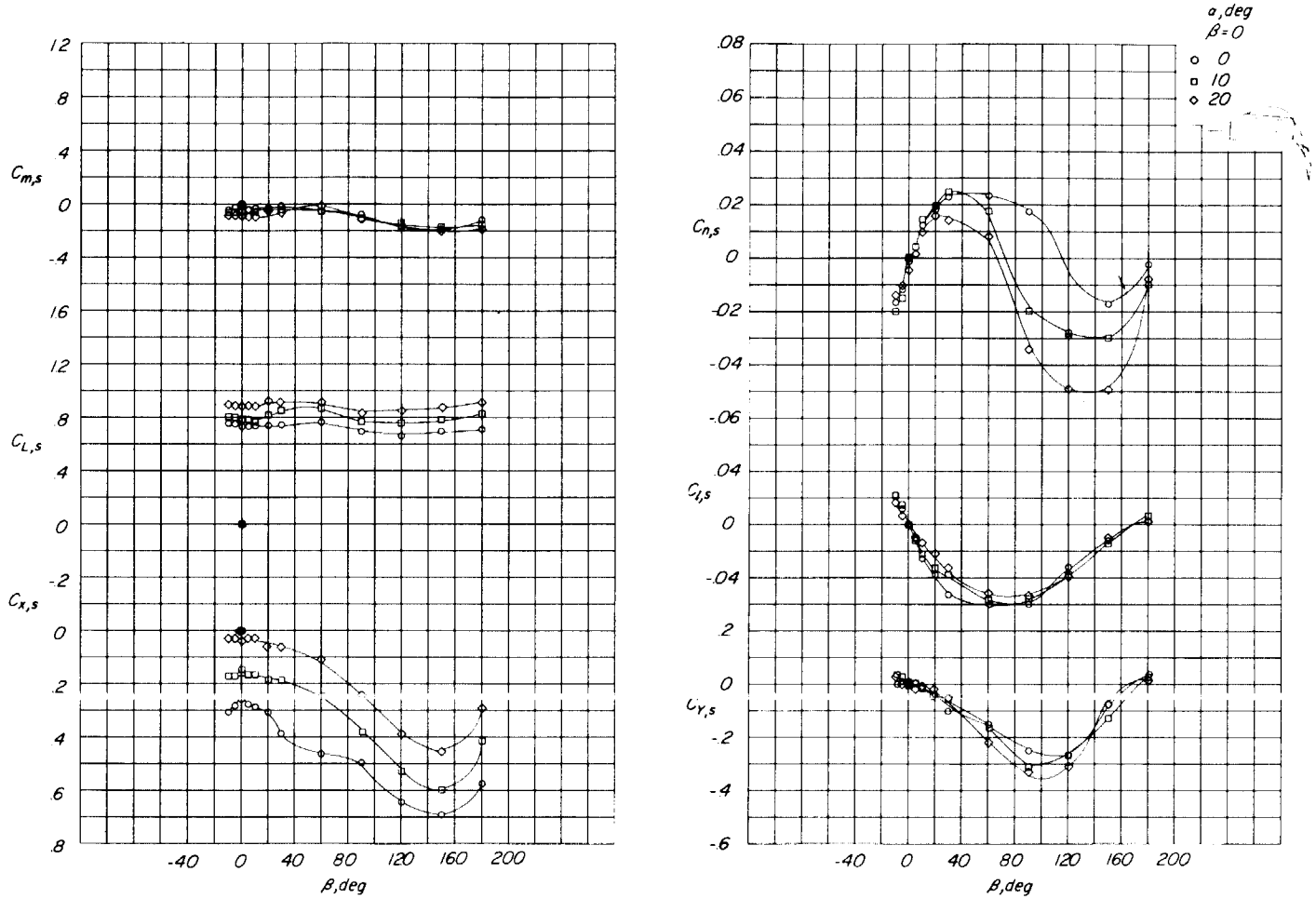

(c) h/D = 0.33; $C_{T,s}$ = 0.944; $\delta_{f,S}/\delta_{f,R}$ = 50/25.

Figure 17.- Continued.

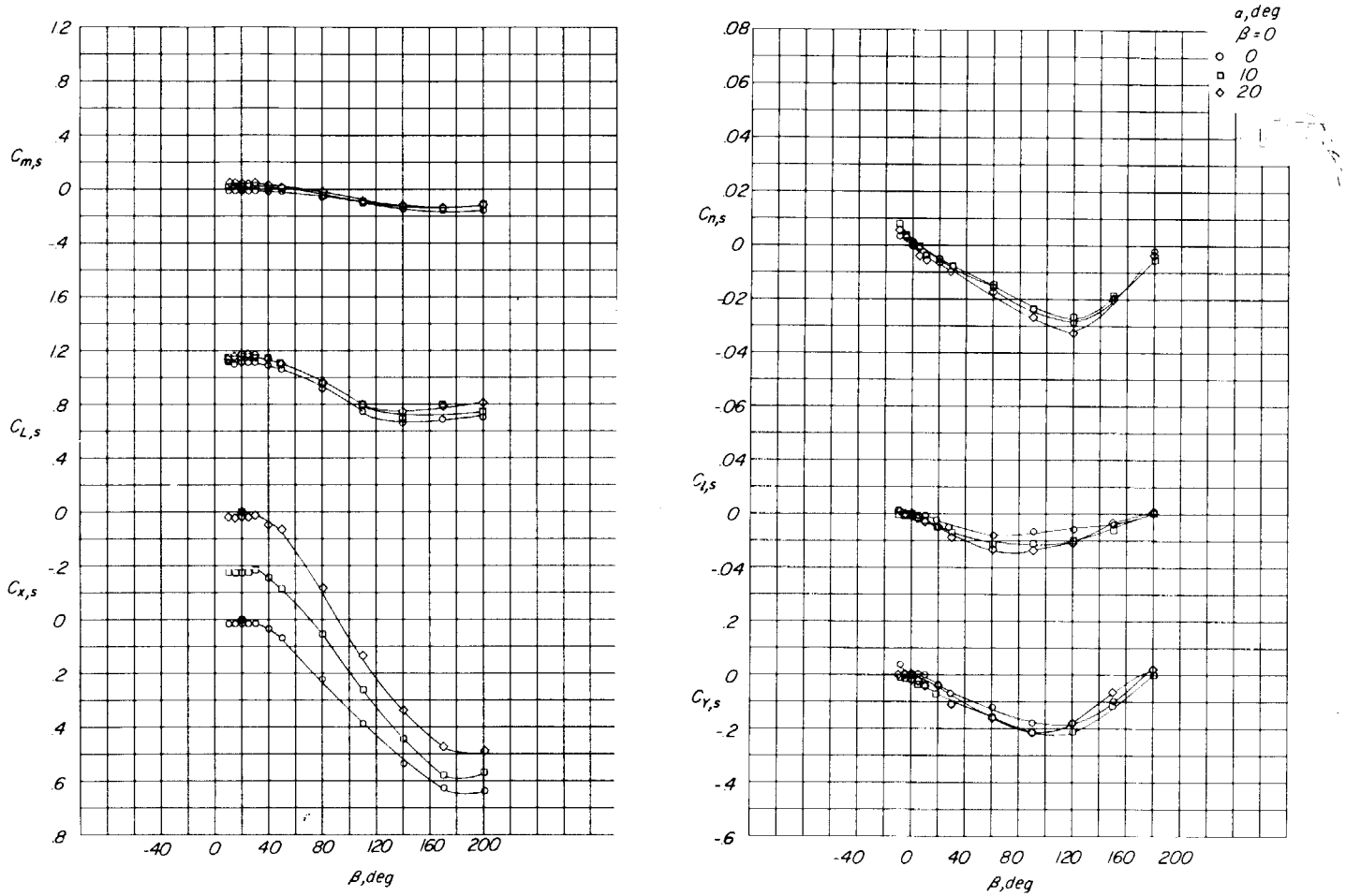

(d) $h/D = \infty$; $C_{T,s} = 0.978$; $\delta_{f,S}/\delta_{f,R} = 50/25$.

Figure 17.- Continued.

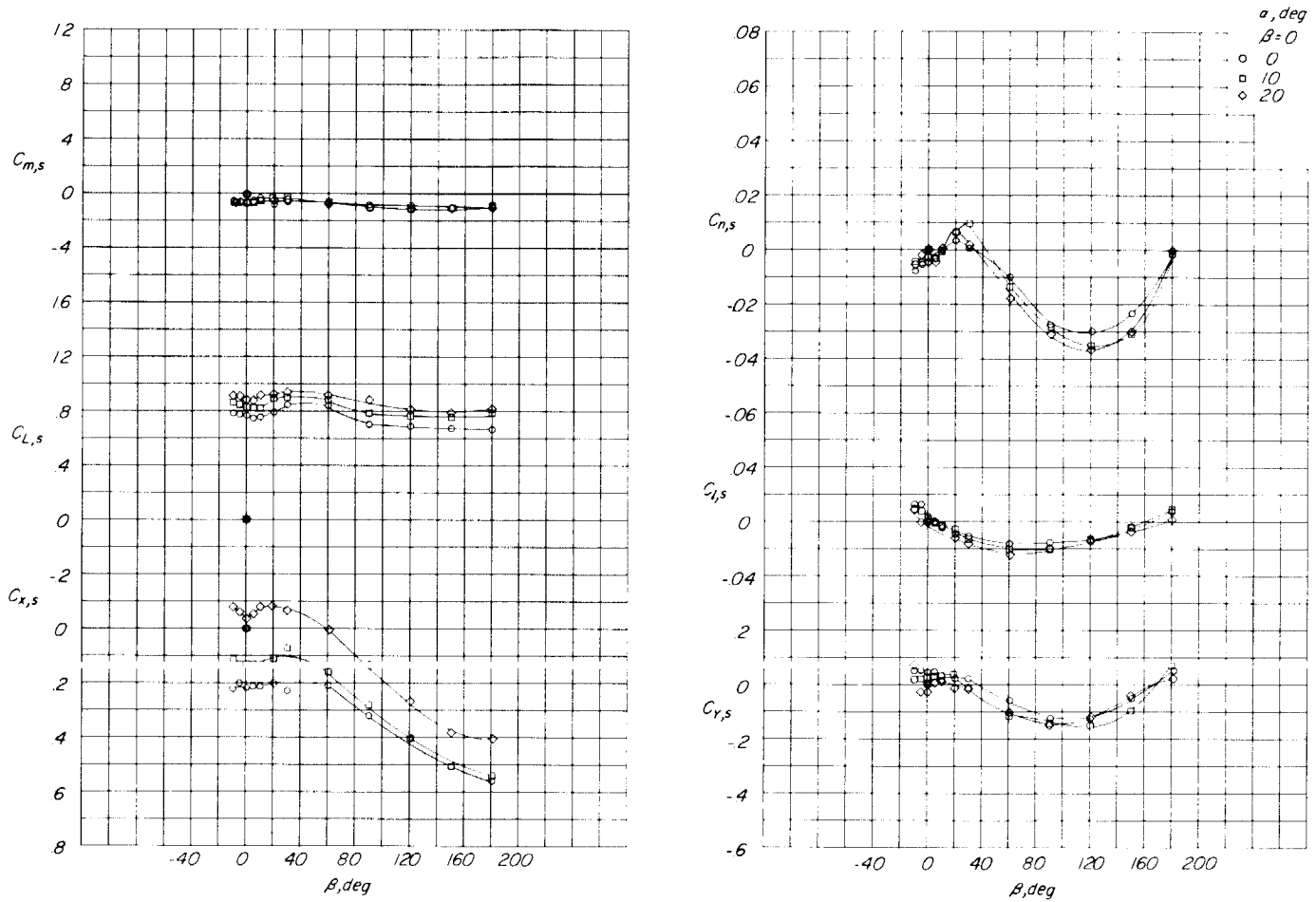

(e) h/D = 1.0; $C_{T,s}$ = 0.978; $\delta_{f,S}/\delta_{f,R}$ = 50/25.

Figure 17.- Continued.

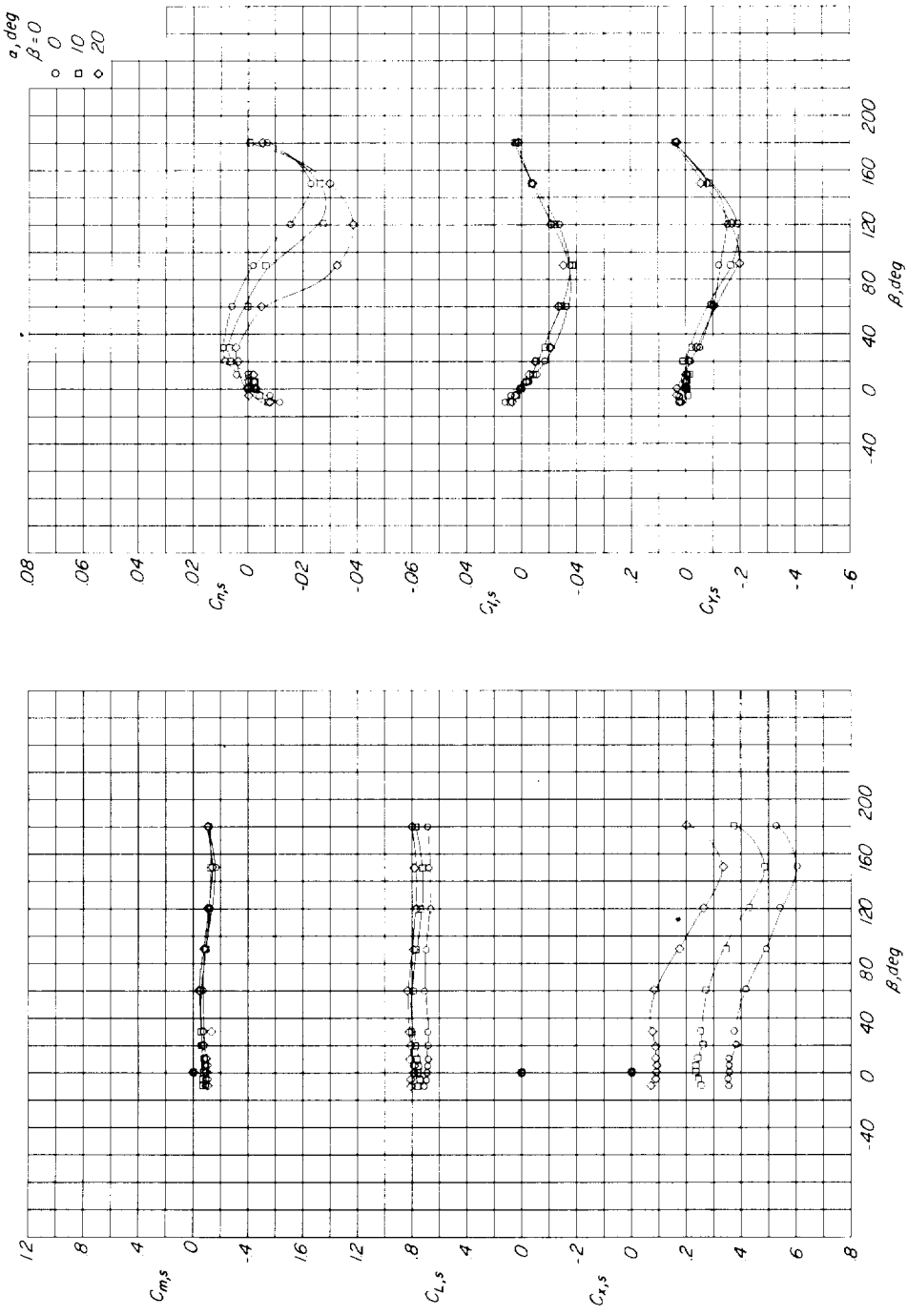

(f) h/D = 0.33; $C_{T,s}$ = 0.978; $\delta_{f,s}/\delta_{f,R}$ = 50/25.

Figure 17.- Concluded.

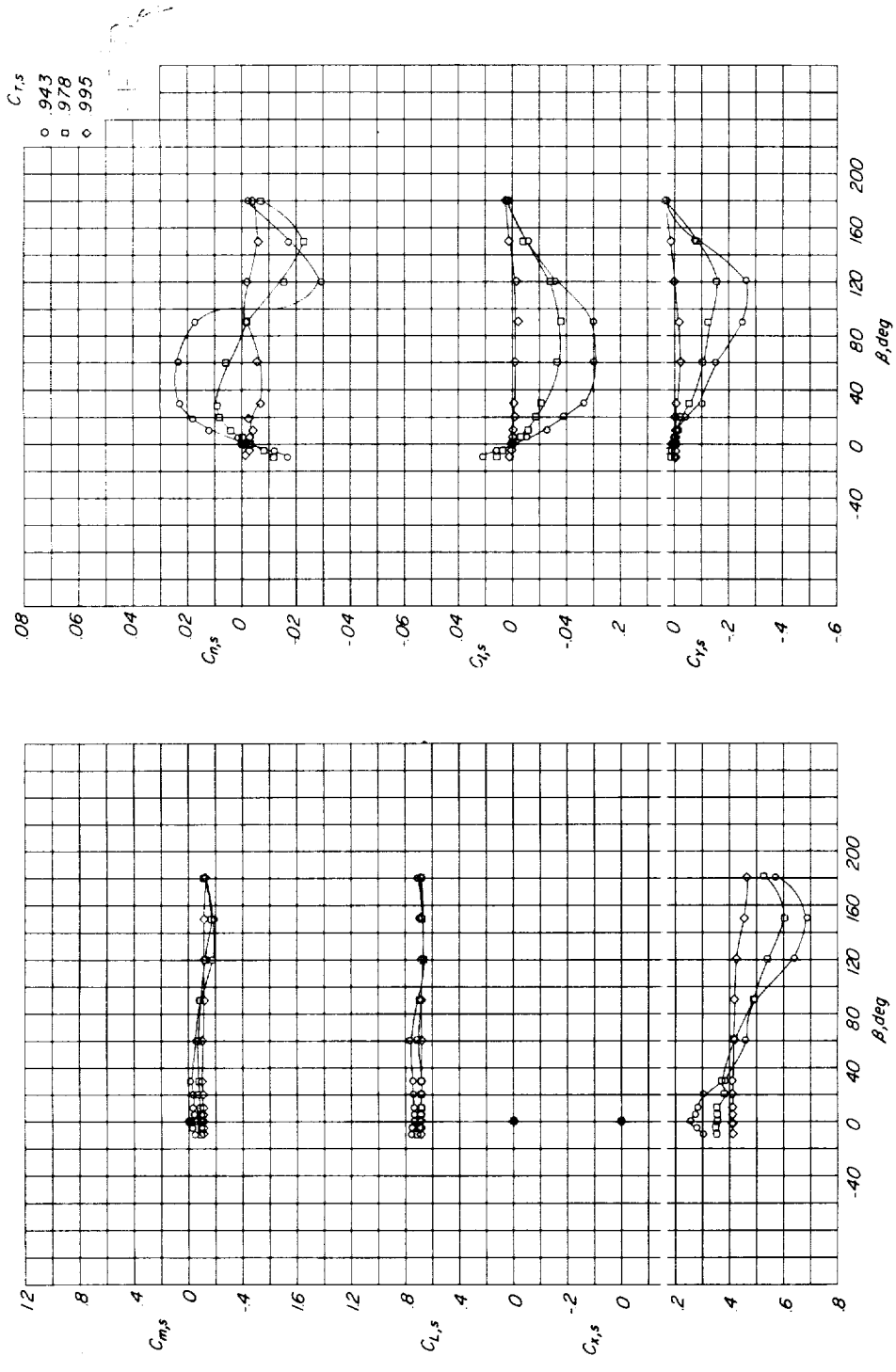

(a) h/D = 0.33; $\delta_{f,S}/\delta_{f,R}$ = 50/25.

Figure 18.- Effect of thrust coefficient on aerodynamic characteristics through a 180° sideslip-angle range at β = 0°. Fuselage fairing on; α = 0°; i_t = 0°.

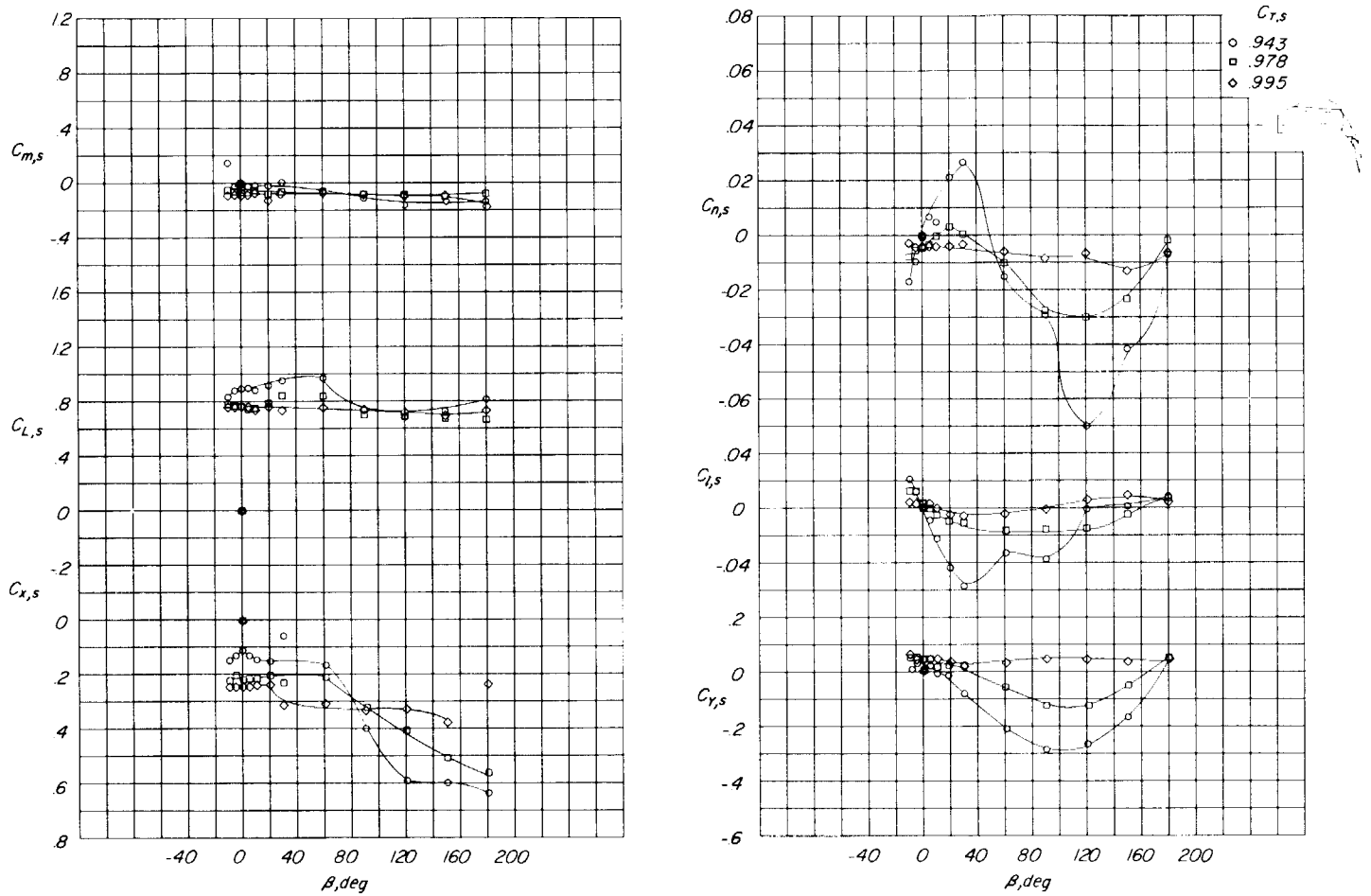

(b) $h/D = 1.0$; $\delta_{f,S}/\delta_{f,R} = 50/25$.

Figure 18.- Concluded.

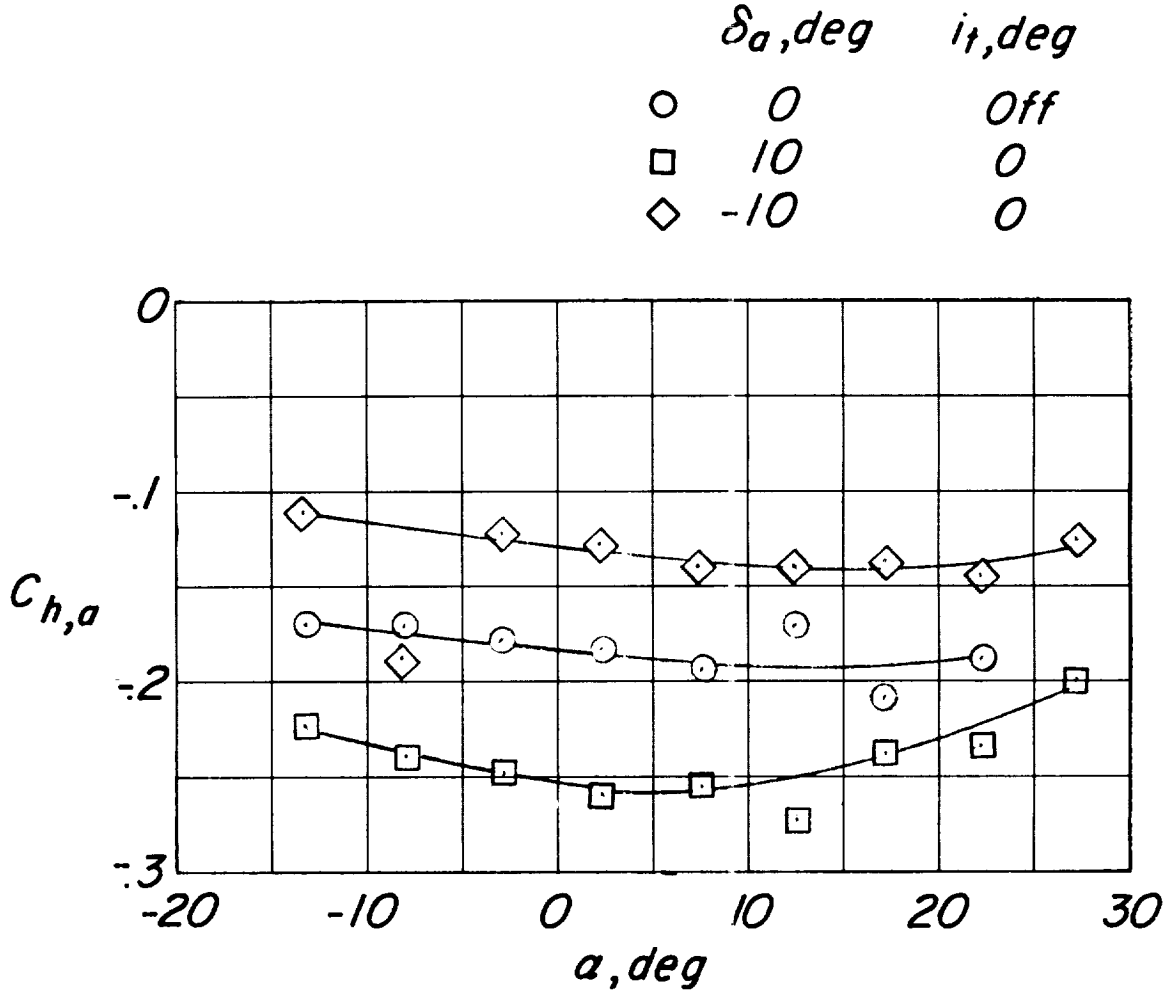

(a) $\delta_{f,S}/\delta_{f,R}$ = 30/20.7; $C_{T,\varepsilon}$ = 0.75.

Figure 19.- Aileron hinge moment out of the region of ground effect.

L-895

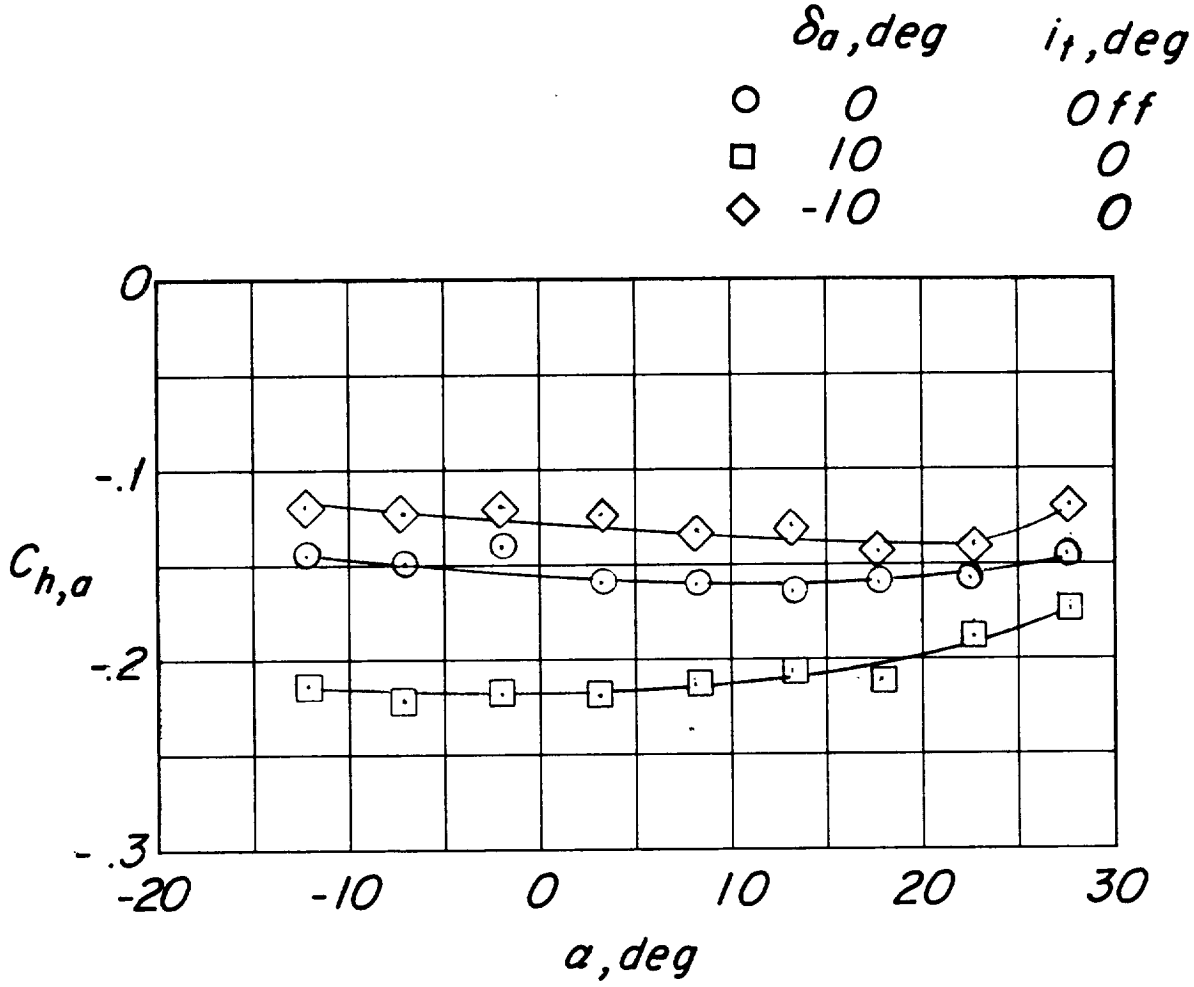

(b) $\delta_{f,S}/\delta_{f,R}$ = 40/24; $C_{T,s}$ = 0.89.

Figure 19.- Continued.

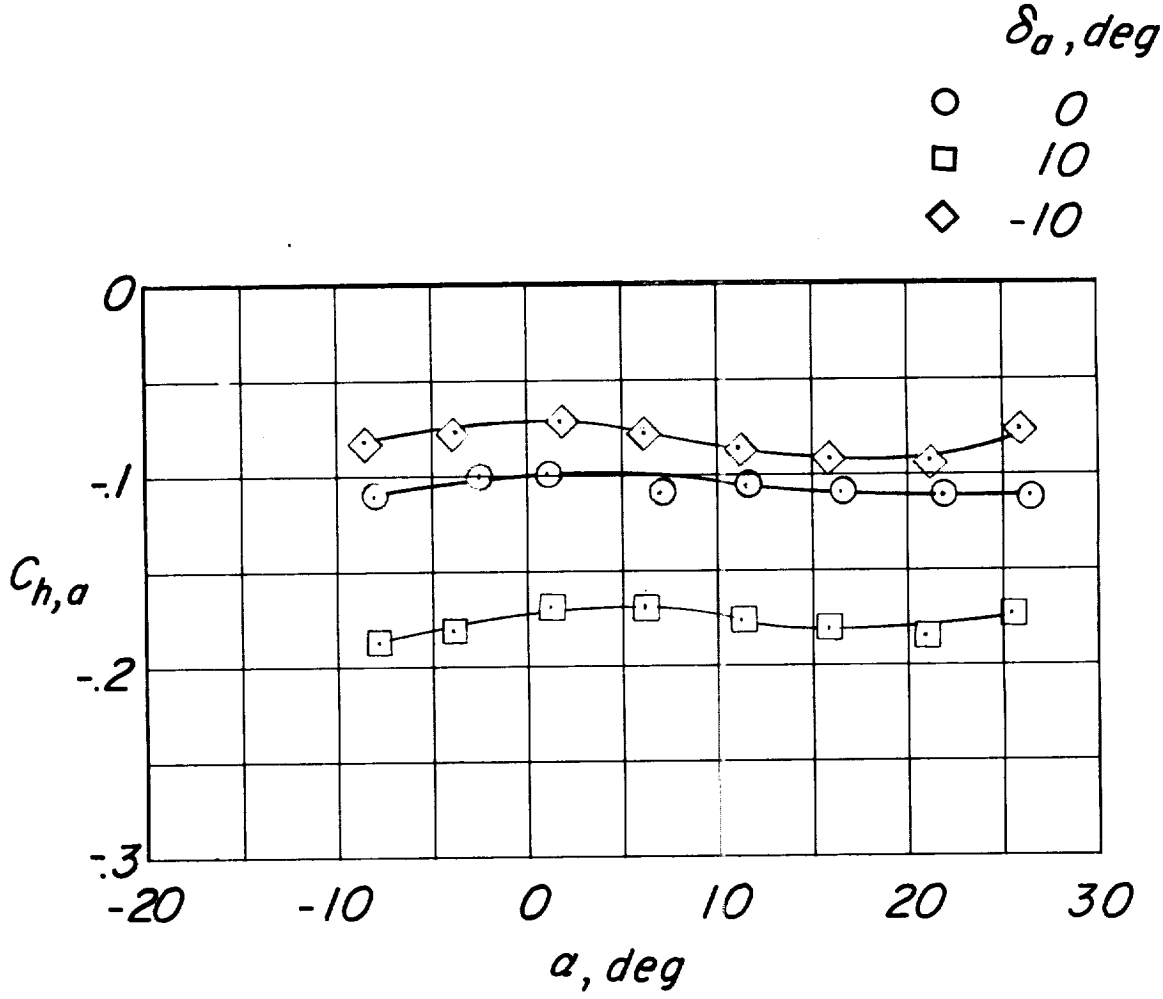

(c) $\delta_{f,S}/\delta_{f,R}$ = 50/25; $C_{T,s}$ = 0.98.

Figure 19.- Concluded.

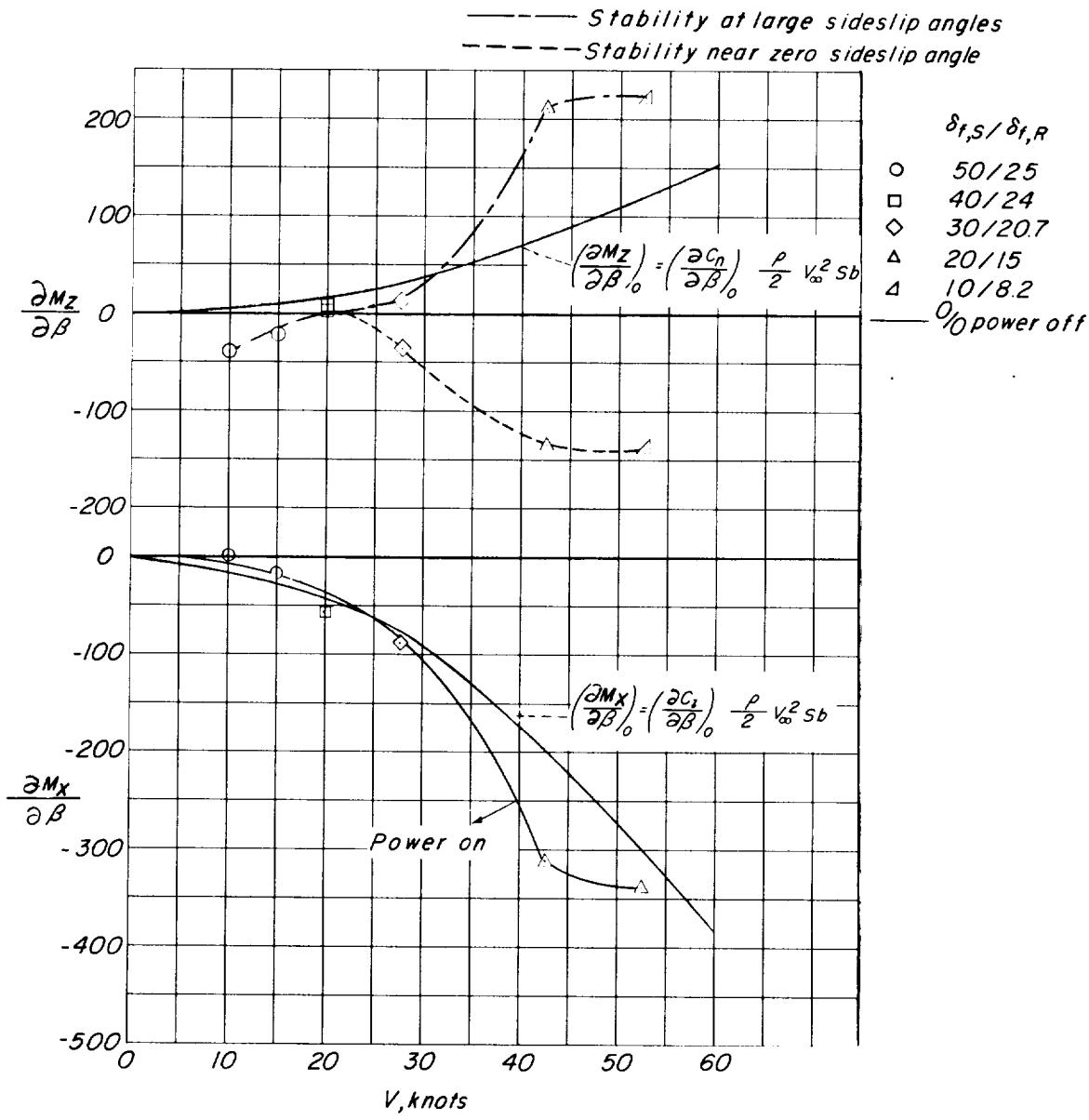

Figure 20.- Directional stability and dihedral effect in steady-level-flight transition out of the region of ground effect.

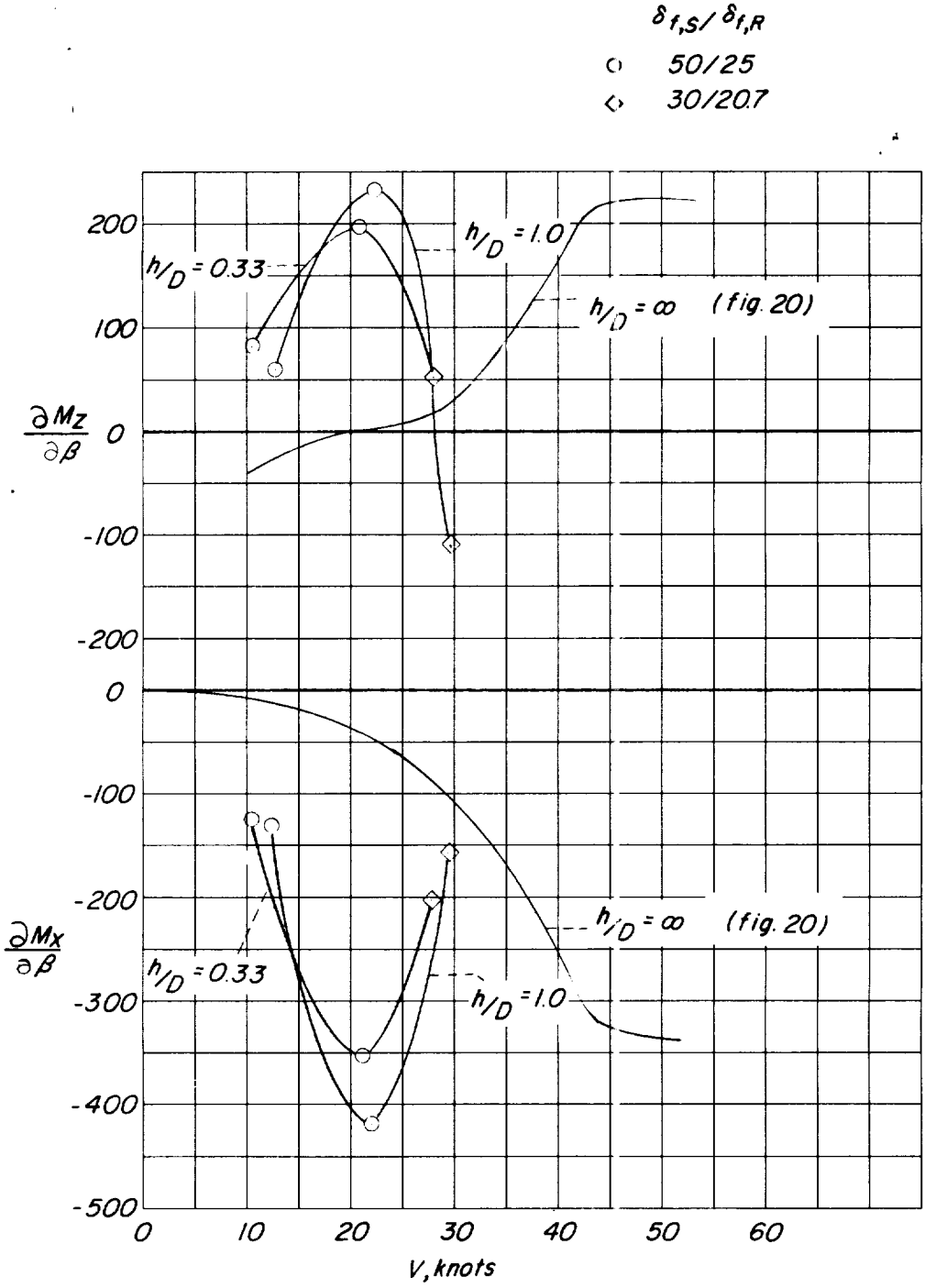

Figure 21.- Directional stability and dihedral effect in steady-level-flight transition in the region of ground effect. Power on.

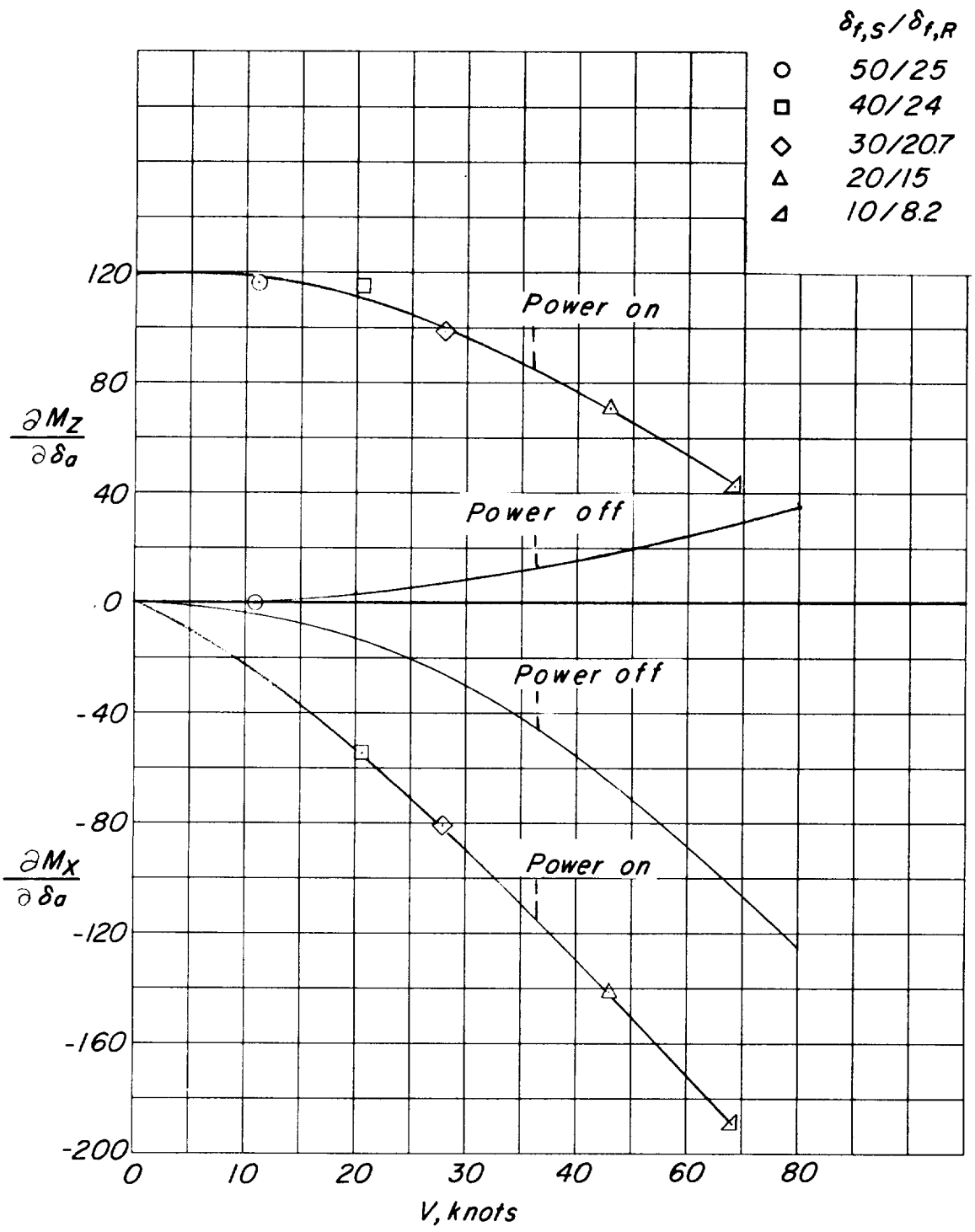

Figure 22.- Aileron effectiveness in steady-level-flight transition.

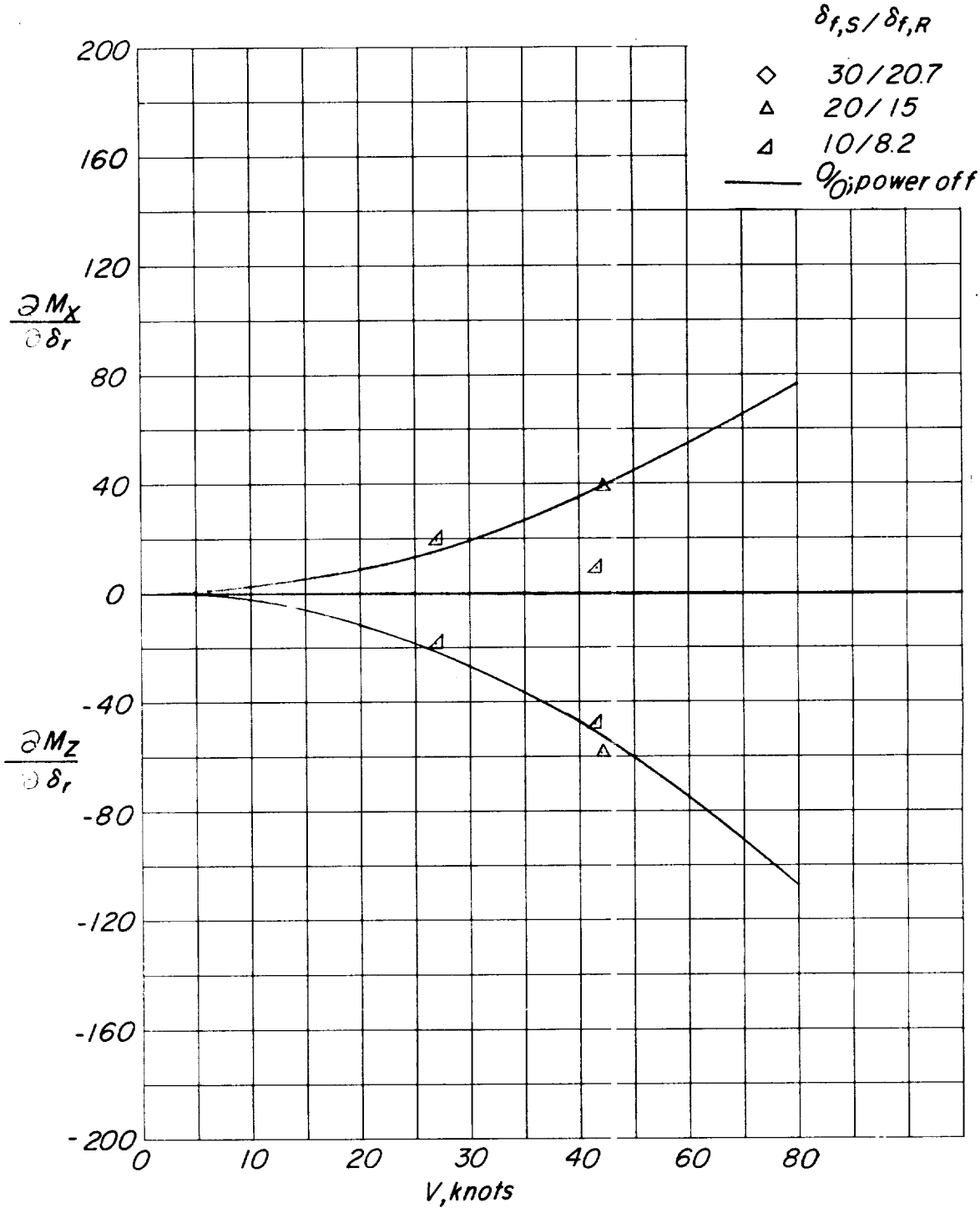

Figure 23.- Rudder effectiveness in steady-level-flight transition.

L-895